
Masters Theses

Student Theses and Dissertations

Summer 2015

Optimum acquisition and processing parameters for multichannel analysis of surface waves using 3D electrical resistivity tomography as control

Uchenna Chibuzo Nwafor

Follow this and additional works at: https://scholarsmine.mst.edu/masters_theses



Part of the [Geological Engineering Commons](#)

Department:

Recommended Citation

Nwafor, Uchenna Chibuzo, "Optimum acquisition and processing parameters for multichannel analysis of surface waves using 3D electrical resistivity tomography as control" (2015). *Masters Theses*. 7437.
https://scholarsmine.mst.edu/masters_theses/7437

This thesis is brought to you by Scholars' Mine, a service of the Missouri S&T Library and Learning Resources. This work is protected by U. S. Copyright Law. Unauthorized use including reproduction for redistribution requires the permission of the copyright holder. For more information, please contact scholarsmine@mst.edu.

**OPTIMUM ACQUISITION AND PROCESSING PARAMETERS FOR
MULTICHANNEL ANALYSIS OF SURFACE WAVES USING 3 D
ELECTRICAL RESISTIVITY TOMOGRAPHY AS CONTROL**

by

UCHENNA CHIBUZO NWAFOR

A THESIS

Presented To the Faculty of Graduate School of the

MISSOURI UNIVERSITY OF SCIENCE AND TECHNOLOGY

In Partial Fulfillment of the Requirements for the Degree

MASTER OF SCIENCE

IN

GEOLOGICAL ENGINEERING

2015

Approved

**Neil Anderson, Advisor
J. David Rogers
Maochen Ge**

ABSTRACT

Multichannel Analysis of Surface Waves (MASW) and Electrical Resistivity Tomography (ERT) data were acquired in the Newburg, Missouri with the goal of determining optimum MASW acquisition parameters. Users of the MASW tool generally state that greater geophone intervals and greater shot-to-receiver offsets provide for more accurate results. The objective was to determine if this “rule of thumb” applies in karst terrain.

ERT data were acquired along four traverses with eighty-four (84) electrodes at five feet spacing with SuperSting R8 Resistivity System using dipole- dipole array. The data were processed using Earth Imager to generate 2-D resistivity inversion and thereafter, Voxler software was used to collate the 2-D ERT data into a 3-D resistivity model. MASW data on the other hand, were acquired along the same ERT traverses on the same locations using a suite of different geophone intervals (1-ft, 2.5-ft, 5-ft, 7.5-ft, and 10-ft) and shot-to-receiver spacings (0-ft, 10-ft, 20-ft, 30-ft, 40-ft, and 50-ft) with a 20lb sledge hammer as the source. The data were processed using Surfseis software to generate the dispersion curves and 1-D shear wave velocity profiles of the area.

On the basis of the comparative analyses of the ERT and MASW data, it was determined that 2.5-ft and 5-ft geophone gave generated depth of bedrock that was consistent with ERT data. With 5-ft geophone spacing it is possible to image the subsurface to greater depth, but with the 7.5-ft and 10-ft, unidentifiable dispersion curves would be generated. Therefore, in this study area, on the basis of data that were acquired it is recommended that 2.5ft spacing be used if depth of investigation is about 40ft, but if the depth of investigation is about 80-ft, using a sledge hammer source then 5-ft geophone spacing at 20-ft shot-receiver offset distance is recommended.

ACKNOWLEDGEMENT

I would like to thank my advisor Dr. Neil Anderson for his encouragement and support during the period of this research. Also, my appreciation goes to members of the committee; Dr. J. David Rogers and Dr. Maochen Ge, for their time and participation in the completion of this project.

The completion of this thesis would not have been possible without the corroborative efforts of several individuals. The following individuals have contributed time and resources to the completion of this study: Stanley Nwokebuihe, Rafael Araujo, and Dennis Duru.

I would like to thank Mr. Ben and his family for providing us with their farm sites to carry out this research.

Specifically, I would like to thank my wife Miss Ebere Nwafor, for her patience and support throughout my graduate study years, Ebere you have been a great wife.

This work is dedicated to my loving wife, Ebere. Without your love and sacrifice, I would not be achieving this milestone.

Thank you.

TABLE OF CONTENTS

	Page
ABSTRACT	iii
ACKNOWLEDGEMENT	iv
LISTS OF FIGURES	ix
LISTS OF TABLES	xii
 SECTION	
1. INTRODUCTION	1
1.1 OBJECTIVES	2
1.2 ORGANIZATION	3
2. OVERVIEWS OF MULTICHANNEL ANALYSIS OF SURFACE WAVES	4
2.1 INTRODUCTION	4
2.2 BASIC WAVE THEORY	4
2.2.1 Body Waves and Surface Waves	8
2.2.2 Rayleigh Waves Velocity	12
2.2.3 Relationship between Shear Waves and Soil/Rock Conditions	13
2.3 MULTICHANNEL ANALYSIS OF SURFACE WAVES METHOD.....	15
2.3.1 Overview	17
2.3.2 MASW Using Impulsive Source (MASWI)	19
2.4 MASW EQUIPMENT	21
2.4.1 Seismic Source	21
2.4.2 Trigger Mechanism	22
2.4.3 Geophones	23

2.4.4 Geophone Cable	24
2.4.5 Seismograph	25
2.5 MASW FIELD SURVEY SETUP	25
2.5.1 Overviews of MASW Data Acquisition	26
2.5.2 Overviews of Data Processing	27
3. OVERVIEWS OF ELECTRICAL RESISTIVITY TOMOGRAPHY METHOD.....	31
3.1 INTRODUCTION	31
3.2 BASIC THEORY	32
3.3 ARRAYS	37
3.4 RELATIONSHIP BETWEEN RESISTIVITY AND SOIL/ROCK CONDITION.....	39
3.4.1 Overviews of Two-Dimensional Electrical Resistivity Surveying	40
3.4.2 Three-Dimensional Electrical Resistivity Surveying (3-D)	42
3.5 FIELD EQUIPMENT	43
3.5.1 Transmitter/Receiver	43
3.5.2 Cables	44
3.5.3 Current and Potential Electrodes	44
3.5.4 Power Source	45
3.6 OVERVIEW OF ERT DATA ACQUISITION	45
3.7 DATA PROCESSING AND INTERPRETATION	47
4. RESEARCH METHODS	50
4.1 OVERVIEW	50
4.2 SITE LOCATION	50

4.3 MASW TESTING	55
4.3.1 Site Setup	55
4.3.2 Field Procedures and Equipment	57
4.3.3 Data Acquisition	59
4.3.4 Data Processing and Inversion	68
4.4 ELECTRICAL RESISTIVITY TOMOGRAPHY (ERT)	85
4.4.1 Site Setup	85
4.4.2 Field Procedures and Equipment	87
4.4.3 Data Acquisition	89
4.4.4 Data Processing and Inversion	91
4.5 CONCLUSIONS	98
5. RESULTS	99
5.1 OVERVIEW	99
5.2 RESULTS FROM MASW DATA	99
5.3 RESULTS FROM ERT DATA	106
5.4 MUTING	109
5.4.1 Results from Muting	113
5.4.2 Importance of Muting	114
6. DISCUSSIONS	115
6.1 OVERVIEW	115
6.2 COMPARISON OF MASW RESULTS WITH 2-D ERT RESULTS.....	115
6.3 FINAL ANALYSIS	124
7. CONCLUSIONS	125

8. RECOMMENDATIONS.....	127
BIBIOGRAPHY.....	128
VITA	131

LISTS OF FIGURES	Page
Figure 2.1: Bulk modulus equations and calculations	6
Figure 2.2: Showing how to determine and calculate shear modulus	7
Figure 2.3: Diagram showing stress and strain relationship	7
Figure 2.4: How P-waves and S- waves travel through a medium.....	9
Figure 2.5: Block models of mode of propagation for Love waves and Rayleigh waves.....	12
Figure 2.6: Showing typical MASW field setup	19
Figure 2.7: Showing typical MASWV field setup	19
Figure 2.8: Showing typical MASWI field setup.....	21
Figure 2.9: Showing different array configurations for the MASWP	21
Figure 2.10: Example of Sledgehammer Triggering Device.....	23
Figure 2.11: Example of spike-coupled Geophone	24
Figure 2.12: Instrumentation of MASW Tomography Survey	26
Figure 2.13: Progression of MASW Tomography Survey	27
Figure 2.14: Processing Steps to Estimate Shear Wave Velocity	28
Figure 3.1: Equipotential and current lines for a pair of current electrodes A and B on a homogeneous half-space.	35
Figure 3.2: Electrode array configurations for resistivity measurements	38
Figure 3.3: Two-dimensional measurement configurations for a dipole-dipole resistivity profile, pseudosection plotting location indicated in red.....	41
Figure 3.4: Examples of measured apparent resistivity, calculated apparent resistivity, and inverted resistivity.....	42
Figure 3.5: Example of Developed Pseudosection Model Using a Wenner Array and 28 Electrodes.....	47
Figure 3.6: Flow Chart of Resistivity Inversion Processing.....	49

Figure 4.1: Newburg map showing the study area located within Mark Twain National Forest.....	50
Figure 4.2: Showing the location of Corn Creek Road	51
Figure 4.3: Alluvium and Surficial geology map of Newburg area.....	52
Figure 4.4: Bedrock Geologic map of the study area.....	53
Figure 4.5: MASW traverses (blue lines) oriented NE-SW and NE-NW and ERT lines (red lines) oriented NW-SE.....	55
Figure 4.6: 4.5 Hz Geophones with spikes.....	56
Figure 4.7: Showing cable (red), connectors (yellow), knob (black) and geophones with spike.....	56
Figure 4.8: A one square foot metal plate.....	58
Figure 4.9: Shot gather for each of the array record at different offset distances.....	60
Figure 4.10: A flowchart detailing the processing steps used for analyzing MASW profiles (Kansas Geological Survey, 2014).	68
Figure 4.11: All the generated dispersion curves and the inverted shear wave velocity model for the different tests	70
Figure 4.12: Switch box and SuperSting	86
Figure 4.13: Four ERT traverses (red) and two MASW traverses (blue).....	87
Figure 4.14: SuperSting Manager App, Plot pseudo section.....	89
Figure 4.15: Equipment set up for the ERT acquisition.....	90
Figure 4.16: Pseudo sections and data points generated for the ERT traverses.....	92
Figure 4.17: Final inverted section for the resistivity analysis.....	94
Figure 4.18: 3-D ERT Model generate with Voxler software.....	96
Figure 5.1: Final inverted section for the resistivity analysis for ERT line 1 showing top of bedrock in black dotted lines, pockets of consolidated sand layer, moist soil and very intact bedrock.....	107

Figure 5.2: Final inverted section for the resistivity analysis for ERT line 2 showing top of bedrock in black dotted lines, pockets of consolidated sand layer, moist soil and very intact bedrock.....	108
Figure 5.3: Final inverted section for the resistivity analysis for ERT line 3 showing top of bedrock in black dotted lines, pockets of consolidated sand layer, moist soil and very intact bedrock.....	108
Figure 5.4: Final inverted section for the resistivity analysis for ERT line 4 showing top of bedrock in black dotted lines, pockets of consolidated sand layer, moist soil and very intact bedrock.....	109
Figure 5.5: 3-D model generated by combining the four ERT traverses using Voxler software.....	109
Figure 5.6: Raw shot gather from a 2.5-ft geophone spacing and 0-ft receiver offset before and after muting.....	111
Figure 5.7 Dispersion curve for 2.5-ft spacing and 0-ft offset.....	112

LISTS OF TABLES

	Page
Table 5.1: Results from all the dispersion curves and generated shear wave velocity profiles.....	106
Table 6.1: Final result analysis for MASW and ERT testing.....	124

1. INTRODUCTION

When important structures are built in active seismic zones or when the dynamic properties of a soil are of interest, testing of the in-situ soil is required to determine its shear wave velocity. The shear wave velocity of the soil is directly related to its shear modulus and the shear modulus of the soil strongly influences how it will react during dynamic loading. Several methods are available to measure the in-situ shear wave velocity profile of a site. The simplest and most accurate methods are borehole seismic methods, but these methods are also fairly expensive due to the need to drill boreholes down to the desired depth of investigation. To reduce the cost and testing time associated with borehole techniques, non-intrusive surface wave methods have been developed. These methods are often significantly cheaper, faster, and easier to use and are subsequently replacing borehole methods for many shear wave velocity investigations.

Various surface wave methods have been developed over the years to estimate the in-situ shear wave velocity profile. The most common method used today is the multi-channel analysis of surface waves (MASW). The MASW method is a newer technique that has several different ways to collect and analyze data. Because there are several different ways to collect and analyze the data, there are limited guidelines on receiver positioning, source placement and source type that are most effective at producing accurate results.

The purpose of this research is to determine the optimum acquisition and processing parameter for MASW method on alluvium deposited site in Newburg, Missouri.

1.1 OBJECTIVES

The main objective of this research is to determine the optimum acquisition and processing parameters for Multichannel Analysis of Surface Waves (MASW) by using MASW and Electrical Resistivity Tomography (ERT) to estimate the top of bedrock and image the subsurface of the site to 50-ft.

The following are means of accomplishing this objective:

- (1) Acquire ERT data along four traverses along the same direction in the study area
- (2) Acquire MASW data along ERT traverses from 100-ft on the ERT traverse using different geophone spacing (1-ft, 2.5-ft, 5-ft, 7.5-ft, and 10-ft.) at different offset distances (0-ft, 10-ft, 20-ft, 30-ft, 40-ft, and 50-ft).
- (3) Process the ERT data using Earth Imager and Resiv2D to generate 2D resistivity inversion result for the study area
- (4) Collate the four 2D ERT result into a 3D model using Voxler software
- (5) Process MASW data using Surfeis software to generate dispersion curve and 1D shear wave velocity profile.
- (6) Estimate the acoustic top of bedrock and depth to top of bedrock using the generated 1D shear wave velocity and ERT in the study area and image subsurface to 50-ft.
- (7) Compare MASW with ERT results and determine the optimum acquisition parameters for MASW based on their accuracy with ERT result.

1.2 ORGANIZATION

This thesis is divided into eight sections. Section one started with the introduction of Multichannel Analysis of Surface Waves method (MASW), objectives of this research and organization of the works done in this research. In section two, overviews of MASW method was discussed starting with the basic wave theory, body waves and surface waves, Rayleigh wave's velocity to the relationships between shear waves and soil/rock conditions. Also, details of MASW method was discussed including the equipment, field survey set up, data acquisition, data processing and interpretations. Then, section three emphasized on the overviews of Electrical Resistivity Tomography (ERT) Method, the basic resistivity theory, array types, relationship between resistivity and soil/rock conditions. Also, 2D and 3D ERT methods were discussed with emphasis on the equipment, data acquisition, data processing and interpretations.

In section four, research methodology was discussed with focus on the site selection, MASW testing and ERT testing. Results of MASW and ERT testing including muting and muting results were discussed in chapter five. While in section six, MASW and ERT results were discussed and compared with each other in the final analysis.

Finally, section seven concluded the research and future recommendations for further studies stated in section eight.

2. OVERVIEWS OF MULTICHANNEL ANALYSIS OF SURFACE WAVES

2.1 INTRODUCTION

Multichannel Analysis of Surface waves (MASW) is a non-destructive seismic survey method, introduced by Park et al., (1999), that has been found by the geotechnical community to be an efficient method for detecting the subsurface shear wave (S) velocity variation. This method is beneficial for analyzing variations in subsurface stiffness (Park et al., 2003). MASW analyses dispersion properties of horizontal travelling Rayleigh waves. The following commentary provides a discussion of basic wave theory, body waves and surface waves, Rayleigh wave velocity, relationship between shear wave and soil/rock condition, and background information pertaining to MASW theory and analysis.

2.2 BASIC WAVE THEORY

Seismic theory is built on the idea that elastic waves travel at speeds which correlate with the physical properties of their respective media (Parasnis, 1997). The knowledge of this idea requires an initial physical understanding of material elastic behavior and wave velocity. Hooke's law states that the strain, ϵ , experienced by a material is directly proportional to the imposed stress, σ , on that given material. At the point of elastic deformation, the elastic material property that directly correlates strain to stress is termed the elastic modulus, E (Callister Jr., 2001).

Seismic wave propagation is dependent on its ability to elastically deform particles within a given media as it propagates through the material. The size and shape

of a solid body can be changed by applying forces to the external surface of the body. These external forces are opposed by internal forces, which resist the changes in size and shape. As a result, the body tends to return to its original condition when the external forces are removed.

Similarly, a fluid resists changes in size (volume) but not changes in shape (i.e. supports compressive stresses but not shear stresses). This property of resisting changes in size or shape and of returning to the undeformed condition when the external forces are removed is called elasticity. A perfectly elastic body is one that recovers completely after being deformed.

Many substances including rocks can be considered perfectly elastic without appreciable error provided the deformations are small, as they are in seismic surveys. The theory of elasticity relates the forces that are applied to the external surface of a body to the resulting changes in size and shape.

An elastic modulus, or modulus of elasticity, is a number that measures an object or substance's resistance to being deformed elastically (i.e., non-permanently) when a force is applied to it. The elastic modulus of an object is defined as the slope of its stress–strain curve in the elastic deformation region. A stiffer material will have a higher elastic modulus.

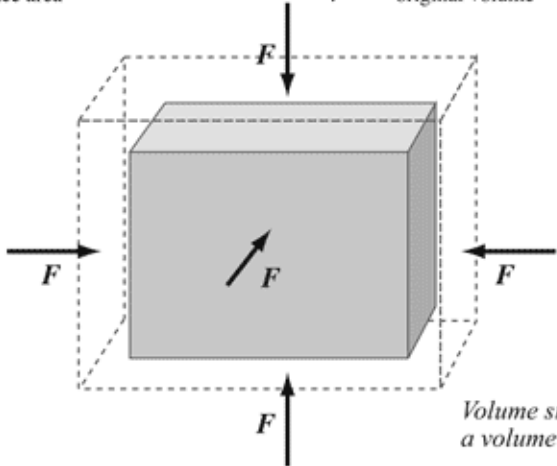
Bulk modulus of a material determines how much it will compress under a given amount of external pressure. The ratio of the change in pressure to the fractional volume compression is called the bulk modulus of the material. Figure 2.1 below show details about bulk modulus calculations.

$$\text{bulk modulus} = - \frac{F/A}{\Delta V/V}$$

$$\text{volume stress} = \frac{F}{A} \qquad \text{volume strain} = \frac{\Delta V}{V}$$

F = normal force
 A = surface area

ΔV = change in volume
 V = original volume



Volume strain produced by a volume stress

Figure 2.1: Bulk modulus equations and calculations
 (<http://www.wikipremed.com/01physicscards.php?card=316>)

Shear modulus known as Modulus of Rigidity - G - is the coefficient of elasticity for a shearing force. It is defined as "the ratio of shear stress to the displacement per unit sample length (shear strain). Figure 2.2 shows equations and calculations for the shear modulus.

$$\text{shear modulus} = \frac{F/A}{\Delta x/h}$$

$$\text{shear stress} = \frac{F}{A}$$

F = tangential force
 A = area of face being sheared

$$\text{shear strain} = \frac{\Delta x}{h}$$

Δx = horizontal distance sheared face moves
 h = height of object

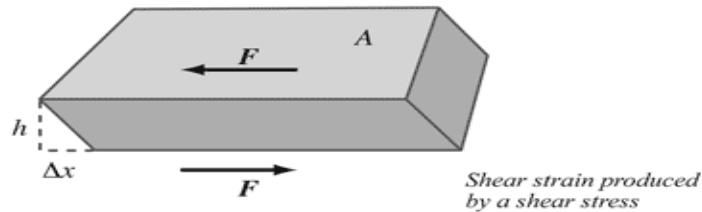


Figure 2.2: Showing how to determine and calculate shear modulus
<http://www.wikipremed.com/01physicscards.php?card=312>

The relations between the applied forces and the deformations are most conveniently expressed in terms of the concepts of stress and strain which are shown in Figure 2.3 below.

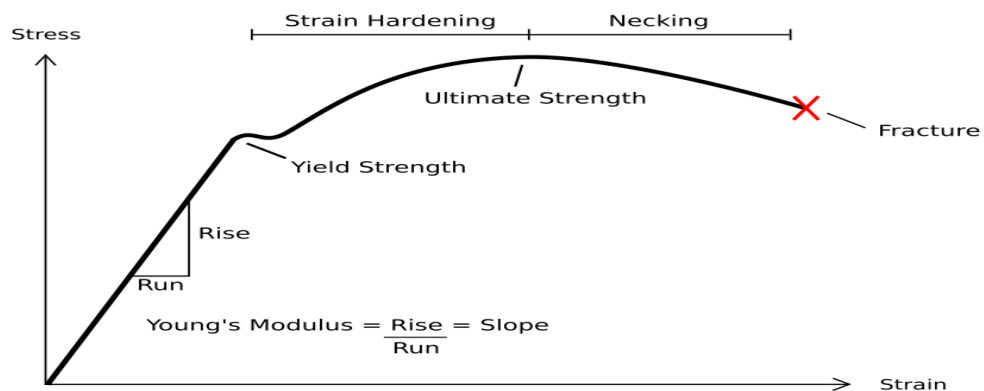


Figure 2.3: Diagram showing stress and strain relationship
http://upload.wikimedia.org/wikipedia/commons/8/84/Stress_Strain_Ductile_Material.png

Yield strength, or the yield point, is defined in engineering as the amount of stress that a material can undergo before moving from elastic deformation into plastic deformation.

The Ultimate Tensile Strength - *UTS* - of a material is the limit stress at which the material actually breaks, with sudden release of the stored elastic energy.

The propagation of different wave types is caused by the different forms of stress imposed (e.g. compressive stress, shearing stress). In different situations, the applicability of the small strain assumption has been questioned and other models relating stress and strain have been applied to seismic analysis. However, the principle of Hooke's law remains one of the prominent models for elasticity in seismic theory (Parasnis, 1997).

The wave velocity, v , is directly proportional to the frequency of the wave, f , and the wave length, λ , as shown in Equation 2.1.

$$v = f\lambda \quad (2.1)$$

The wavelength is the distance between two consecutive wave peaks or troughs. The frequency of a wave is the reciprocal of the wave period, t , which is the duration required to complete one wave oscillation. See equation 2.2 below for details.

$$f = 1/t \quad (2.2)$$

Understanding of the basic wave relationships is very crucial when evaluating and interpreting seismic wave activity.

2.2.1 Body Waves and Surface Waves. Seismic waves are grouped into two types, namely; body waves and surface waves. Body waves are non-dispersive and travel through a given media at a speed proportional to the material density and modulus. Body waves are categorized into two types based on their modes of propagation. They can

either travel longitudinal or transverse to the direction of the traveling wave. Longitudinal movements are called P-waves or compression waves, and the transverse movements are called S-waves or shear waves. P-waves transfer energy through media by compressing and dilating particles as the wave passes through the media. Compressional waves (P-waves) are characterized by particle motion (vibratory) that is parallel to the direction the wave is traveling as shown in Figure 2.4 below.

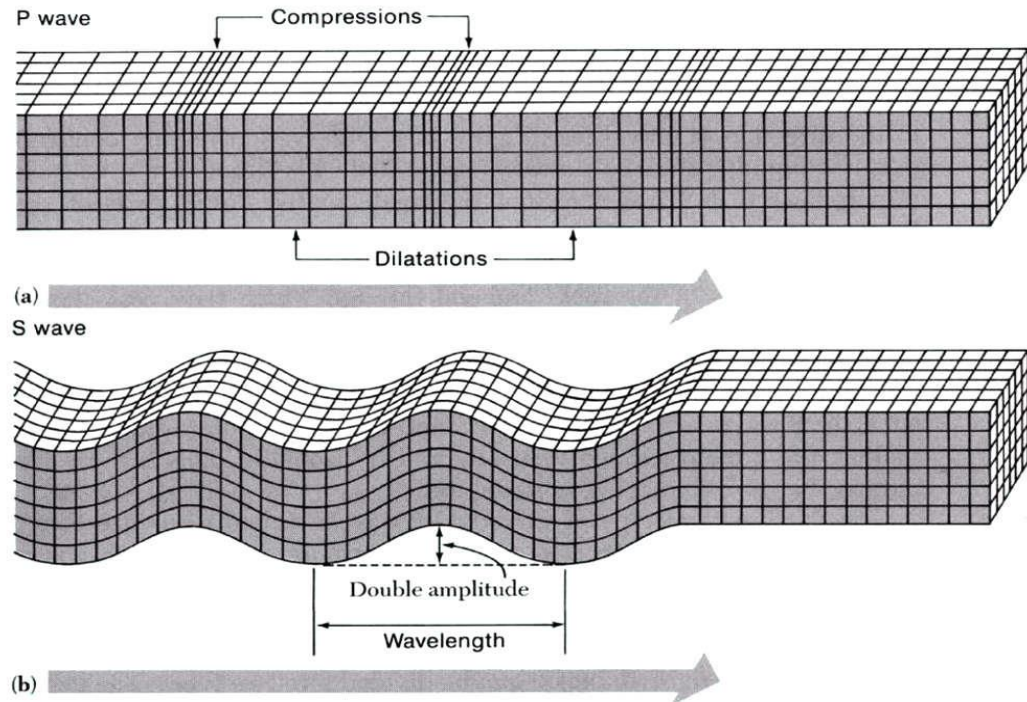


Figure 2.4: How P-waves and S-waves travel through a medium
(<http://geohazardsearthquake.blogspot.com>)

The shear wave or S-wave is characterized by particle motion (vibratory) that is perpendicular to the direction the wave is propagating as shown in the Figure 2.4 above.

In a homogeneous environment, the velocity of a body wave can be expressed by the general equation provided below.

$$V = (\text{Relevant Elastic Modulus/Density})^{1/2} \quad (2.3)$$

For P-waves, the material elastic modulus is related to the bulk modulus, K , and shear modulus μ (Equation 2.4). However, for S-waves, the material modulus is only related to the shear modulus μ (Equation 2.5) (Kearey, Brooks and Hill, 2002).

$$V_P = \sqrt{\frac{K + 4\mu/3}{\rho}} \quad (2.4)$$

$$V_S = \beta = \sqrt{\frac{\mu}{\rho}} \quad (2.5)$$

P-waves transmit faster than S-waves, and S-waves do not propagate through liquids or gases (Parasnis, 1997). The direct measurement of P- and S- waves can be used to calculate soil properties such as Poisson's ratio, bulk moduli and shear moduli (Kearey, Brooks and Hill, 2002).

Surface waves, in contrast, travel along free surfaces or along the boundary of dissimilar materials (Kearey, Brooks and Hill, 2002). Surface waves are tied to the surface and diminish as they get farther from the surface. They represent the strongest portion of the signal received during a seismic survey.

(Park et al., 2009) estimated that over 70 percent of the received signal during a given shot is attributed to the arrival of surface waves. For this reason, the reception of surface waves has been thought of as noise or ground roll during the reflection and refraction seismic survey where only body waves are of interest (Parasnis, 1997).

Surface waves are further categorized in two different types (Love waves and Rayleigh waves) based on their modes of propagation and dispersion. Particle motion

associated with Love waves is parallel to the free surface and perpendicular to the direction of the waves, Rayleigh waves move perpendicular to the surface but travel along the wave path (Kearey, Brooks and Hill, 2002). Love waves are a form of polarized shear wave, and are observed in a multilayer media when the shear wave velocity of the top layer is less than that of the lower layer (Parasnis, 1997). They are the fastest surface wave and move the ground from side-to-side and are confined to the surface of the crust. Because their particle motion is always horizontal, Love waves are seldom recorded in seismic surveying where only vertical source and receivers are used (Park et al., 1997).

Particle motion associated with Rayleigh waves, in contrast, is retrograde elliptical. Because it rolls, it moves the ground up and down and side-to-side in the same direction that the wave is moving. Most of the shaking felt from an earthquake is due to the Rayleigh wave, which can be much larger than the other waves. The shape of the Rayleigh waveform is described as a retrograde, elliptical motion (Park and Miller, 1999). The retrograde elliptical motion can be compared to the observable path of a cork present in a gentle wave motion of a pond or lake. Ground roll is Rayleigh-type surface waves generated most effectively in all kinds of surface seismic surveys using vertical seismic sources. More than two thirds of seismic energy generated is imparted to ground roll (Loke, 2000). A block model of how Love waves and Rayleigh waves propagate is shown in Figure 2.5.

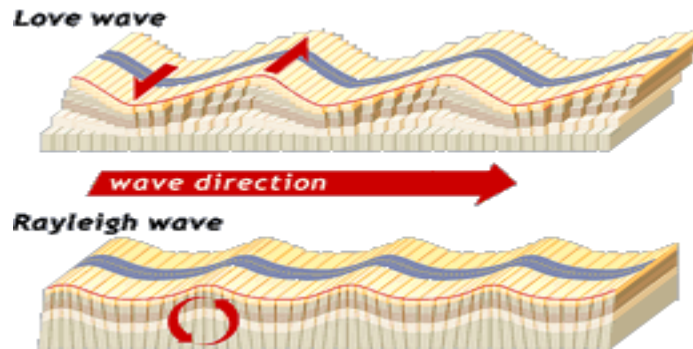


Figure 2.5: Block models of mode of propagation for Love waves and Rayleigh waves (<http://geohazardsearthquake.blogspot.com>)

Rayleigh waves are used for MASW, ReMi and SASW surveying. Therefore, herein the focus is on Rayleigh wave velocity.

2.2.2 Rayleigh Waves Velocity. Rayleigh waves are dispersive in nature (different frequencies travel with different phase velocities). The highest useable Rayleigh wave frequency (geotechnical purposes) recorded involves particle motion within the shallowest depth range (~ 1 wavelength; typically upper few feet) and travels with a velocity that is mostly a function of the average shear wave velocity within that depth range. Intermediate frequencies for Rayleigh waves involve particle motions to intermediate depths (to ~ 1 wavelength) and travel with velocities that are a function of the average shear wave velocity over those intermediate depth ranges. Also the lowest useable frequency recorded involves particle motion to greatest depth (1 wavelength) and travels with a velocity that is a function of the shear wave velocity over that depth range. Rayleigh wave velocities are generally assumed to be about 90% of the corresponding shear wave velocities; hence Rayleigh wave phase velocity vs. frequency data can be transformed into depth vs. shear wave velocity data.

In uniform medium, Raleigh wave phase velocities are constant, and can be determined using the formula:

$$V_R^6 - 8\beta^2 V_R^4 + (24 - 16\beta^2 / \alpha^2) \beta^4 V_R^2 + 16(\beta^2 / \alpha^2 - 1) \beta^6 = 0 \quad (2.6)$$

V_R is Rayleigh wave velocity, β is shear-wave velocity, α is compression-wave velocity (Kearey, Brooks and Hill, 2002).

Although the Rayleigh wave phase velocity is a function of both compressional (α) and shear wave (β) velocities, it is much more sensitive to variations in β than variations in α . Hence, for computational purposes and when dealing with Rayleigh waves propagating through soil and rock, a value of Poisson's Ratio is often assumed such that V_R is approximately equal to 0.9β (Equation 2.7).

$$V_R \sim 0.9 \beta \quad (2.7)$$

In non-uniform medium (like typical soils and rock), α and β vary with depth. Hence, Rayleigh wave phase velocities vary with frequency (wavelength and depth extent of particle motion). If we can determine how V_R varies with frequency, we can determine how V_R varies with depth. If we assume that V_R and β are directly related ($V_R \sim 0.9 \beta$), we can also determine how β varies with depth.

2.2.3 Relationship between Shear Waves and Soil/Rock Conditions. The shear wave velocity of a material is very important when predicting the impact earthquake seismic waves will have on the material as it pass through it (Wood, 2009). By knowing the S-wave velocity of a material the shear modulus can be determined using the relationship:

$$\mu = \rho V_s^2 \quad (2.8)$$

Where μ = shear modulus, ρ = mass density, and V_s = shear wave velocity. The shear modulus of a material describes how it will react (in terms of stress-strain behavior) in response to strong ground motion. Hence, shear modulus helps in predicting the vulnerability of a material to an impending earthquake. The equation above helps to calculate small strain shear modulus of a material (μ_{max}), when seismic surface wave methods are used to develop sub-surface V_s profiles at a site. This is due to the small levels of strain induced in the materials during testing. The sub-surface shear modulus profile of a site is used to predict ground motion amplification of earthquake waves along with the possible liquefaction potential of a site (Wood, 2009). Because knowledge of shear wave velocity can provide critical information about how a material will respond to different types of loads (static and dynamic), many methods have been developed to measure this property.

Downhole and crosshole techniques were the earliest methods used to measure in-situ shear wave velocity profiles (Wood, 2009). These two techniques involve drilling(s) to the actual depth needed for testing and they directly measure the V_s by determining the time it takes for shear waves to travel from a known source position (either at the ground surface or in a borehole) to a known receiver position (in a borehole). The downhole method involves drilling of one borehole and placing the source at the ground (mostly a sledge hammer striking a metal plate), while the crosshole method involves drilling more than one borehole, then placing a source in one borehole and a receiver(s) in the other hole(s) (Wood, 2009). In this method, the waves propagate between the boreholes and the source and receivers are both moved to different depths. These methods directly measure the in-situ shear wave velocity and are therefore considered the most accurate methods

for measuring shear-wave velocity (V_s). Although downhole and crosshole methods provide the most accurate V_s of a sub-surface, they are limited by large cost of drilling boreholes and are being replaced by surface wave methods which are faster, cost effective and better alternatives to estimating sub-surface shear wave velocity (V_s) profiles. The earliest surface wave's method used was the steady state Rayleigh waves method followed by Spectral Analysis of Surface Waves method (SASW) (Park et al., 2000). The steady state Rayleigh waves method uses a mechanical vibrator to produce a vertical sinusoidal signal that is measured using a single receiver while SASW uses only two receivers to record ground roll that is usually generated by impact source like a sledge hammer. Both methods are time and labor intensive due to necessity of repeated tests with different field configurations, therefore, Multichannel Analysis of Surface Waves (MASW) method was introduced to mitigate the impending problems of SASW and Steady State method. For the purpose of this research, the focus is on the Multichannel Analysis of Surface Waves (MASW) method.

2.3 MULTICHANNEL ANALYSIS OF SURFACE WAVES METHOD

In a layered medium in which seismic velocity changes with depth, both types of the surface waves have dispersion property that is indicative of elastic moduli of near-surface earth materials: different wavelength has different penetration depth and propagates with different velocity. Short wavelength has shallow penetration and longer one has deeper penetration. The propagation velocity for each wavelength, called phase velocity (Bath, 1973), depends primarily on the shear (S)-wave velocity (V_s) of the medium over the penetration depth and is influenced only slightly by the compressional

(P)-wave velocity, density (ρ), and Poisson's ratio (σ). Therefore, the surface-wave velocity is a good indicator of shear (S)-wave velocity (V_S). It is normally assumed the phase velocity of ground roll is about 92 percent of V_S (Stokoe et al., 1994), and the ratio changes between 0.88 and 0.95 for the entire range of Poisson's ratio (0. - 0.5) (Ewing et al., 1957).

Theoretical values for the phase velocities of different wavelengths can be found by solving the above elastic wave Equation 2.6 with boundary conditions set by the layered model (Loke, 2000).

Therefore, by analyzing the dispersion feature of ground roll represented in recorded seismic data, the near-surface S-wave velocity (V_S) profiles can be constructed and the corresponding shear moduli (μ) are calculated from the relation between the two parameters:

$$v_s = \sqrt{\frac{\mu}{\rho}}, \quad \text{or} \quad \mu = v_s^2 \rho \quad (2.9)$$

ρ represents density of material. Change of density with depth is usually small in comparison to the change in μ and is normally ignored or guessed. With known (or guessed) Poisson's ratio, one can also obtain P-wave velocity (V_P) profile from V_S profile. The entire procedure of generating V_S profile consists of three steps: acquiring ground roll data in the field, processing the data to determine dispersion curve (a plot of frequency vs. phase velocity), and back calculation of the V_S for different depths. The wavefields of horizontally traveling ground roll are recorded by receivers (geophones) laid at the surface with certain spacing dx . Recorded wavefields are then analyzed at

different frequencies (f) for the phase velocities (C_f) based upon the difference (Δt_f) in the arrival times of ground roll at two receivers as

$$C_f = \frac{dx}{\Delta t_f}. \quad (2.10)$$

This analysis produces a set of data (f vs. C_f), the dispersion data, that are in turn passed into next step of analysis, the inversion process. The inversion process back calculates S-wave velocity (V_S) profile from the measured dispersion data. Two different approaches are possible for inversion: forward modeling and least-squares algorithm. The forward modeling involves assuming a V_S profile, and then comparing the theoretical dispersion curve with the empirical (Stokoe et al., 1994). The assumed profile is modified until the two curves match closely. The least-squares algorithm seeks the V_S profile whose dispersion curve matches best with the empirical curve in least-squares sense (Nazarian, 1984; Sanchez-Salinerio et al., 1987; Rix and Leipski, 1991). It is an automated, but computationally intensive method.

2.3.1 Overview. MASW technique was first reported in late 1990s and was developed by Kansas Geological Survey as an improvement to SASW method (Park et al. 1998, 1999, 2001). It makes use of more than two receivers (array of 12 to 48) deployed in a linear pattern at equal spacing attached to a single recording system to detect the higher modes present in the surface waves (Amit Goel and Animesh Das, 2008). The multiple receiver spread allows for data acquisition over a larger area, improves modal separation and provides a means of efficient and continuous data acquisition (Park et al., 2000). The basic field procedures and acquisition parameters are generally the same as those used in conventional common midpoint body-wave reflection surveys. Because of

these commonalities, the MASW method can be applied to reflection or refraction data if low frequency receivers are used and no analog low-cut filter is applied during data acquisition (Park et al., 2001). A typical MASW field setup is shown in Figure 2.6.

Three types of MASW method have been developed at Kansas Geological Survey Agency (KGS) : multi-channel analysis of surface waves using Vibroseis (MASWV), multi-channel analysis of surface waves using impulsive source (MASWI) and multichannel analysis of surface waves using passive source MASWP (Park et al., 1997a). Each type has difference in type of source used and data processing technique to generate dispersion curve. MASWV uses a swept source like Vibroseis (Figure 2.7), MASWI uses an impulsive source like sledge hammer (Figure 2.8) while MASWP uses ambient noise from a passive source especially moving vehicle along a road side (Figure 2.9). The data processing techniques are a time-domain approach for MASWV (Park et al., 1999) and a frequency-domain approach for MASWI and MASWP (Park et al., 1997a). When a combined dispersion curve of an extended frequency range is prepared from analyses of both passive and active surface waves it increases the maximum depth of Vs estimation (Park et al., 2001).

For the purpose of this research, the focus is on the Multichannel Analysis of Surface Waves using an impulsive source.

Multi-Channel Analysis of Surface Waves (MASW)

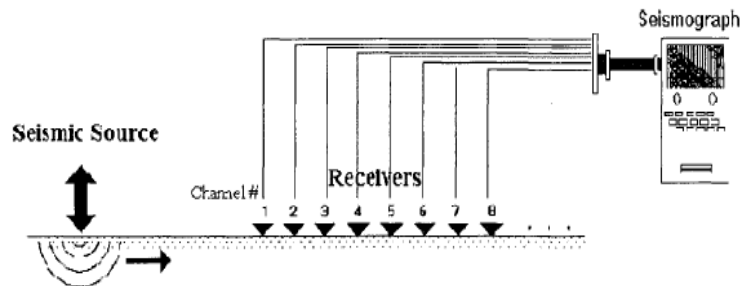


Figure 2.6: Showing typical MASW field setup (Park et al., 1997)

Multi-Channel Analysis of Surface Waves using Vibroseis (MASWV)

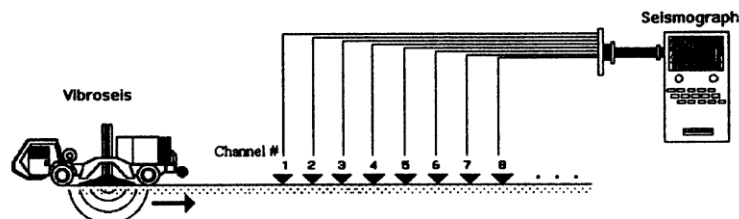


Figure 2.7: Showing typical MASWV field setup (Park et al., 1997)

2.3.2 MASW Using Impulsive Source (MASWI). The method of multi-channel analysis of surface waves using impulsive source (MASWI) is a similar method to multichannel analysis of surface waves using Vibroseis (MASWV) method. Two main differences are, however, in type of the source used and the data processing technique to generate dispersion curve. Instead of a swept source like Vibroseis, an impulsive source like a sledge hammer is used. The data processing technique is a frequency-domain technique, instead of a time-domain technique of CCSAS in MASWV method, similar to the spectral analysis technique used in SASW method. The technique, however, does not

involve calculation of phase difference of recorded surface waves that is the case in SASW method. The calculation of phase difference is prone to generate erroneous results because of the so-called wraparound phenomenon. Instead, the technique calculates phase velocities based upon a spectral correlation parameter (Park et al., 1997a). Therefore, the calculated dispersion curve can have much a greater confidence than that calculated by SASW method. Computational speed of this technique is also faster than those of MASWV and SASW techniques. Because of the type of source used, MASWI method is much a cheaper, simpler, and faster method than MASWV method. However, there can be two main drawbacks in comparison to MASWV method. First, it is very difficult in MASWI method to control the spectral contents of the generated surface waves. In consequence, bandwidth of recorded surface waves is often narrower than that by MASWV method. This narrowness can significantly limit maximum investigation depth and the resolution within the investigable depth range (Park et al., 1999). Second, the data processing technique to generate dispersion curve tends to have slightly less tolerance for the inclusion of body waves than the technique (CCSAS) used in MASWV method. This drawback in data processing, however, is currently being investigated thoroughly and expected to be alleviated soon. Efforts are also being made to alleviate the first drawback of MASWI method by examining various types of impulsive source with various conditions near the impact point.

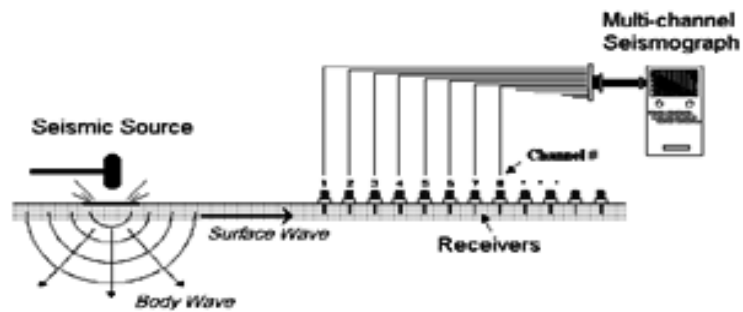


Figure 2.8: Showing typical MASWI field setup (Park et al., 1997)

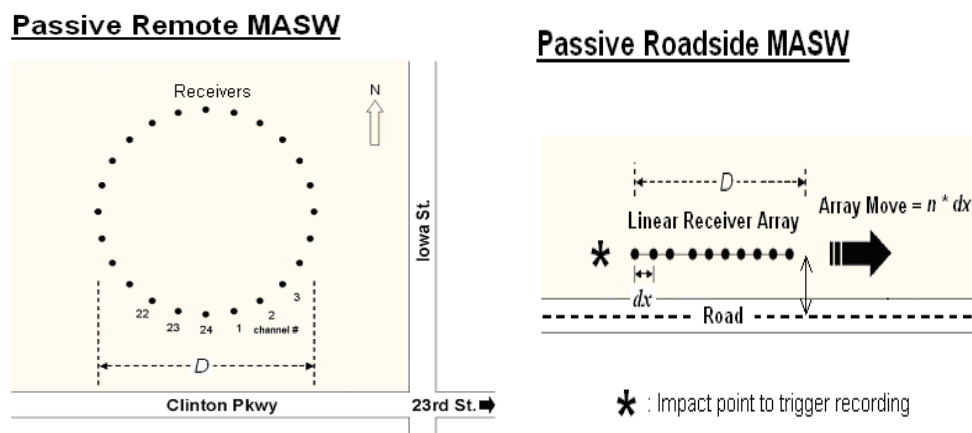


Figure 2.9: Showing different array configurations for the MASWP (Park et al., 1997)

2.4 MASW EQUIPMENT

Equipment required to conduct MASW analyses is comprised of five elements: a seismic source, a triggering device, receivers, transmitting cables and a multichannel seismograph.

2.4.1 Seismic Source. A seismic source is used to transfer energy to the ground for the purposes of inducing seismic wave activity. In practice, a source can be an impact force applied to the ground by a hammer or falling weight, a small scale explosion

detonated within the subsurface, or a mechanical vibratory device (Loke, 2000). A sledgehammer with either a metallic or stiff rubber strike plate provides an inexpensive and easily transferrable impact source. However, for surveys requiring a higher degree of energy transfer, a falling weight may also be used to provide an impact source. Explosive sources such as downhole gun fire or explosives used during quarry operations are less frequently used due to expense and safety; however, given the application explosive sources can provide strong surface wave signals for data acquisition (Loke, 2000). Swept frequency sources provide a signal with a constant frequency. The selection of a seismic source should be based on the signal requirements of the survey, cost and relative safety (Kearey, Brooks and Hill 2002). For most shallow surface evaluations, the use of a sledgehammer and striker plate provides an adequate seismic signal (Park et al., 2009).

2.4.2 Trigger Mechanism. The triggering mechanism is needed to signal the seismography and synchronize the time with the arrival of the transmitted surface wave (Loke, 2000). For impact sources, such as a sledgehammer or drop weight, an open circuit mechanism is attached to the source, which closes at the moment of contact. An example of a simple triggering system attached to a sledgehammer is provided in Figure 2.10. In an ideal situation, the trigger would provide an instantaneous signal marking the initiation of the survey (Milson, 1996). However, in practice it is understood that there is a small lag in between the actual strike event and the time for which the signal is transmitted to the seismography that the strike event has occurred. Lag time can be predetermined for a particular trigger instrument and subsequently programmed into seismograph use during data acquisition (Geometrics Incorporated, 2003).

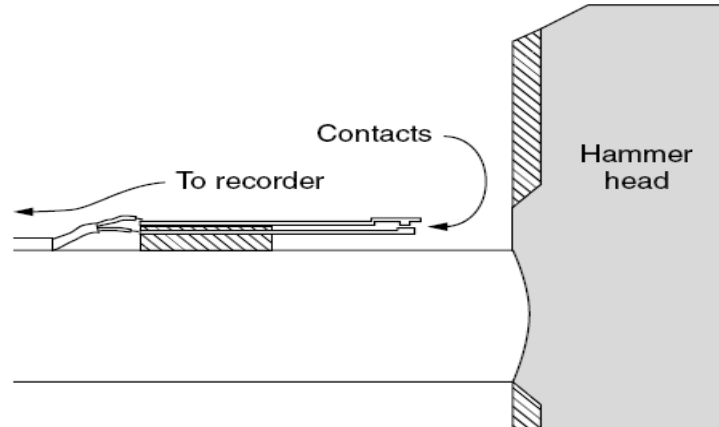


Figure 2.10: Example of Sledgehammer Triggering Device (Milson, 1996)

2.4.3 Geophones. Receivers, or geophones, are electromechanical transducers that convert ground motion into an electrical analog signal (Pelton, 2005). The current, or signal, produced is proportional to the velocity of the oscillating coil system through the internal magnetic core (Milson, 1996). The movement of the internal core is relative to the ground movement below the geophone, as the seismic wave(s) pass the respective receiver (Kearey, Brooks and Hill, 2002). Figure 2.11 provides an example of the configuration of a spike-coupled geophone. Geophones with single, vertical axis of vibration are commonly used to measure incoming signals immediately below the receiver. Other geophones with horizontal or multiple axis capabilities are available, but are not commonly used for MASW applications (United States Corps of Engineers, 1995). For the purpose of this research, 4.5 Hz geophones with steel spikes were used. The geophone must be well coupled with the earth. Steel spikes are typically used for coupling geophones; however, in some applications the use of steel plates has proven to be comparable to the use of steel spikes. Advancements in receiver deployment have led

to towable instruments such as the land streamer, which uses a weighted geophones and cable system equipped with robust steel plates for coupling. For MASW applications, lower frequency receivers (e.g. 2 Hz, 4.5 Hz) provide better performance due to the ability to capture deeper transmitted signals (Park et al., 2009).

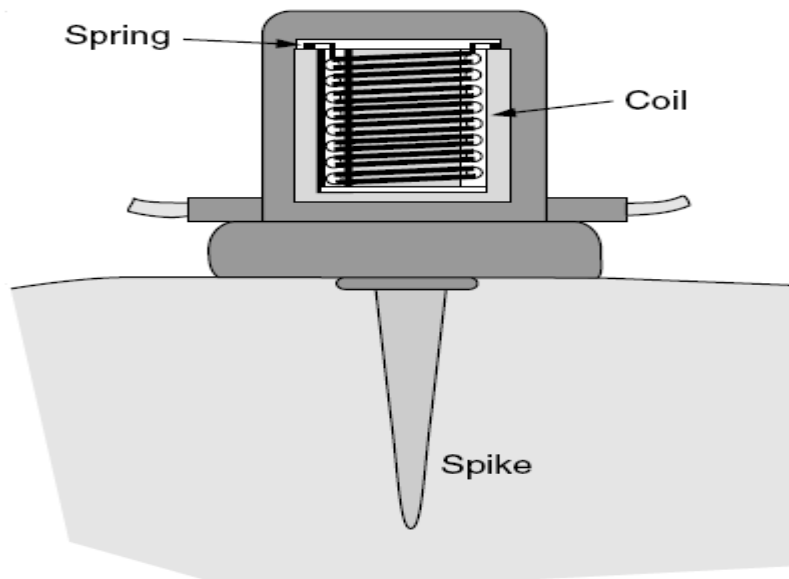


Figure 2.11: Example of spike-coupled Geophone (Milson, 1996)

2.4.4 Geophone Cable. Analog electrical impulses are transmitted from the individual geophones to the seismograph through a cable system. The cable is metallic and transmits the signal with little resistance; however, due to the potential for “cross-talk” between the geophone cable and the trigger switch, consideration should be given during data acquisition to maintaining a sufficient distance between the two elements (Milson, 1996).

2.4.5 Seismograph. Seismographs are used to record and interpret the transmitted signal from the geophone into a discernable trace or shot record (Milson, 1996). Seismographs can range in complexity from simple timing instruments to microcomputers capable of digitizing, storing and displaying received shot records. Multichannel seismographs allow for the acquisition of multiple independent readings. Systems with 24 channels are common in shallow surface investigations; however, deeper applications may utilize a greater number of channels (Milson, 1996). RAS-24 Seistronix seismograph was used for this research because it was available and has all the required specifications.

2.5 MASW FIELD SURVEY SETUP

Field setup for data acquisition is similar to that of the common midpoint reflection survey. Figure 2.13 is an exhibit showing the typical linear layout and the progressive movement of a survey during a profiling application (Park et al., 2009). While Figure 2.12 is array configurations of MASW survey.

Consideration should be given to the geophone interval spacing, as an increased length will improve depth and modal separation but will also increase the amount of spatial averaging of data during processing (Park, 2005).

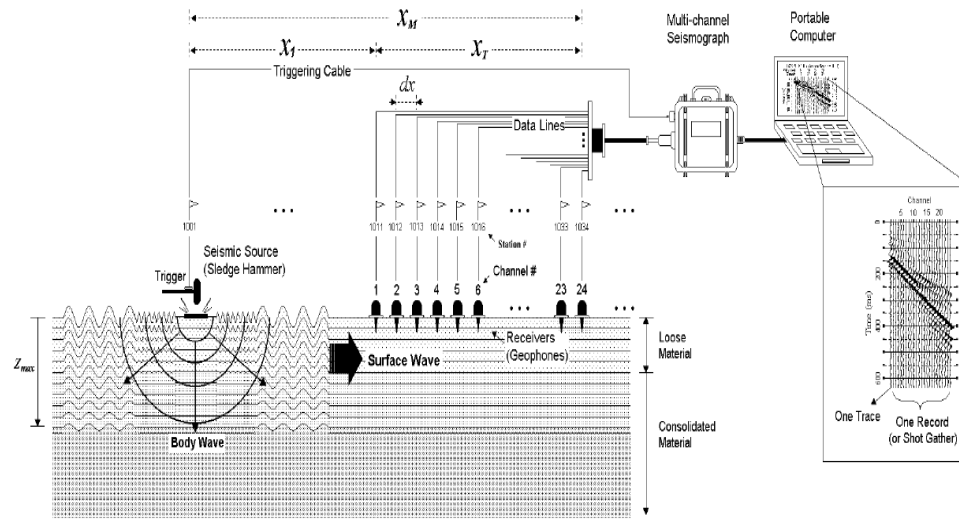


Figure 2.12: Instrumentation of MASW Tomography Survey (Park et al., 2004)

2.5.1 Overviews of MASW Data Acquisition. The survey begins at the instance that the seismic source initiates the wave signal. The triggering system notifies that seismograph when data recording should begin. In order to acquire strong surface signals, it is recommended that sampling intervals range from 0.5 to 1.0 millisecond and recordings times range from 500 milliseconds to 1,000 milliseconds. A variation in required recording times and sampling intervals is generally a function of subsurface conditions (e.g. slower velocities from softer soil conditions). As demonstrated in Figure 2.13, the shot record is created from the trace signals returned to the seismography by the geophones. The individual geophone records are known as traces. After recording the first shot record, the line of geophones is advanced a predetermined interval down the survey line, and preparations are made to collect the next shot (Park et al., 2009). The length of the geophone array shift dictates the resolution of the tomography profile. Shot

Interval distances beyond the spread length increased the required averaging of soil properties and introduced smearing to the imagery. Due to MASW testing requiring a constant receiver spacing, it is very important that the spacing be small enough to prevent far offset effects. The spacing also controls the minimum wavelength that can be measured by the array due to spatial aliasing. Spatial aliasing occurs when receiver pairs measure wavelengths that are less than 2 times the spacing between the receivers. Park et al. (2001) advises that receivers should normally be spaced at 1 meter intervals with a maximum source offset of 100 meters. For the purpose of this research, an active source (20-lbs sledge hammer) was used. The geophone spacings used were 1-ft, 2.5-ft, 5-ft, 7.5-ft and 10-ft, while offset distances chosen were 0-ft, 10-ft, 20-ft, 30-ft, 40-ft and 50-ft.

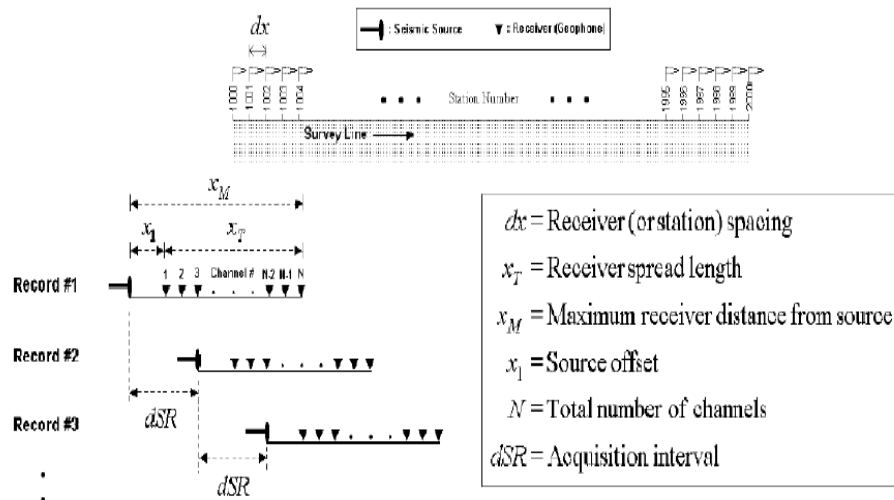


Figure 2.13: Progression of MASW Tomography Survey (Park et al., 2004)

2.5.2 Overviews of Data Processing. Three steps must be performed in order to convert shot record data to estimations of shear wave velocity: initial processing of shot

record for surface wave phase velocity and frequency for development of dispersion curves, identification of fundamental mode, and inversion of the fundamental mode curvature into a representative shear wave profile (Figure 2.14).

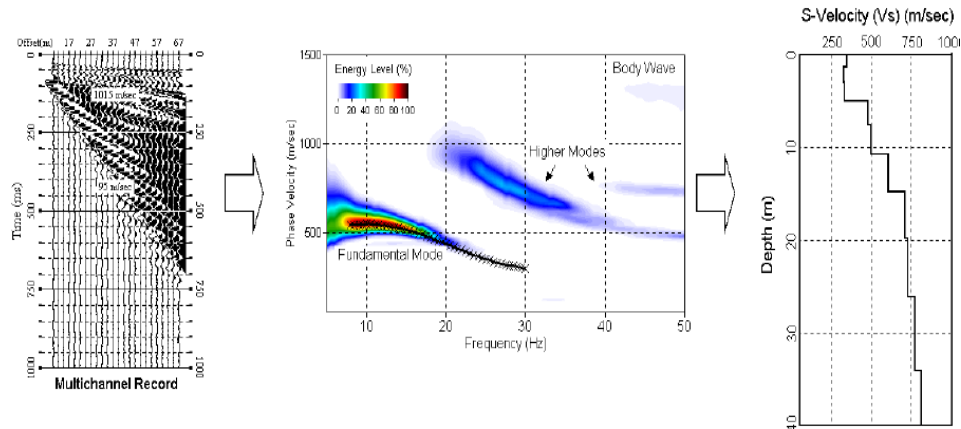


Figure 2.14 Processing Steps to Estimate Shear Wave Velocity (Park et al., 2004)

After field surveying is complete, each collected shot record is processed, highlighting the present surface wave signatures. The raw shot record may contain other wave forms, such as refracted waves, body waves, and sources of cultural noise. However, one of the main advantages of the MASW seismic technique is that the strength of the utilized surface wave is much greater than other wave forms; therefore surface waves are more discernable in the presence of noise. In a record presenting good signal to noise (S/N) ratio, the signal strength of the surface wave should be evident by the linear sloping features of the dispersive wave forms. Surface waves, on an active shot record, are often identified noted by the smooth sloping behavior as the wave travels down the geophone array (Park et al., 2009). This linear slope represents the phase velocity of the particular surface wave, and can be used to transform the shot record data

into a dispersion curve relating phase velocity to wave frequency (Park et al., 2000). Developed analysis software, such as Surfeis, can process shot records and extract dispersion curves through the initial processing sequences (Park et al., 2009). Before the phase velocity and frequency information can be inverted, the fundamental mode of the surface wave must be identified. The dispersion curve is produced by processing the shot record data using specialized algorithms (e.g. frequency-wavenumber spectrum, slowness-frequency transformation, KGS wavefield transformation). The resulting dispersion curve plot relates phase velocity within the frequency domain. As shown in Figure 2.14, the generated image contains the fundamental mode, as well as artifacts from higher modes and other wave forms. The fundamental mode of the dispersion curve is identified by the strongest energy signature in the dispersion curve. At this time, automated selection of dispersion curves is not available, therefore it is still necessary to manually identify the curvature of the fundamental mode. Higher mode contamination of the shot record can hinder the selection of the fundamental mode, and introduce error into the MASW analysis (Park et al., 2009).

The inversion process for MASW is similar to the inversion process used for ERT analysis. A forward modeling algorithm is used to generate an earth model with layers of varying shear wave velocity. The generated model is an attempt to match an actual layered earth model, for which the exhibited shear wave condition could exist. A root mean square analysis is used to evaluate the fitting of the derived curve with the actual curve extracted from the field data. Before the iterative process is ended, the derived model must either satisfy the error tolerance or the number of iterations performed must exceed the number of iterations allowed for convergence. The inverted section represents an

estimate of shear wave velocity with respect to depth (Park et al., 2009). The inverted section represents an averaged condition below the given geophone spread. To assign a spatial coordinate to the reading, it is assumed that the layered earth model is representative of subsurface conditions below the mid span, or mid station location of the geophone array. Downhole measurements have been used to test the validity of the mid station assumption. Results from testing have indicated that the use of MASW, with the mid station assumption, provides a reasonable estimation of profiled shear wave properties when compared against downhole measurements of the same area (Park et al., 2000).

The inversion process for MASW is performed prior to the development the tomography profile. Since a unique shear wave velocity profile is generated for each shot along the survey line, the individual profiles can be interpolated to create a single two-dimensional image representing lateral and vertical variations in shear wave velocity. No additional inversion is required. Interpolation can be performed using an equal weighting or variant weighting system (Park et al., 2009).

3 OVERVIEWS OF ELECTRICAL RESISTIVITY TOMOGRAPHY METHOD

3.1 INTRODUCTION

Just as soil and rock materials have both physical and chemical properties; subsurface materials also present unique electrical characteristics. Surface electrical resistivity surveying is based on the principle that the distribution of electrical potential in the ground around a current-carrying electrode depends on the electrical resistivities and distribution of the surrounding soils and rocks. Mineral grains comprised of soils and rocks are essentially nonconductive, except in some exotic materials such as metallic ores, so the resistivity of soils and rocks is governed primarily by the amount of pore water, its resistivity, and the arrangement of the pores. To the extent that differences of lithology are accompanied by differences of resistivity, resistivity surveys can be useful in detecting bodies of anomalous materials or in estimating the depths of bedrock surfaces. In coarse, granular soils, the groundwater surface is generally marked by an abrupt change in water saturation and thus, by a change of resistivity. In fine-grained soils, however, there may be no such resistivity change coinciding with a piezometric surface.

Generally, since the resistivity of a soil or rock is controlled primarily by the pore water conditions, there are wide ranges in resistivity for any particular soil or rock type, and resistivity values cannot be directly interpreted in terms of soil type or lithology. Commonly, however, zones of distinctive resistivity can be associated with specific soil or rock units on the basis of local field or drill hole information, and resistivity surveys

can be used profitably to extend field investigations into areas with very limited or nonexistent data.

Practitioners in geologic, environmental and engineering fields utilize electrical resistivity soundings and tomography to map fluctuations in conductive behavior (Milson, 1996). Recent advancements in equipment and software have automated both data acquisition and processing, making electrical resistivity one of the most versatile methods for both the practicing geophysicist and engineering professionals (Steeple, 2001).

3.2 BASIC THEORY

The fundamental principle behind collection and interpretation of electrical resistivity measurements originates in the electrical physical theory of Ohm's Law. Ohm's Law, Equation 2.10, states that the product of the electrical current, I , through a conductor and the resistance of the conductor, R , for which the current passes, is equivalent to the potential difference, V , across the conductor.

$$V = IR \tag{2.10}$$

This relationship is best represented by envisioning current passing through a thin wire. The expounded application of the Ohm's Law has made this relationship a capstone concept in the study of electrical theory (Gibson and George, 2003). Units for electrical potential, current, and resistance are volts, amperes, and ohms, respectively.

As suggested, the conductor element can tangibly be described as a wire element. The resistance of the wire is related to both the geometric shape and material attributes of the wire (Milson, 1996). The geometry of the wire is typically cylindrical, therefore

possessing a length and cross-sectional area, and is made of a conductive material. The total resistance of the wire element, R , is the product of the material resistivity, ρ , and the ratio of the wire length and cross-sectional area.

$$R = \rho (L/A) \quad 2.11$$

Considering the physical relationship between the geometry of the conductor and the material property, Equation 2.11 can be manipulated to determine the material resistivity of the conductor element.

$$\rho = R (L/A) \quad 2.12$$

This form states that the units for resistivity are dependent on the volume of space for which the current travels. Typical units for resistivity, ρ , include ohm-meter and ohm-centimeter (Gibson and George, 2003).

In similar context, the measurement of potential difference can be related to the dissipation of electrical current within an infinite, homogenous half-space. In this scenario, the application of an electrical current is travels in radial fashion out from the point of origin. During the current application, the resistance at any location away from the point of origin within the homogeneous mass can be found by determining the radius from the point of origin and the surface area of the respective hemispherical equipotential surface. Relating this model to the original wire example, Equation 2.11 can be rewritten using the radius, r , as the distance for which the current travels and the surface area of the resulting equipotential surface, $2\pi r^2$. Equation 2.13 describes the system resistance at any point away from the point source, within the homogeneous mass.

$$R = \rho(r/2\pi r^2) = (\rho/2\pi r) \quad 2.13$$

Using the resistance term from the aforementioned homogeneous earth model, Equation 2.14 relates the resistance of the earthen model to Ohm's Law.

$$U = \rho \frac{I}{2\pi r}, \quad 2.14$$

U = potential, in V , ρ = resistivity of the medium, r = distance from the electrode

Likewise, the potential difference between any two points within the homogeneous mass would be the difference between the two equipotential surfaces, as expressed in Equation 2.15 (Gibson and George, 2003).

$$U = \frac{\rho I}{2\pi r_A} - \frac{\rho I}{2\pi r_B} = \frac{\rho I}{2\pi} \left[\frac{1}{r_A} - \frac{1}{r_B} \right], \quad 2.15$$

Where r_A and r_B = distances from the point to electrodes A and B

$$\text{Therefore, } \rho = (2\pi U/I) [1/[(1/r_A)-(1/r_B)]] \quad 2.16$$

Equation 2.16 relates the applied current, I , and measured potential difference, V , to a constant value which accounts for spatial considerations, or the way in which the reading was acquired. This model and concept of equipotential surfaces and means of measuring potential differences between various surfaces is fundamental to the interpretation of collected field data (Gibson and George, 2003).

Figure 3.1 illustrates the electric field around the two electrodes in terms of equipotential and current lines. The equipotential represent imagery shells, or bowls, surrounding the current electrodes, and on any one of which the electrical potential is everywhere equal. The current lines represent a sampling of the infinitely many paths followed by the current, paths that are defined by the condition that they must be everywhere normal to the equipotential surfaces.

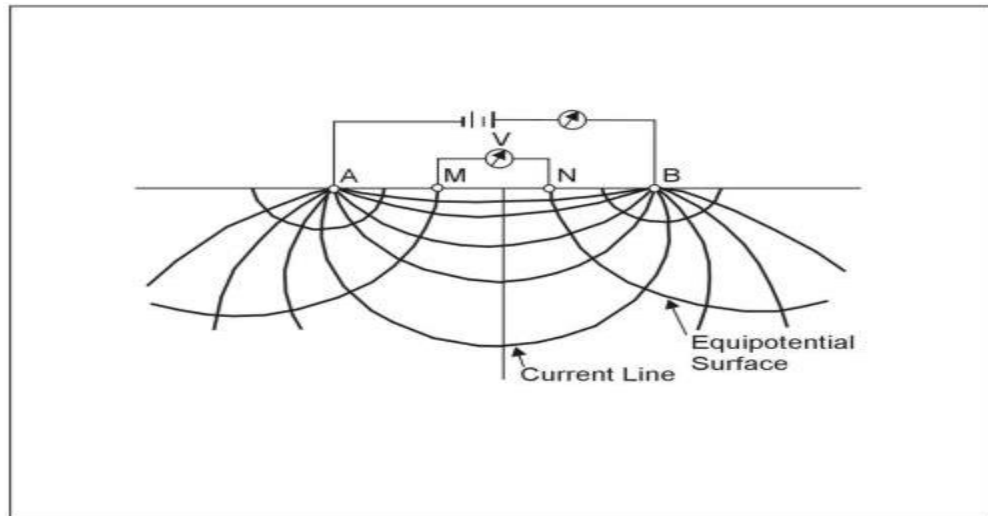


Figure 3.1: Equipotential and current lines for a pair of current electrodes A and B on a homogeneous half-space.

In addition to current electrodes A and B, Figure 3.1 shows a pair of electrodes M and N, which carry no current, but between which the potential difference V may be measured. Following the previous equation, the potential difference V may be written

$$V = U_M - U_N = \frac{\rho I}{2\pi} \left[\frac{1}{AM} - \frac{1}{BM} + \frac{1}{BN} - \frac{1}{AN} \right], \quad 2.17$$

Where U_M and U_N = potentials at M and N ,

AM = distance between electrodes A and M , etc.

These distances are always the actual distances between the respective electrodes, whether or not they lie on a line. The quantity inside the brackets S is a function only of the various electrode spacing. The quantity is denoted $1/K$, which allows rewriting the equation as:

$$V = \frac{\rho I}{2\pi} \frac{1}{K}, \quad 2.18$$

Where K = array geometric factor.

Equation 2.18 can be solved for ρ to obtain:

$$\rho = 2\pi K \frac{V}{I}, \quad 2.19$$

The resistivity of the medium can be found from measured values of V , I , and K , the geometric factor. K is a function only of the geometry of the electrode arrangement.

In a homogenous media, the measured resistivity will be equivalent to the true value of resistivity at a given location with the media. However, the occurrence of a homogenous condition is rare, if not non-existent in practice. In order to account for the inherent heterogeneity of the earth, a collected reading is considered an apparent resistivity measurement. Apparent resistivity is the resistivity of a theoretical, homogeneous half-space which complements the measured current and potential difference for a particular measurement scheme (United States Corps of Engineers, 2001). Essentially, the apparent resistivity value is an average reading of the energized soil mass engaged during the measurement. Wherever these measurements are made over a real heterogeneous earth, as distinguished from the fictitious homogeneous half-space, the symbol ρ is replaced by ρ_a for apparent resistivity. The resistivity surveying problem is reduced to its essence, the use of apparent resistivity values from field observations at various locations and with various electrode configurations to estimate the true resistivities of the several earth materials present at a site and to locate their boundaries spatially below the surface of the site. An electrode array with constant spacing is used to investigate lateral changes in apparent resistivity reflecting lateral geologic variability or localized anomalous features. To investigate changes in resistivity with depth, the size of the electrode array is varied. The apparent resistivity is affected by material at increasingly greater depths (hence larger volume) as the electrode spacing is increased.

Because of this effect, a plot of apparent resistivity against electrode spacing can be used to indicate vertical variations in resistivity.

The geometric coefficient, K , varies with array types. The spacing and layout of current and potential electrodes impacts the induced equipotential fields generated within the earthen mass (refer to Figure 3.2 for Wenner, Schlumberger, and Dipole-Dipole arrays). Referencing Equation 2.16, the geometric factor for a general four probe system can be derived (Gibson and George, 2003).

3.3 ARRAYS

Theoretically, soil resistivity could be measured by using a single current source and receiver element. In practice, this is not feasible due to the contact resistance between the earth and the electrode pair. To overcome this phenomenon, four electrodes are used for measurement; two electrodes providing current to the earth and two electrodes for measuring potential difference within the earth (Milson, 1996). Current electrodes are identified as C1 and C2 (or A and B), and potential electrodes are identified as P1 and P2 or (M and N) (Loke, 2000).

The types of electrode arrays that are most commonly used are Schlumberger, Wenner, and dipole-dipole. There are other electrode configurations that are used experimentally or for non-geotechnical problems or are not in wide popularity today. Some of these include the Lee, half-Schlumberger, polar dipole, dipole -dipole, and gradient arrays. In any case, the geometric factor for any four-electrode system can be found from Equation 2.17 and can be developed for more complicated systems by using the rule illustrated by Equation 2.15 (United States Environmental Protection Agency,

2011). It can also be seen from Equation 2.19 that the current and potential electrodes can be interchanged without affecting the results; this property is called reciprocity (Milson, 1996). For the purpose of this research, the discussion will focus on the dipole-dipole array which was used for this research.

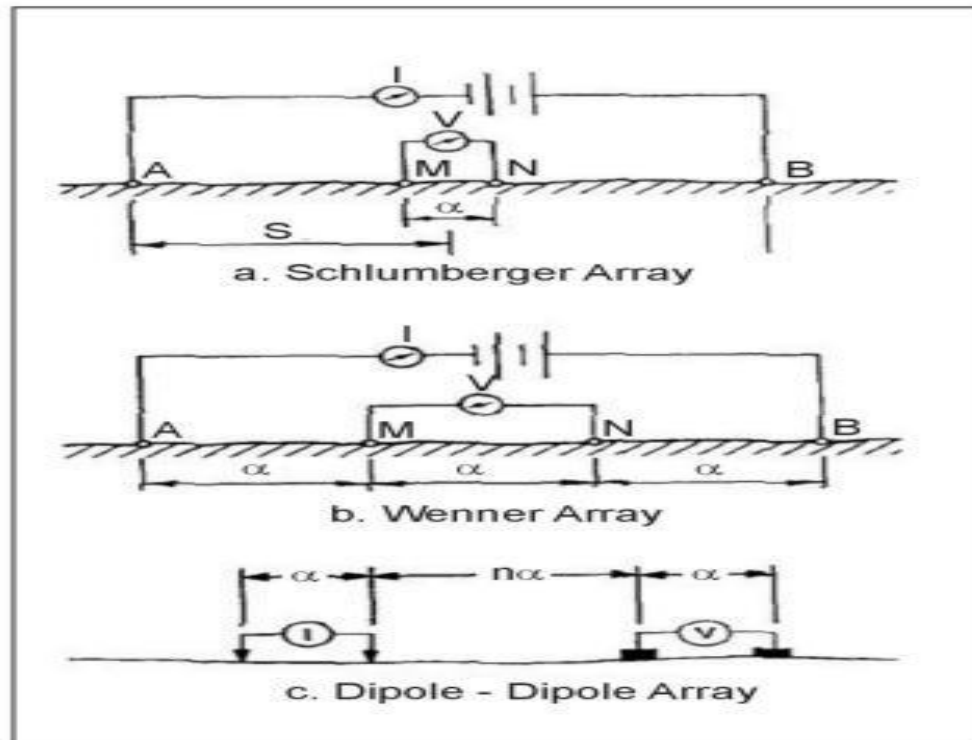


Figure 3.2: Electrode array configurations for resistivity measurements (United States Environmental Protection Agency, 2011).

Unlike the Wenner and Schlumberger arrays, the configuration of the dipole-dipole array does not place the potential electrode pair inside the current electrode pair. Current and potential electrode pairs have common interior spacing, and separated by a distance ten times the interior spacing of the electrode pair. The dipole-dipole array is commonly used for performing tomography surveying due to the array's ability to resolve

lateral variations. In comparison to the Wenner and Schlumberger arrays, the dipole-dipole array has a weaker signal and is more susceptible to the effects of ambient or cultural noise (United States Environmental Protection Agency, 2011).

If the separation between both pairs of electrodes is the same a , and the separation between the centers of the dipoles is restricted to $a(n+1)$, the apparent resistivity is given by:

$$\rho_a = \pi a n(n+1)(n+2) \frac{V}{I}, \quad 2.20$$

3.4 RELATIONSHIP BETWEEN RESISTIVITY AND SOIL/ROCK CONDITION

Electrical resistivity testing represents a broad category of geophysical testing, including measurements of spontaneous potential, induced polarization, and apparent resistivity measurements (Loke, 2000). Spontaneous potential (SP) is a method designed to measure variations in conductive behavior occurring without introducing an auxiliary current source. Induced polarization is a method measuring the time-rate decay of polarizing effects resulting from the induced current (Loke, 2000). This method is effective in delineating contaminant plumes and mineral ore bodies, which often present with unique decay signatures when compared against other ambient conditions (Gibson and George, 2003). Among the electrical resistivity testing methods, apparent resistivity measurement is the most utilized method for engineering applications (Loke, 2000). Apparent resistivity can be analyzed in either by vertical sounding, two dimensional profile, three dimensional models, or time variant analysis (Gibson and George, 2003).

3.4.1 Overviews of Two-Dimensional Electrical Resistivity Surveying. Two-dimensional surveying, or electrical resistivity tomography (ERT) surveying, is performed by measuring fluctuations in both the vertical and lateral planes. The 2D profiles take the VES techniques and integrate them into a 2D plane transecting the desired target area (United States Environmental Protection Agency, 2011). The most common configuration of the 2D survey employs dipole-dipole electrode configurations. During this type of survey, readings are assumed to lie within a single, vertical plane. Two dimensional surveys are generally performed at the surface; however, readings may also be collected using downhole or surface to borehole methods of measurement. For surface measurements, the dipole-dipole array is preferred due to the array's sensitivity in both lateral and vertical directions, as well as the versatility of the array setup and progression when used with multi-channel equipment transmitters and receivers (Advanced Geosciences, Incorporated, 2009).

However, alternative resistivity measurements can be made using towed surface or marine arrays, which would maintain the above configuration, and build up the 2D image by moving the entire measurement array for each series of measurements. In both cases the resulting image plots the apparent resistivity with depth, which is then contoured (commonly krigged) using a commercially available program. The color contoured image displays the distribution of apparent resistivity values and associated gradients within the area of interest. In order to convert the apparent resistivity data to true resistivity, the data are inverted.

Figure 3.3 shows a transmitting current dipole (I) followed by a series of potential dipoles (V) which measure the resulting voltage gradient at each station along the line.

Subsequent measurements are completed by sequentially moving the current dipole down the line

2 Dimensional Resistivity Profiling: Dipole-dipole Array

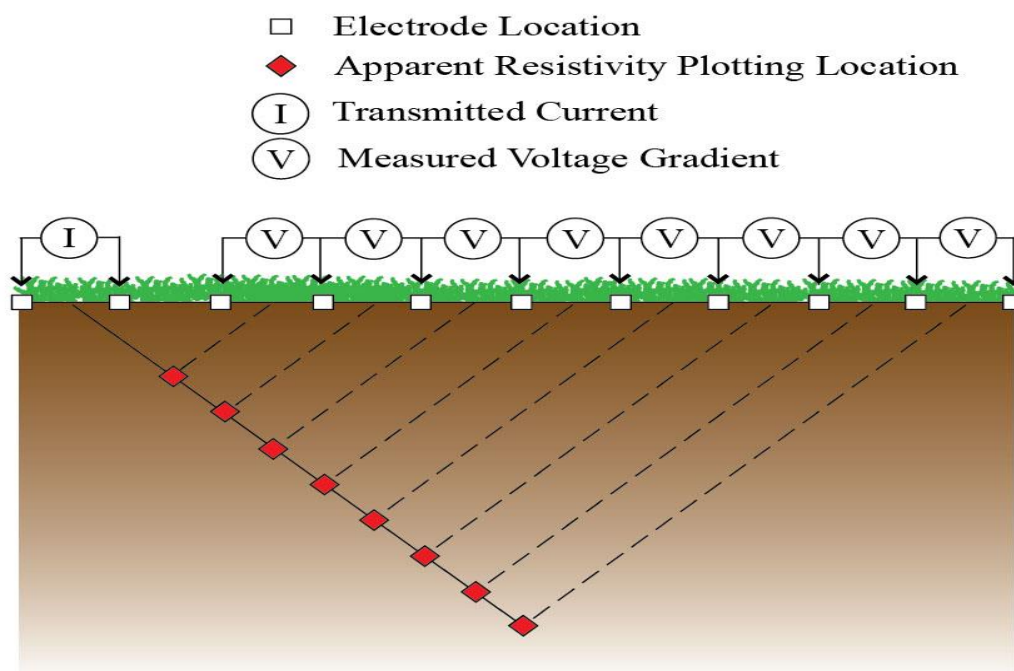


Figure 3.3: Two-dimensional measurement configurations for a dipole-dipole resistivity profile, pseudosection plotting location indicated in red (United States Environmental Protection Agency, 20011)

Figure 3.4 displays an example of a measured apparent resistivity pseudosection at the top, followed by a calculated apparent resistivity pseudosection, and resulting in the inverted true resistivity 2D section. The numbers presented at the bottom of the inverted section display goodness of fit criteria used to assess the accuracy of the calculated resistivity model. Finally note that the surface elevations have been included in the final model, accounting for variations in measurement geometry due to changing topography.

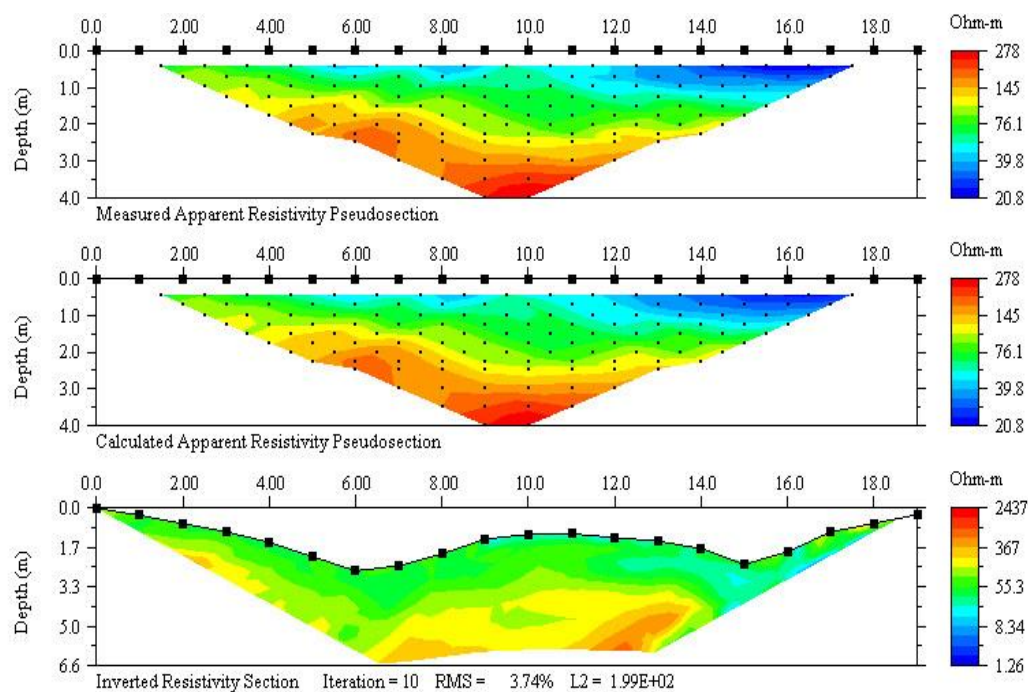


Figure 3.4: Examples of measured apparent resistivity, calculated apparent resistivity, and inverted resistivity (Advanced Geosciences, Incorporated, 2009).

3.4.2 Three-Dimensional Electrical Resistivity Surveying (3-D). During a three-dimensional survey, measurements of potential difference are made in all three spatial coordinate planes. This allows for the analysis of a target volume, as opposed to planar section. Three-dimensional surveys may either be performed along the surface, using crosshole methods, or using surface to borehole measurements. Analytical software now allows for the compilation of multiple two-dimensional survey data, into a three-dimensional representation (Advanced Geosciences Incorporated, 2008). For this research Voxler software was used to compile multiple 2-D survey data into a 3-D model.

3.5 FIELD EQUIPMENT

The basic setup required for field measurements includes a transmitter, receiver, conductive cables, a set of electrodes and a power source (United States Corps of Engineers, 1995).

3.5.1 Transmitter/Receiver. The function of the transmitter is to apply and regulate a known current through the instrumentation, to the earth. To acquire the desired survey penetration and resolution, it is important that the chosen transmitter is capable of emitting ample current through the system. Previous instrumentation required manual current adjustments until applicable readings were made. However, with advancements in technology, newer transmitters are capable of self-regulating current flow to promote the best possible signal for data acquisition. In addition, various instruments are now capable of conveying larger currents, also improving signal strength and resolution. Advanced Geosciences, Incorporated (AGI) produces three different automated units, with maximum current outputs ranging from 500 milliamps to 2,000 milliamps. The most recent development by AGI is a system capable of transmitting a current up to 27 amps (Advanced Geosciences, Incorporated, 2009).

As the transmitter applies a known current, a receiver is needed to measure the resulting potential reading. Newer instrument, equipped with digital processing capabilities, are capable of sending the required current, as well as measuring and receiving the respective potential difference measurement. The sensitivity of the receiver should be established prior to initiating a survey to ensure that goals of the survey are met (Advanced Geosciences Incorporated, 2008). Single channel transmitters/receivers are only capable of collecting one reading at a time. Although single channel instruments are

still in use for VES surveys, two and three dimensional surveys are optimized by multi-channel systems allowing for the acquisition of multiple readings in a single current output (Advanced Geosciences Incorporated, 2008).

3.5.2 Cables. Metallic cables are used to convey current from the transmitter and to return measurements of difference to the receiver. The use of highly conductive metallic material, such as copper, helps minimize losses during data acquisition. Depending on the transmitter/receiver system utilized, the cables are either composed of a single wire strand, or a core housing multiple strands accommodating each of the available channels. Cables are needed for connecting the transmitter/receiver with the potential electrodes (Advanced Geosciences Incorporated, 2008).

3.5.3 Current and Potential Electrodes. Electrodes are used by the transmitter to transfer current to the subgrade, and by the receiver to detect fluctuations in electrical potential. For general use, steel, copper or bronze stakes are common. For applications requiring refined measurements, readings taken in noisy environments or areas with high contact resistance, using electrodes with of ceramic components emitting a metallic aqueous solution, such as copper sulfate, is a viable alternative (Loke, 2000). Sufficient bedding of electrodes is required in order to couple the resistivity setup with the earth. As noted, surface conditions with high contact resistance can be overcome by using ceramic electrodes with a metallic aqueous solution, or, if using metallic stakes, by placing a saline solution around the base of the electrode (Advanced Geosciences Incorporated, 2008).

When using a direct current for testing purposes, there is a potential that the charges on the exterior of the electrode will take on a common charge over the surface of

the electrode, effectively polarizing the electrode, if the current is applied in one direction for an extended period of time. In order to prevent polarization, most modern instruments routinely reverse signals to reverse potential charge buildups (United States Corps of Engineers, 1995).

3.5.4 Power Source. The transmitter requires a power source in order to pull a current for the data acquisition system. Required power sources vary by instrument, and range from internal rechargeable batteries to external generator power sources. For newer instruments, due to the low power emission required and short duration of discharge, dry cell batteries can be used for this application. Dry cell batteries are preferred because the ability to drain and recharge the battery without damaging the core (Advanced Geosciences Incorporated, 2008). A wet cell battery was used in this survey because of its availability and durability

3.6 OVERVIEW OF ERT DATA ACQUISITION

Newer instruments are equipped with multiple channels, which allows for multiple electrodes to be engaged and measurement to be taken through each channel. For instance, the SuperSting R8 resistivity meter, produced by Advanced Geosciences, Incorporated, is equipped with eight channels. Therefore, for each current injection, the system engages nine electrodes to collect eight different potential difference measurements (Advanced Geosciences, Incorporated, 2006).

Unlike the single channel transmitter, multiple channel equipment has to receive instruction on the proper triggering sequence of electrodes. This information can either be programmed directly into the instrument through manual entry, or indirectly by uploading

coded command file (Loke, 2000). The sequencing information considers the array style and information pertaining to the electrode locations or electrode address during each measuring sequence. There are no theoretical limits to the depth of penetration. However, as the electrode spacing increases signal strength decreases. At a certain electrode separation distance, the signal strength is too low to provide reliable measurements of potential difference. Practical limits should be instilled considering the signal strength of the particular array type and equipment capabilities. (Advanced Geosciences Incorporated, 2008) suggested that when considering depth of penetration for tomography applications, practitioners can generally assume that the depth of penetration is approximately 15 to 25 percent of the length of the electrode spread. Survey resolution is also related to electrode spacing. Current practices suggest that the electrode spacing not be greater than twice the size of the object or feature to be imaged. The design of the survey (i.e. Survey run length, electrode spacing, and array type) directly impacts the depth of penetration and resolution (Advanced Geosciences Incorporated, 2008).

It is not always possible or practical to image a survey line or area in one deployment of electrodes. To continue a survey after completion of the initial data collection, electrodes may be configured to collect additional data along a common survey line or area, using roll-along survey techniques (Loke, 2000). In this research, 5-ft electrode spacing was used. The metal stakes are made of steel and SuperSting R8 was used to measure the resistivities.

3.7 DATA PROCESSING AND INTERPRETATION

Field measurements must be converted into a visual representation for analysis purposes. Referring to Equation 2.18, calculation of apparent resistivity requires a geometric factor. Measurements taken from the field provide readings of induced current and respective potential difference, so by coordinating field data with respective electrode coordinates and known array type, the geometric factor can be determined and apparent resistivity is calculated. In addition, recorded field measurements are assigned a coordinate location, which correlate to the array type used and electrode spacing at the time of the potential difference reading. The mapping of apparent resistivity values creates a profile termed a pseudosection (Milson 1996, Loke 2000, Gibson and George 2003). Pseudosections (Figure 3.5) provide a crude representation of the resistive environment surveyed, and attempting an interpretation from a pseudosection can be misleading (Zonge, Wynn and Urquatt, 2005).

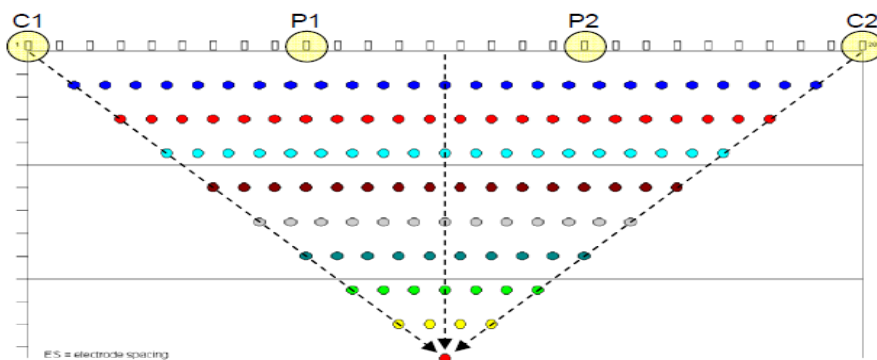


Figure 3.5: Example of Developed Pseudosection Model Using a Wenner Array and 28 Electrodes (Loke, 2000)

Although the “true” point measurements is unattainable using surface survey methods, apparent values can be effectively used to estimate “true” subsurface conditions (Loke, 2000). Apparent resistivity pseudosections provide the necessary data to complete an iterative inversion process. The purpose of the inversion is to produce a matching or representative earth model which would produce a like psuedosection. Iterations continue until the modeled psuedosection approaches convergence with the measured psuedosection. Currently there are no means of directly correlating apparent resistivity measurements to an earthen model (Zonge, Wynn and Urquatt, 2005).

Figure 3.6 provides a generalized flow chart demonstrating the typical processes required to complete the inversion process. The convergence criterion is usually a predetermined tolerance for calculated error between the measured and modeled resistivity. Statistical analysis of data (e.g. root mean square error analysis, L2 normalization) is used to gauge the refinement of the final model. Smoothing algorithms are also used to eliminate or lessening the impact of data points not conforming to the trends of the model (Advanced Geosciences, Incorporated 2009, Zonge et al., 2005). The inversion process is best performed using numerical analysis software due to the quantity of data involved and iterative processes. Software packages such as RES2DINV, RES3DINV and EarthImager 1D, 2D, and 3D are examples of products available for inversion processing and inversion (Advanced Geosciences Incorporated, 2008, 2009).

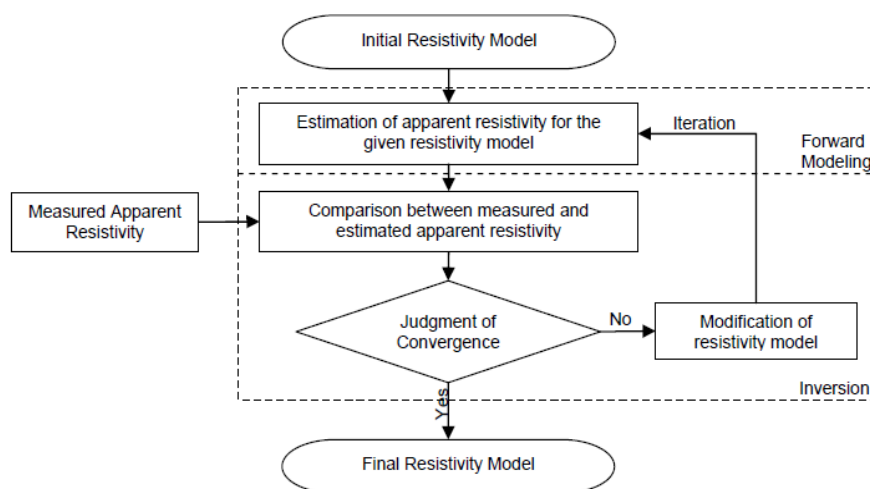


Figure 3.6: Flow Chart of Resistivity Inversion Processing (Society of Exploration Geophysicist of Japan, 2004)

In survey situations with significant variations in terrain, estimated resistivity measurements may mask subsurface features if site topography is not considered (Zonge et al., 2005).

Therefore, site conditions should be considered; excessive dip of subsurface strata along the survey line (more than about 10 percent), unfavorable topography, or known high lateral variability in soil or rock properties may be reasons to reject field data as unsuitable for interpretation in terms of simple vertical variation of resistivity. But the effects of topographic changes on generated tomography images can be resolved during the inversion process (Advanced Geosciences Incorporated, 2008).

4 RESEARCH METHODS

4.1 OVERVIEW

This section presents the methodology behind the site selection, data collection setup, and data collection procedures used in this acquisition and processing. The focus will be on the MASW and Electrical Resistivity Tomography methods, and will provide a guide to those collecting these types of data in the similar environment.

4.2 SITE LOCATION

A single site was chosen for this research. It is located in Newburg, Missouri Area. This site was chosen due to its proximity to the university, and it is flat (no complex topography) and has easy accessibility. Newburg map in Figure 4.1 shows that study area is located close to the Corn Creek Road within the Mark Twain National Forest area in south west of Newburg.

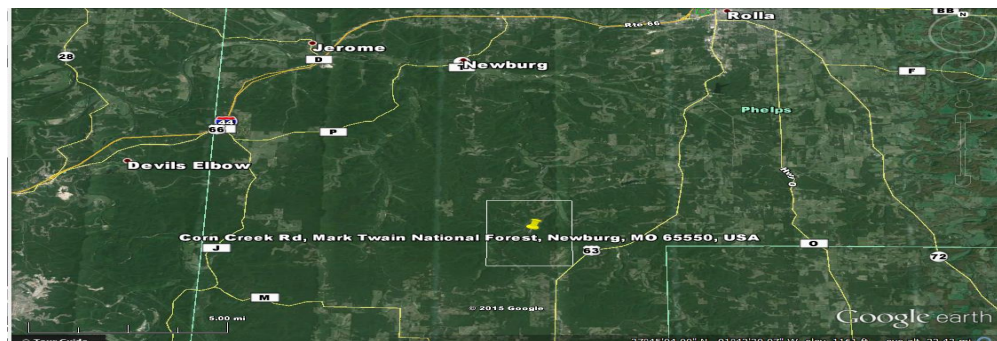


Figure 4.1: Newburg map showing the study area located within Mark Twain National Forest (Courtesy of Google Earth).

The Corn Creek Road is located at the southwest corner of high way 63 and southeast of Interstate 44 (Figure 4.2.)

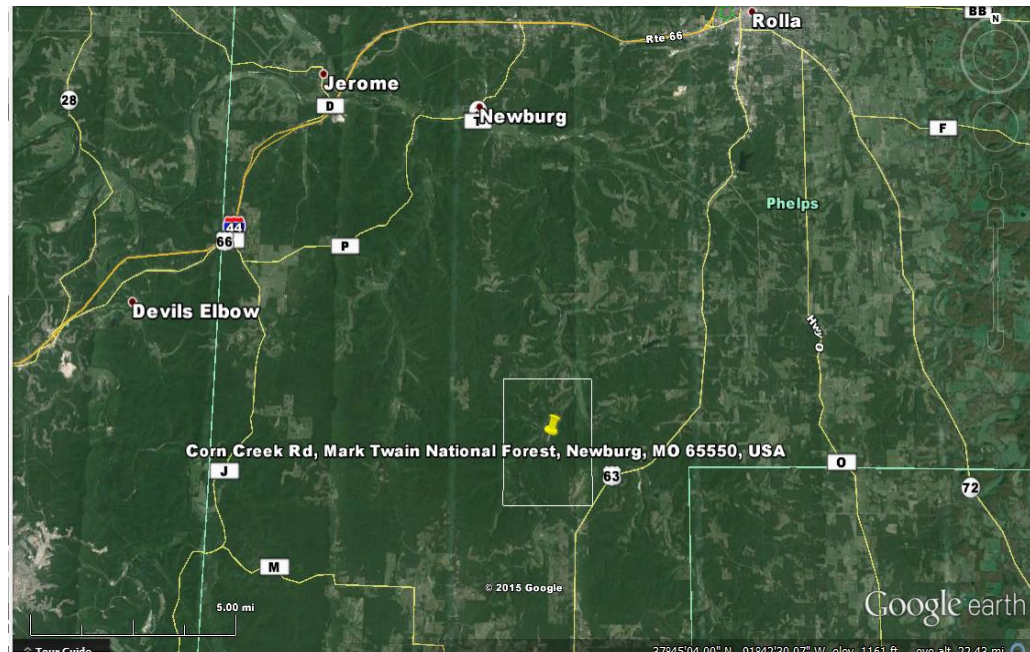
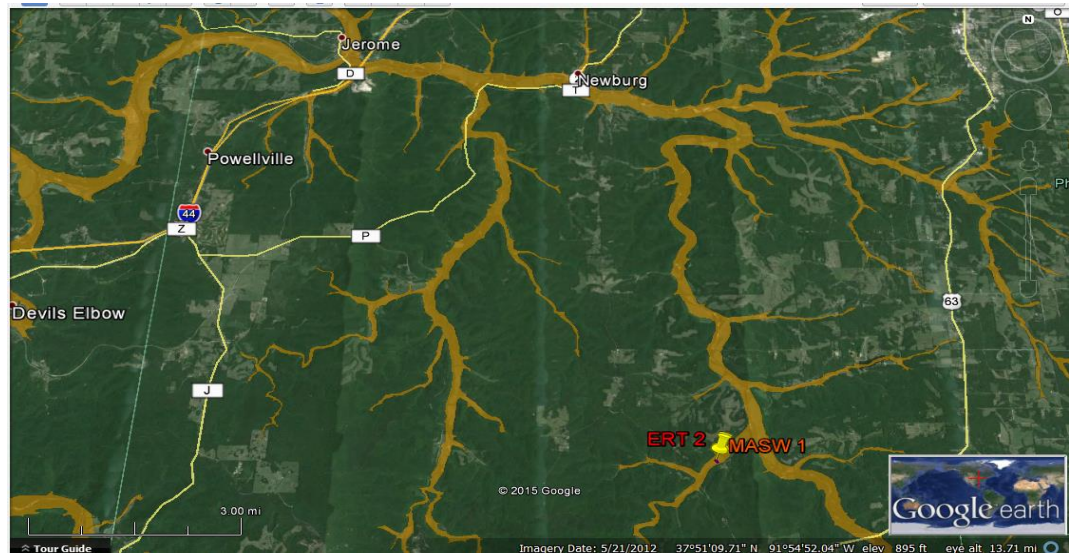


Figure 4.2: Showing the location of Corn Creek Road (courtesy of Google Earth)

The exact location of the site is given by coordinates: 37°48'31.00" N and 91°52'05.70" W and elevation of 955-ft above the sea level.

The site geology consists of alluvium and residuum deposits which depicts an old river channel. Alluvium and Surficial geology map of the area shows that the site is within a flood plain (Figure 4.3).



(a) Broader view



(b) Enlarged view

Figure 4.3: Alluvium and Surficial geology map of the Newburg area (courtesy of Google Earth)

The alluvium deposits are predominately loose soil (regolith) while the K-residuum is comprised of Cherty sandy clay and sandy clay, reddish brown to brown, 1-10-ft. thick, developed as residuum from sandy dolomite, dolomite, sandstone and chert. Residuum is stony clay and clayey sand containing relict layers of sandstone and chert, 5-10-ft. thick, generally covered by coarse cherty colluvium on hillslopes and a thin loess mantle on uplands (<http://dnr.mo.gov/GIS/GEOLOGY.SURFICIAL.XML>). Figure 4.4 show the bedrock, geologic map and geologic unit of the study area.

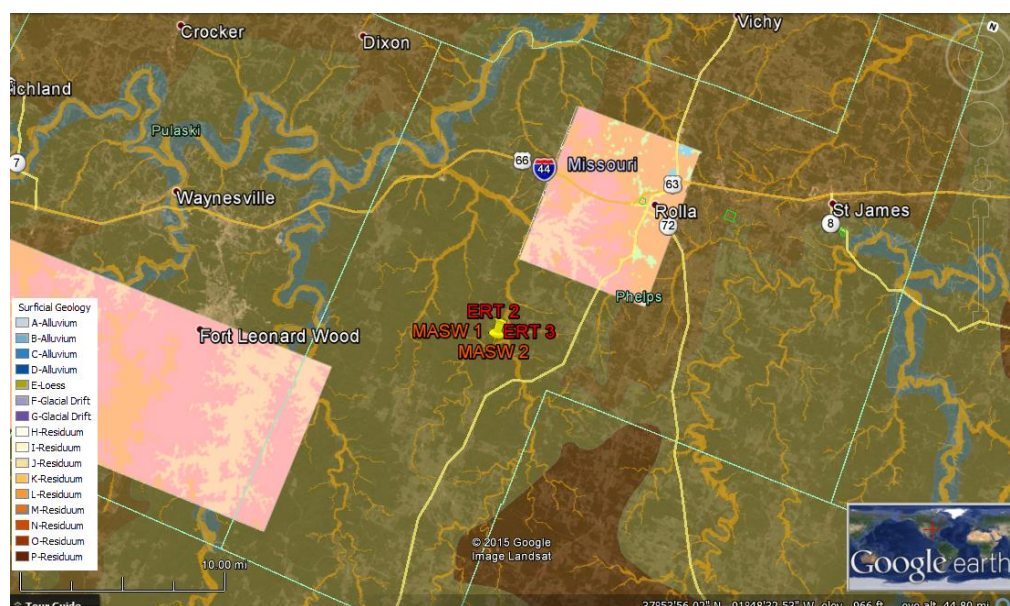


Figure 4.4: Bedrock Geologic map of the study area (Courtesy of Google Earth).

The bedrock is an early Ordovician deposit known as Gasconade Formation which is dominated by dolomite and a little intercalation of chert overlain by the Roubidoux Formation containing mostly dolomite, sandstone, banded chert, shale and some siliceous oolites, respectively, according to their order of dominance. Roubidoux

Formation was severely eroded during the transgression stage of the glaciation age, and few thickness of alluvium was deposited after the transgression age. The K- residuum could be residuals from weathered bedrock.

Multichannel Analysis of surface waves (MASW) were acquired along two lines with five array configurations. The first configuration consisted of 24 geophones (4.5 Hz natural frequency) placed at a uniform spacing of 1-ft. with a total array length of 23-ft. while the offset distances for the geophones were placed at different intervals in the order of 0-ft to 50-ft. For the second array configuration, the 24 geophones were spaced 2.5-ft apart uniformly while maintaining the same offset distances at interval of 0-ft. to 50-ft. The third array configuration had the 24 geophones spaced at 5-ft interval while the offset distances are same as former. In the fourth and five array configurations, the 24 geophones were spaced at 7.5-ft and 10-ft respectively while the offset distances were maintained at interval of 0-ft to 50-ft.

The two MASW traverses were oriented in both northeast – southwest and northeast – northwest directions with the source on both ends of the arrays (Figure 4.5). Also, electrical resistivity tomography (ERT) was acquired along four (4) different lines oriented NW-SE direction which is 20-ft apart (Figure 3.5). ERT data was collected using SuperSting Resistivity unit, dipole-dipole array configuration with 84 electrodes -5ft spacing and the length of the traverse was approximately 415-Ft.



Figure 4.5: MASW traverses (blue lines) oriented NE-SW and NE-NW and ERT lines (red lines) oriented NW-SE.

4.3 MASW TESTING

4.3.1 Site Setup. As noted, the terrain at the site was relatively flat, and little to no change in surface conditions were noted between the times of the two geophysical surveys. The research site provided a relatively quiet atmosphere for seismic data acquisition, as ambient and cultural noise was limited.

For the first MASW traverse a tape measure was placed at the center of the array and extended west to ensure the source had enough room for the farthest desired source offset. Then a second tape measure was extended east to ensure a linear and accurate spacing of the receivers. While in the second MASW traverse a tape measure was placed before the center and extended south to insure the source had enough room for the farthest desired offset. Then a second tape measure was extended north to insure a linear and accurate spacing of the receivers.

The receivers used in testing were 4.5 Hz geophones. The geophones were coupled to the ground using metal spikes hard mounted to the geophone cases, as seen in Figure 4.6

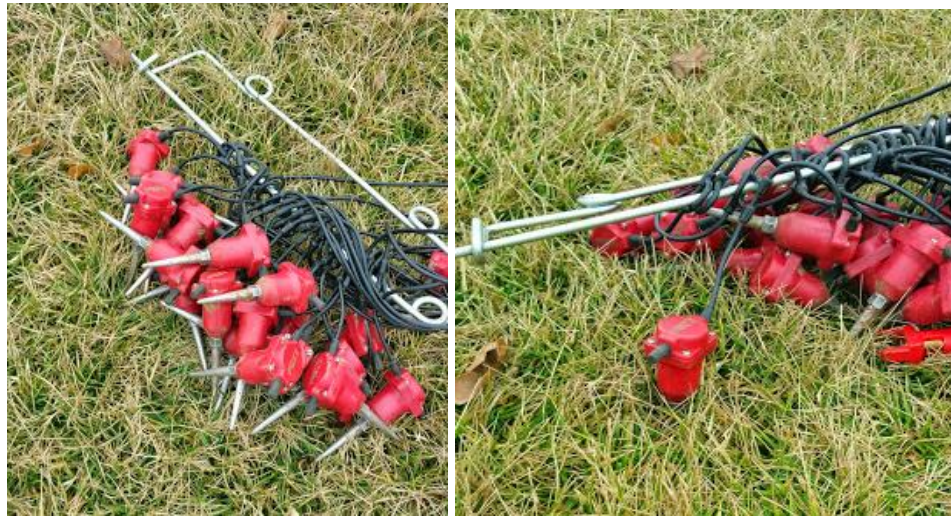


Figure 4.6: 4.5 Hz Geophones with spikes (a) uncoupled (b) coupled

After the geophones were installed, individually shielded paired cable was run to each geophone. The cable has 24 conductive connectors where each geophone was attached and the cable has a knob at both ends which are used to connect the cable to the seismograph. The length of the connecting cable is approximately 240-ft. and the interval between the connectors is approximately 10-ft (See Figure 4.7 for details).



Figure 4.7: Showing cable (red), connectors (yellow), knob (black) and geophones with spike.

For each test setup, the serial number and placement of each geophone and cable were recorded to allow identification of defective equipment if needed. A log sheet of important information was also kept for each setup.

4.3.2 Field Procedures and Equipment. After the field setup was complete, the 24 receiver cables were connected to the RAS-24 exploration seismograph data acquisition system, a full-function dynamic signal analyzer manufactured Seistronix Corporation (<http://www.seistronix.com>). The RAS-24 exploration seismograph is intended for smaller refraction and reflection surveys where cost and ease of use are essential. The RAS-24 offers 24 channels (12 channels optional) of high performance 24-bit A/D conversion in a small, lightweight package, wide dynamic range (117db @ 2ms), intuitive operation under Windows XP/Vista, connect up to 5 boxes (120 channels), 3D on up to 5 lines, automated system performance tests and operates with any laptop.

It is controlled with a windows-based software package produced by Seistronix Corporation known as RAS- 24 that has measurement capabilities in both the time and frequency domain. Software modules are available for auto-power spectrum, transfer function, synchronous average, auto- and cross-correlation, and histogram analysis, throughput to disk with event capture, zoom analysis, stepped sine, and active X communication.

Testing began with a 1-ft receiver spacing with an impulsive source. For the impulsive source, a 20 lbs. sledgehammer was used to strike a one square foot piece of plate steel (Figure 4.8). The sledgehammer had a PCB 350A14 shock accelerometer attached to one end of the head that acted as the trigger for the analyzer. Six source offset

distances were generally used for the 1ft. receiver spacing: 0-ft., 10-ft, 20-ft, 30-ft., 40-ft., and 50-ft. at both ends of the array.



Figure 4.8: A one square foot metal plate

Five hammer impacts were stacked at each shot location and the corresponding resulted shear waves were recorded.

After the 1ft spacing tests were complete, the receiver array was expanded to a 2.5-ft receiver spacing making it 57.5-ft spread length. Then, the 20 lbs. sledgehammer was once again used at source offset distances of 0-ft, 10-ft, 20-ft, 30-ft, 40-ft. and 50-ft. at both ends of the array while five hammer impacts were stacked at each shot location and the corresponding resulted shear waves were recorded.

Immediately the 2.5-ft spacing tests were completed, the receiver array was expanded to a 5-ft. receiver spacing making it 115-ft spread length. Then, the 20 lbs. sledgehammer was once again used at source offset distances of 0-ft, 10-ft, 20-ft, 30-ft,

40-ft. and 50-ft. at both ends of the array while five hammer impacts were stacked at each shot location and the corresponding resulted shear waves were recorded.

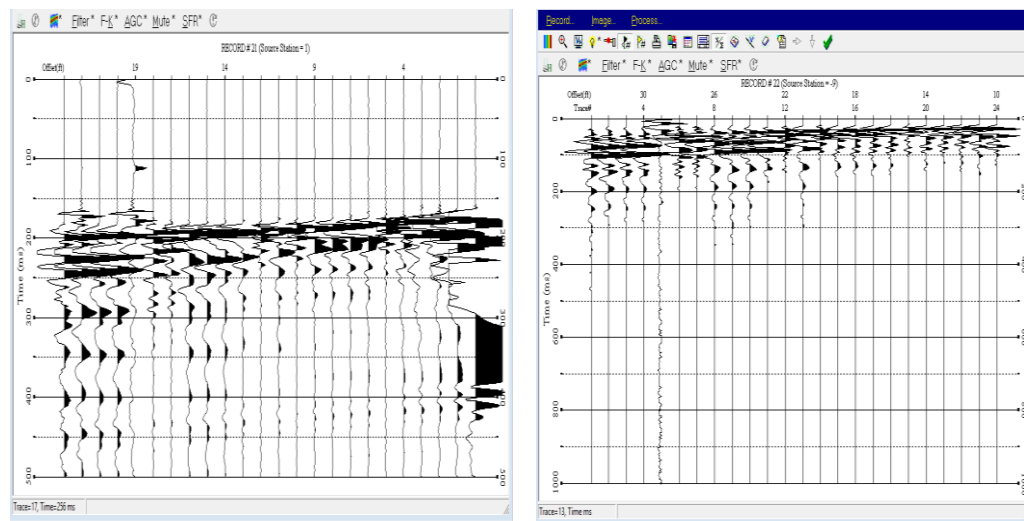
When the 5-ft spacing tests were completed, the receiver array was expanded to a 7.5-ft receiver spacing making it 172.5-ft. spread length. Then, the 20 lbs. sledgehammer was once again used at source offset distances of 0-ft, 10-ft, 20-ft, 30-ft, 40-ft. and 50-ft at both ends of the array while five hammer impacts were stacked at each shot location and the corresponding resulted shear waves were recorded.

Finally, when the 7.5-ft spacing tests were completed, the receiver array was expanded to a 10-ft receiver spacing making it 230-ft spread length. Then, the 20 lbs. sledgehammer was once again used at source offset distances of 0-ft, 10-ft, 20-ft, 30-ft, 40-ft and 50-ft. at both ends of the array while five hammer impacts were stacked at each shot location and the corresponding resulted shear waves were recorded.

4.3.3 Data Acquisition. Prior to beginning the field test, parameters were selected which are related to the geometry of the field survey and data acquisition parameters. The selection of field parameters was based on documented guidance provided by the Kansas Geologic Survey (Ivanov, Park and Xia, 2009). For data acquisition, the recording time and sampling intervals were set at 1 second and 0.5 milliseconds, respectively.

Parameters recommended by Seistronix Inc. were used to coordinate the triggering system with the RAS-24 seismograph. After the initial setup of RAS-24 controller, the system was ready for the first shot record. As a check, the receiver signal window of the RAS-24 controller was monitored while one team member walked by the geophone array. The induced vibrations from the footsteps returned a small, but visible, signal to the receiver indicating proper oscillation of the geophone core.

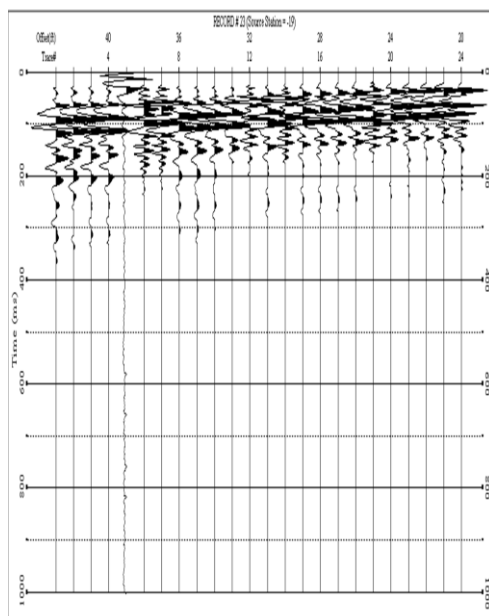
Recording sequence is started by initializing the recording software and arming the trigger system. When ready, the party responsible for swinging the hammer is signaled, and the hammer blow initiates the survey. The response from the triggering system notifies the seismograph that the survey has begun. Signals recorded through the designated recording time and at the designated time interval. Figure 4.8 shows an example of the visual output provided by the processing software after completing one shot. After acceptance of the sounding, either the setup can be moved for the next reading or additional readings can be collected in the same locations for the purpose of stacking records. Stacking records is used to improve the definition of the record, and generally used in noisy environments. Five stacks were used to minimize noise from the environment. Shot gather for each of the array record at different offset distances are shown in Figure 4.9 below.



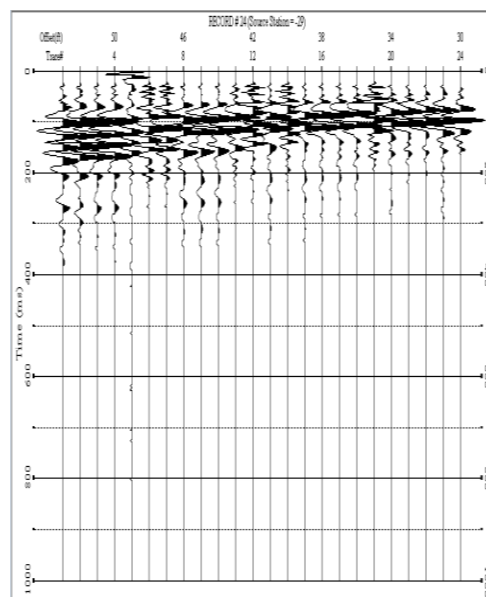
(a) 1-ft spacing and 0-ft offset.

(b) 1-ft spacing and 10-ft offset.

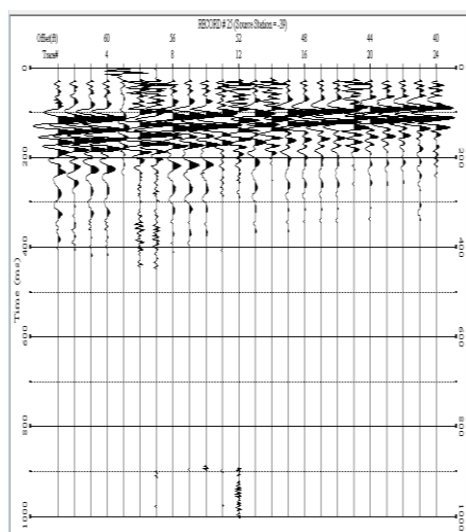
Figure 4.9: Shot gather for each of the array record at different offset distances



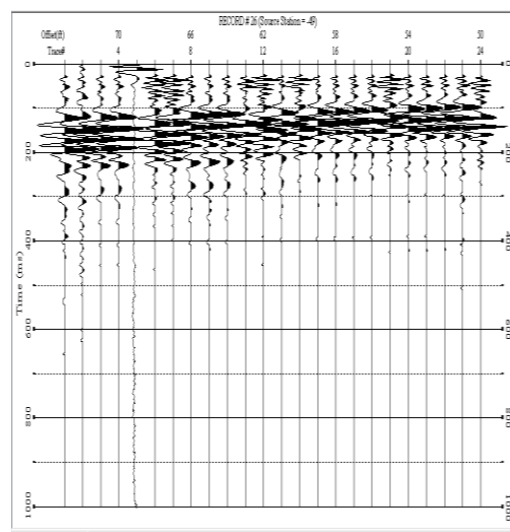
(c) 1-ft spacing and 20-ft offset.



(d) 1-ft spacing and 30-ft offset

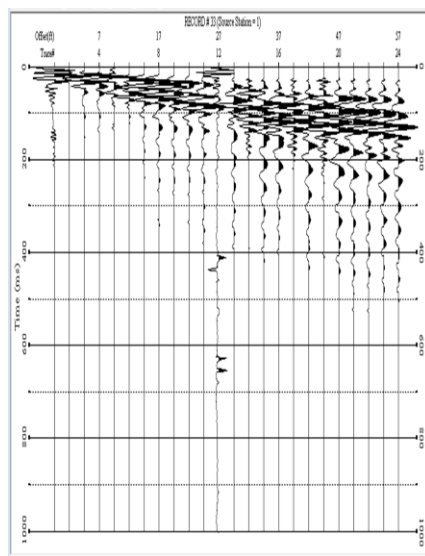


(e) 1-ft spacing and 40-ft offset.

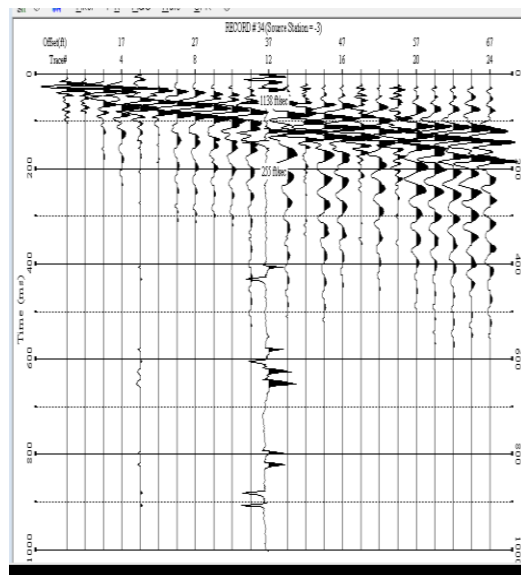


(f) 1-ft spacing and 50-ft offset

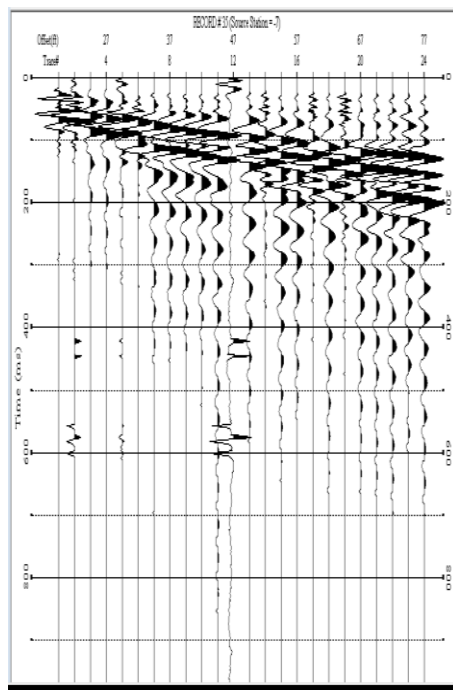
Figure 4.9: Shot gather for each of the array record at different offset distances (Cont.)



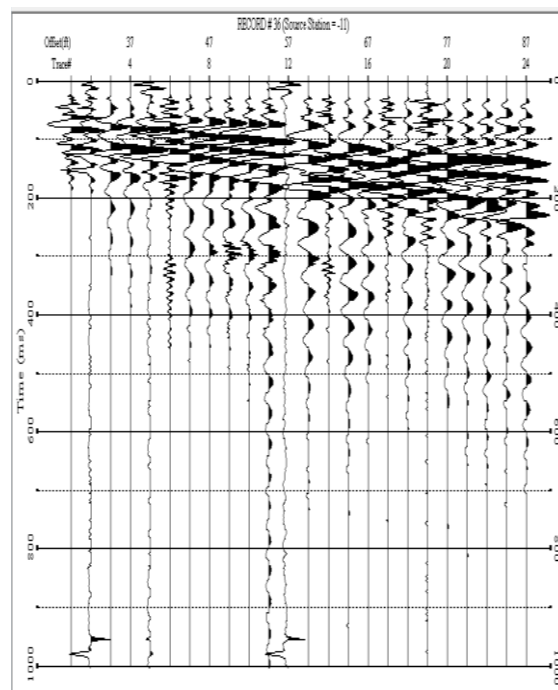
(g) 2.5-ft spacing and 0-ft offset.



(h) 2.5-ft spacing and 10-ft offset

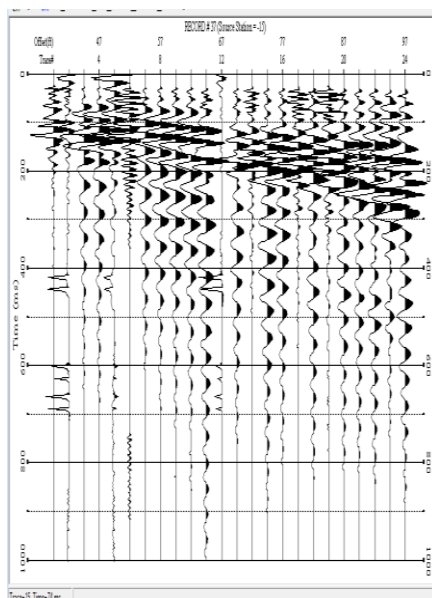


(i) 2.5-ft spacing and 20-ft offset.

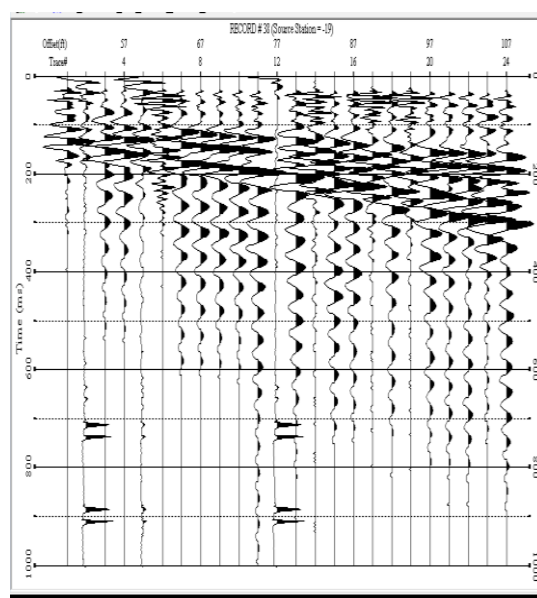


(j) 2.5-ft spacing and 30-ft offset.

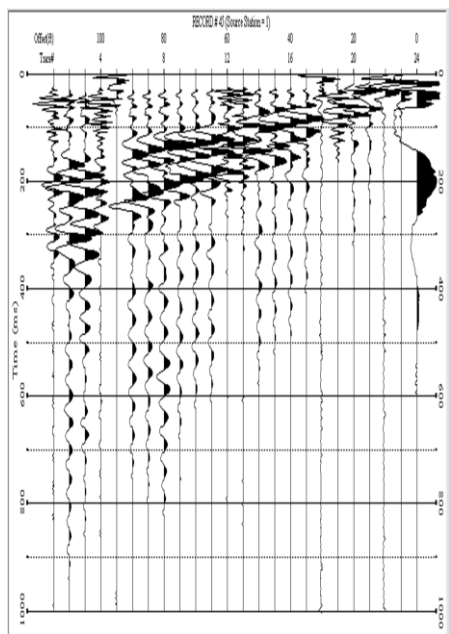
Figure 4.9: Shot gather for each of the array record at different offset distances (Cont.)



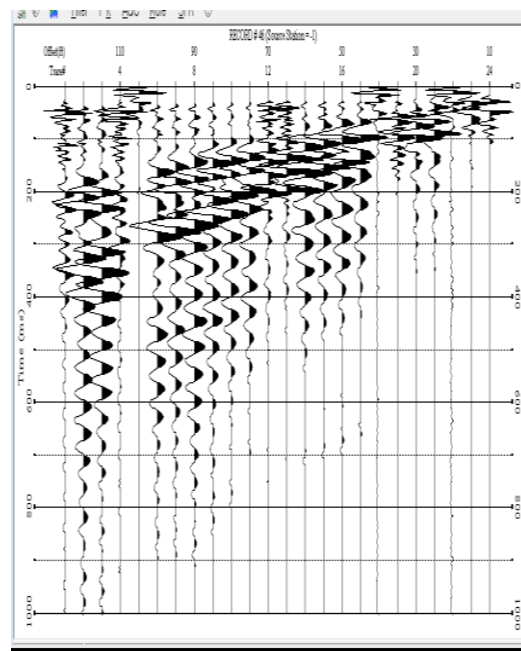
(k) 2.5-ft spacing and 40-ft offset.



(l) 2.5-ft spacing and 50-ft offset.

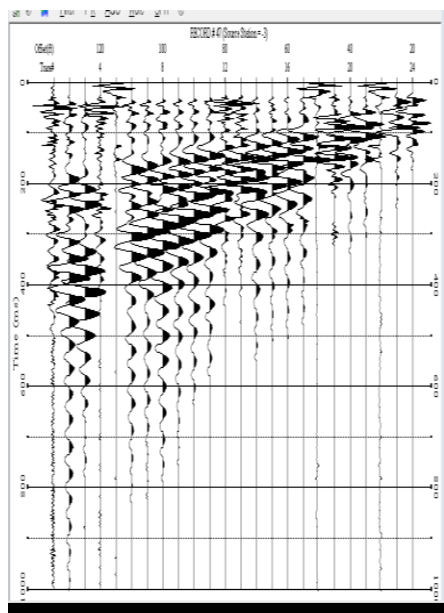


(m) 5-ft spacing and 0-ft offset.

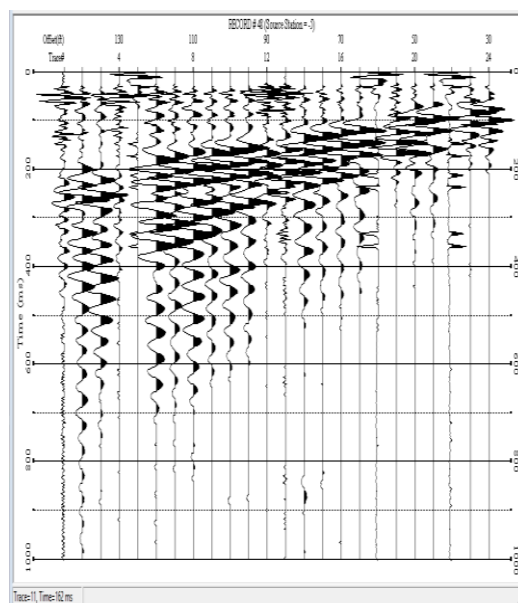


(n) 5-ft spacing and 10-ft offset.

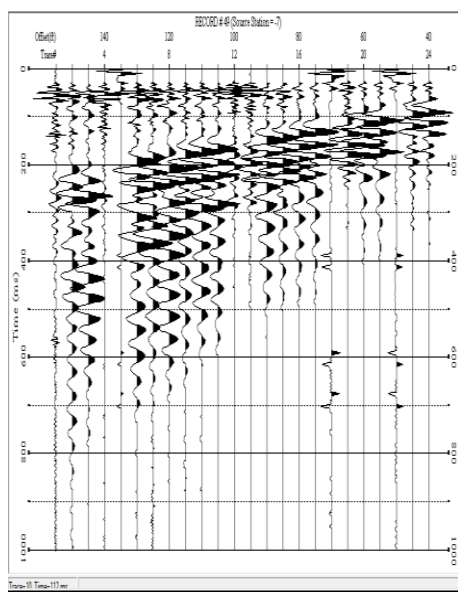
Figure 4.9: Shot gather for each of the array record at different offset distances (Cont.)



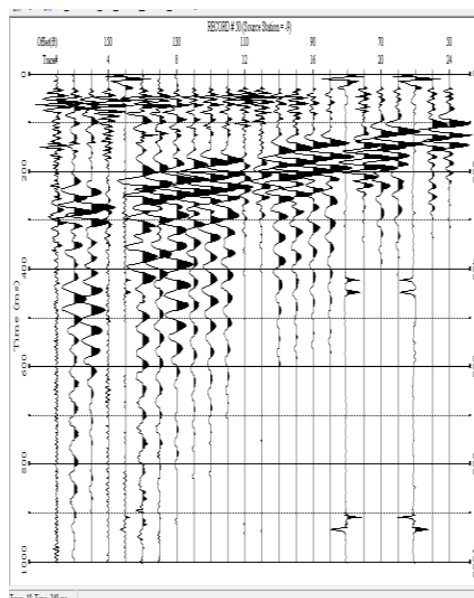
(o) 5-ft spacing and 20-ft offset.



(p) 5-ft spacing and 30-ft offset.

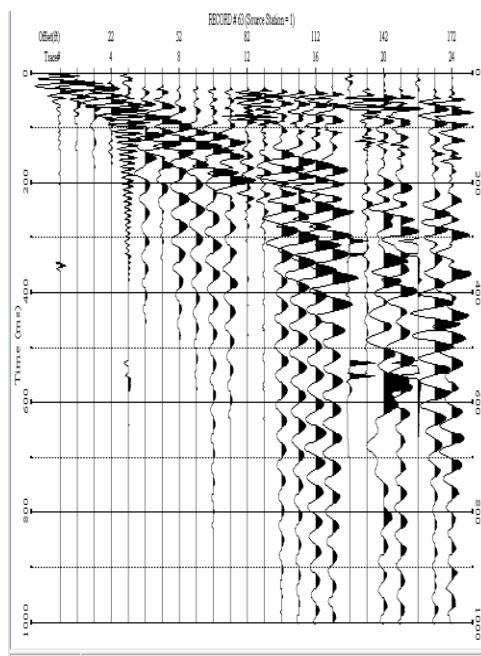


(q) 5-ft spacing and 40-ft offset.

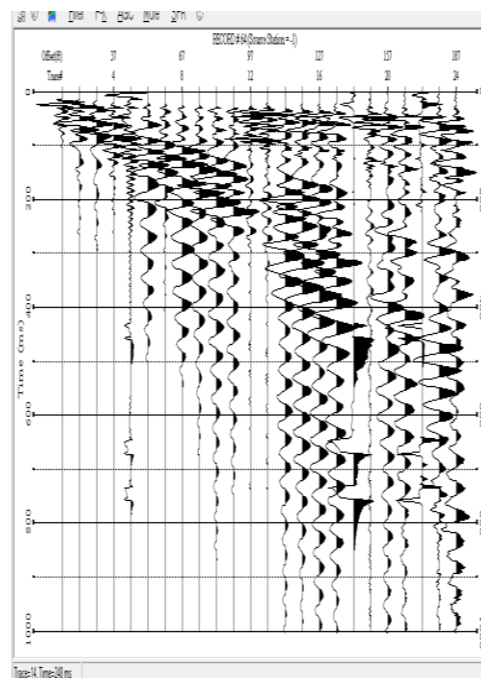


(r) 5-ft spacing and 50-ft offset.

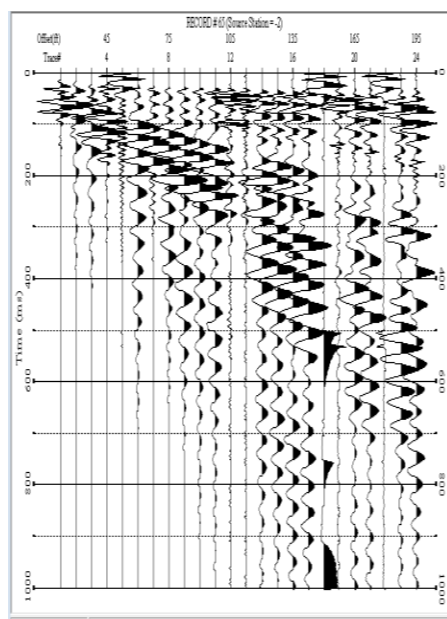
Figure 4.9: Shot gather for each of the array record at different offset distances (Cont.)



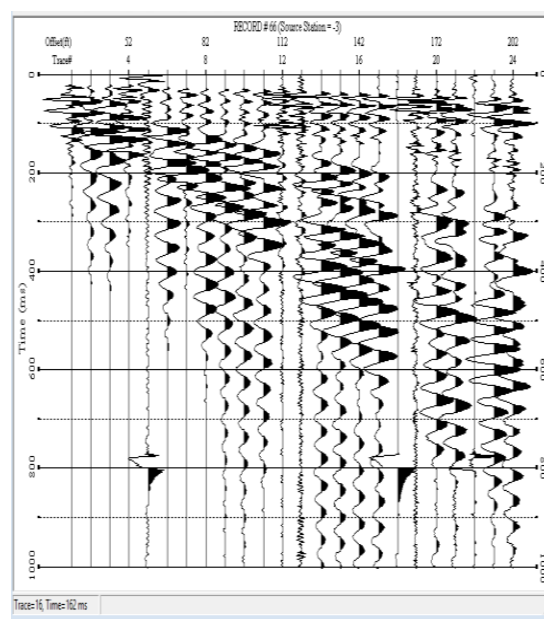
(s) 7.5-ft spacing and 0-ft offset.



(t) 7.5-ft spacing and 10-ft. offset.

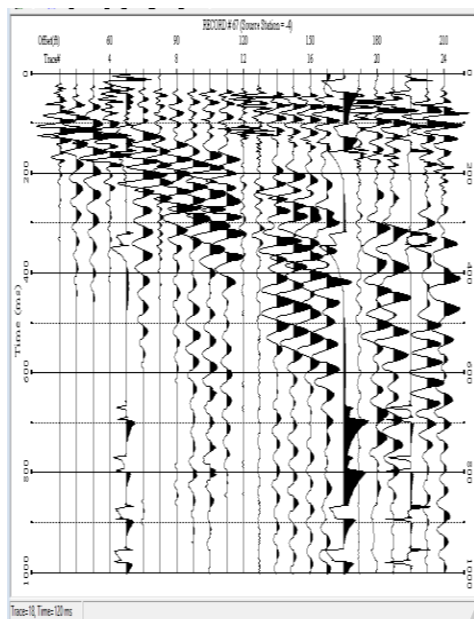


(u) 7.5-ft spacing and 20-ft. offset.

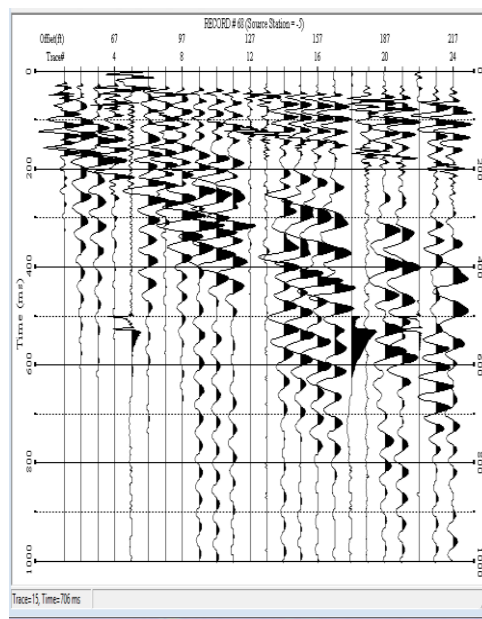


(v) 7.5-ft spacing and 30-ft. offset.

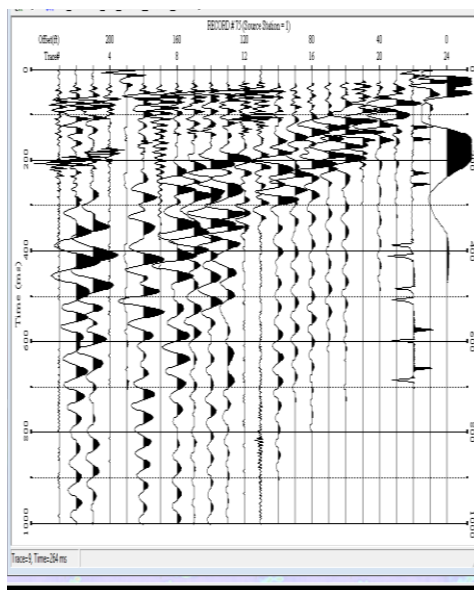
Figure 4.9: Shot gather for each of the array record at different offset distances (Cont.)



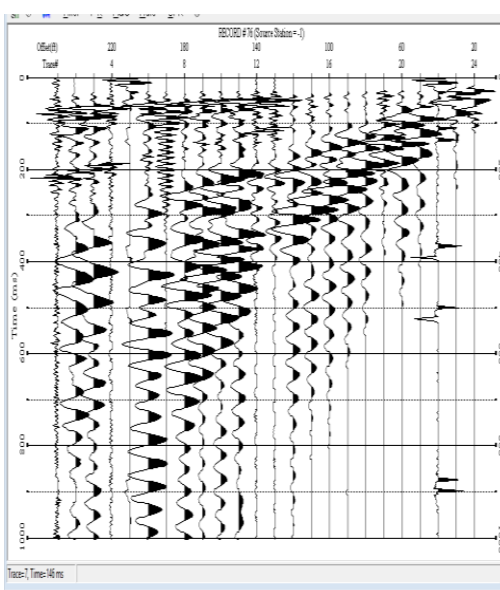
(w) 7.5-ft spacing and 40-ft. offset.



(x) 7.5-ft spacing and 50-ft. offset.

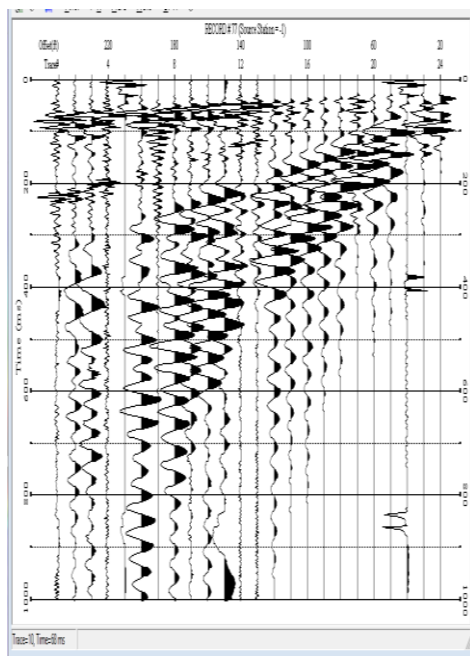


(y) 10-ft spacing and 0-ft. offset.

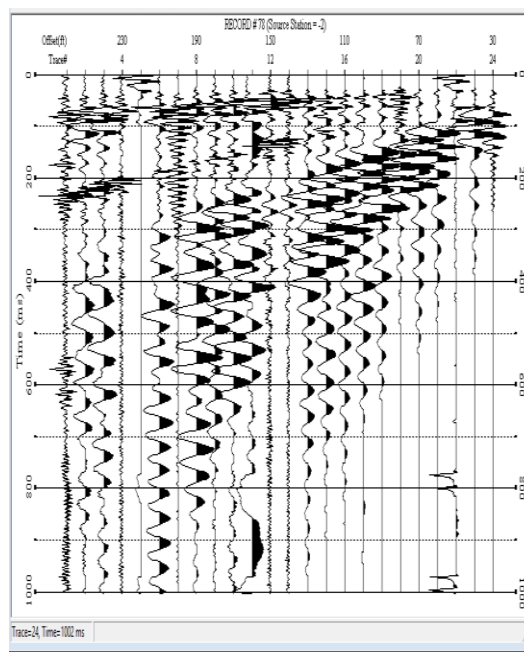


(z) 10-ft spacing and 10-ft. offset.

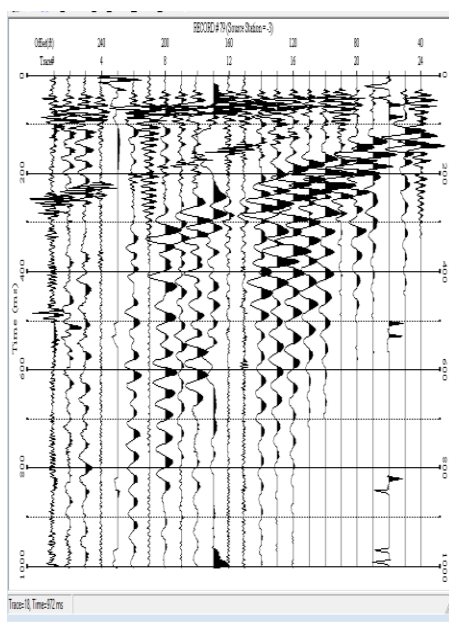
Figure 4.9: Shot gather for each of the array record at different offset distances (Cont.)



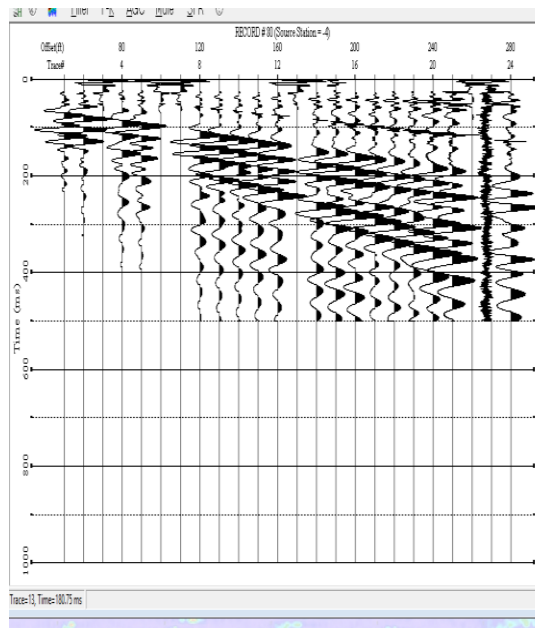
(aa) 10-ft spacing and 20-ft. offset.



(ab) 10-ft spacing and 30-ft. offset.



(ac) 10-ft spacing and 40-ft. offset.



(ad) 10-ft spacing and 50-ft. offset.

Figure 4.9: Shot gather for each of the array record at different offset distances (Cont.)

4.3.4 Data Processing and Inversion. Processing of shot records was performed using the Surfeis software package, developed by the Kansas Geologic Survey (<http://www.masw.com/DispersionAnalysis.html>). The purpose of the software is to process and analyze shot records for Rayleigh wave isolation and extraction of fundamental modes, invert extracted curvatures dispersion characteristics, develop representative dispersion curves, allow manual into one-dimensional shear wave sounds, and interpolate series of one-dimensional models into a single two dimensional tomography image (Park et al., 2009). Figure 4.10 provides a flowchart detailing the processing steps used for analyzing MASW profiles.

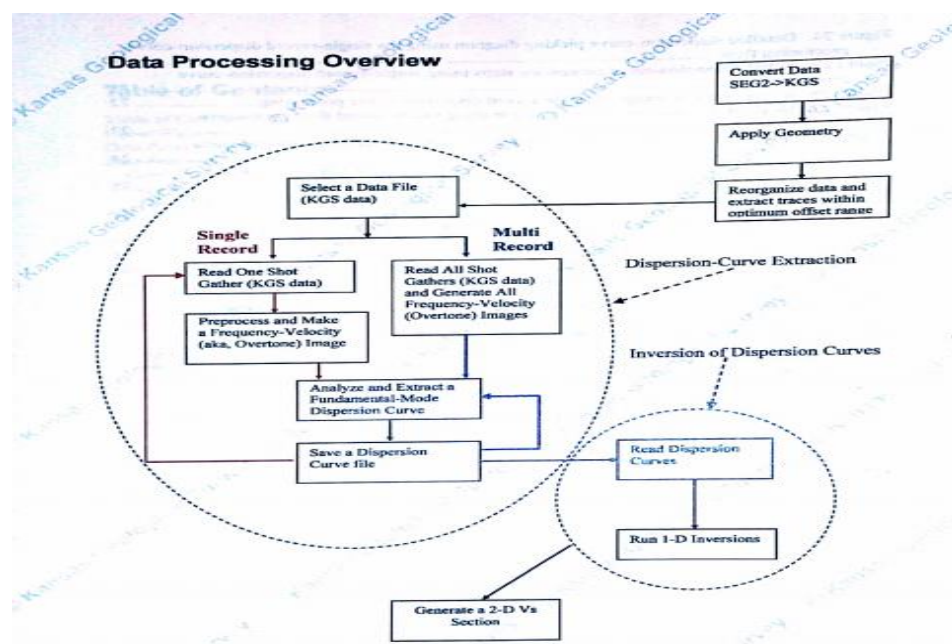


Figure 4.10: A flowchart detailing the processing steps used for analyzing MASW profiles (Kansas Geological Survey, 2014)

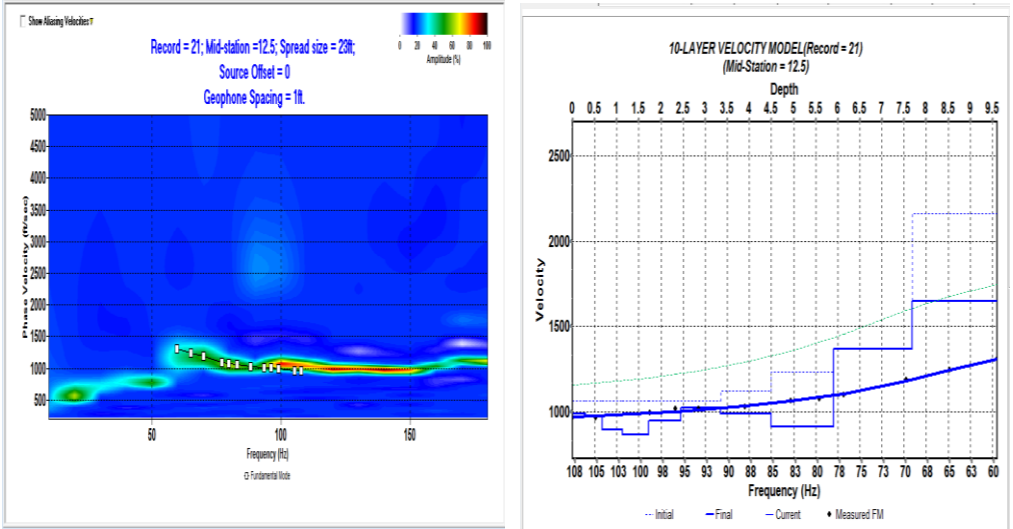
Processing begins by up loading SEG-2 field records into Surfeis. Records are processed and converted into KGS format, which is recognizable by the program. After the conversion into KGS format, the program will collect information pertain to the nature of the survey (i.e. active or passive method of data acquisition), the setup of the survey, and how the survey was advanced. Data files are processed a second time scanning for signatures of surface waves within the record (Ivanov, Park and Xia, 2009).

Algorithms in the Surfeis routine are used to analyze each KGS file and determine surface wave phase velocity and frequency properties, and used to plot representative dispersion curves. Due to the energy of surface waves, related measurements of amplitude can be used to highlight the energy of the fundamental mode (Park et al., 2009). Figure 4.9 show all the dispersion curves generated for the thirty (30) data sets for this research and markings indicating the selected curvature of the fundamental mode. Each shot record has a unique dispersion curve, and each curve must be analyzed manually, by the processor, to identify and select best fit for the fundamental mode (Park et al., 2009).

The dispersion curve can also be used to evaluate the depths of analysis. As seen in Figure 4.9, the fundamental mode is identified by the marked curvature in the bottom left of the exhibit. The lowest frequency generated in the dispersion curve is approximately 10 Hz and a phase velocity of approximately 1,800 feet per second which was found in 5- ft. spacing and 20 ft. offset distance array. The wavelength is equivalent to the phase velocity divided by the frequency. In this example, the corresponding wave length would be approximately 180 feet. Assuming that the maximum depth of penetration is approximately half of the maximum recorded wavelength (Park et al.,

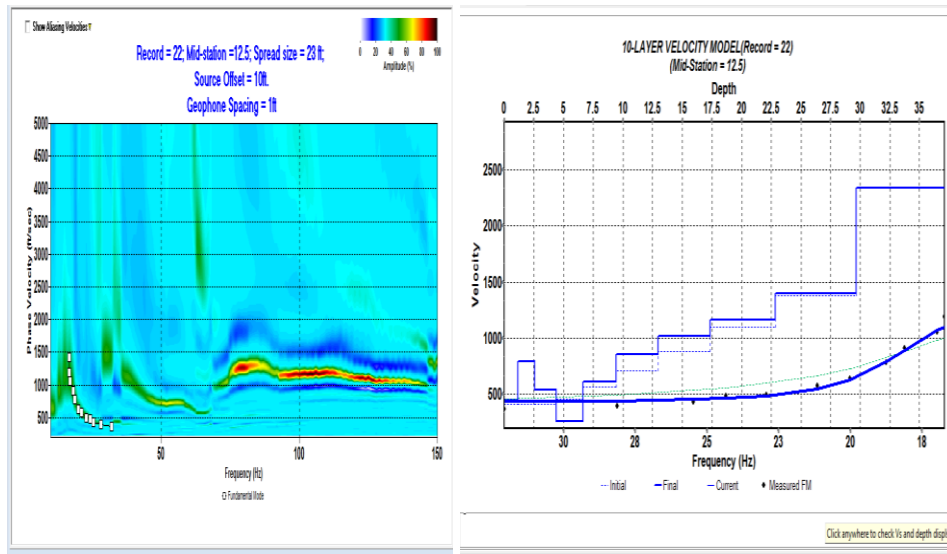
2009), the depth of penetration would be approximately 90 feet. The minimum depth of resolution can be determined in a similar fashion, by using the nodal point to the far right of the extracted curve. For the given example, the shallowest observable depth is approximately 8 to 10 feet below the surface.

After all records have been evaluated and the fundamental modes are selected, curves are then used as comparative tools during the inversion process. Surfeis attempts to generate a layered earth, shear wave model that would produce a similar fundamental mode curvature as that extracted from field testing. The iterative process continues until the predetermined error tolerance is achieved or the maximum number of iterations is performed. All the generated dispersion curves and the inverted shear wave velocity model for the different tests are shown in Figure 4.11.

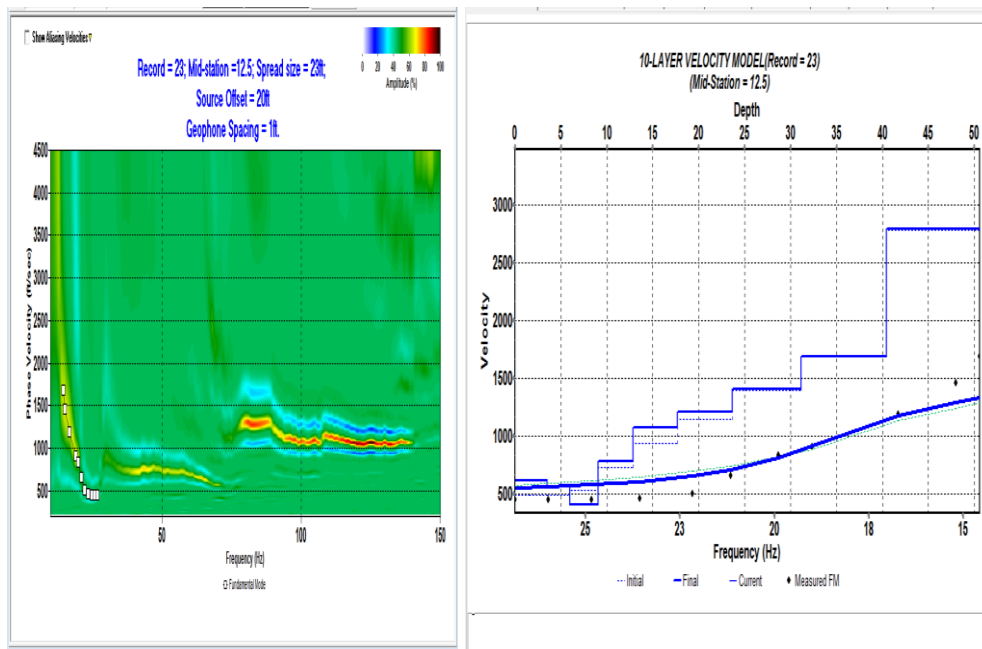


(a) 1-ft spacing and 0-ft offset.

Figure 4.11: All the generated dispersion curves and the inverted shear wave velocity model for the different tests.

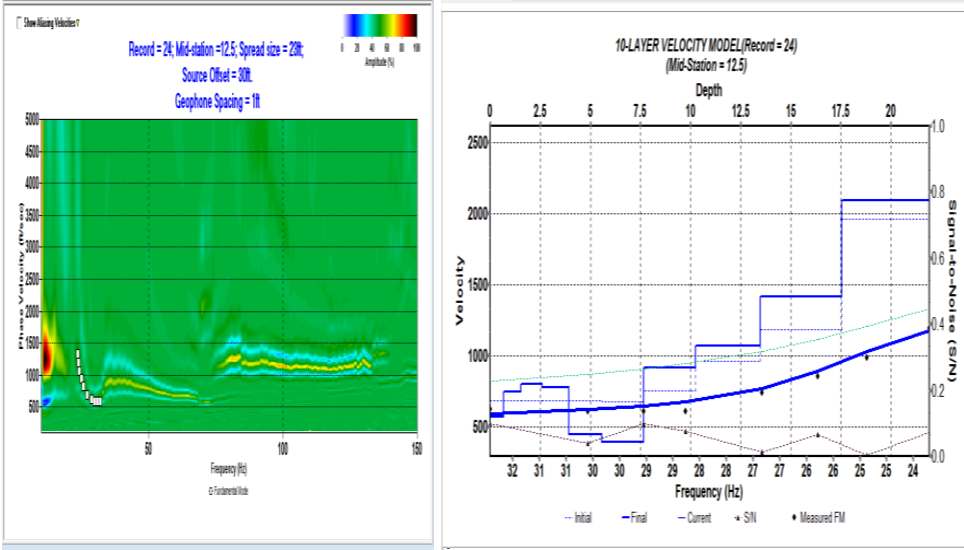


(b) 1-ft spacing and 10-ft offset

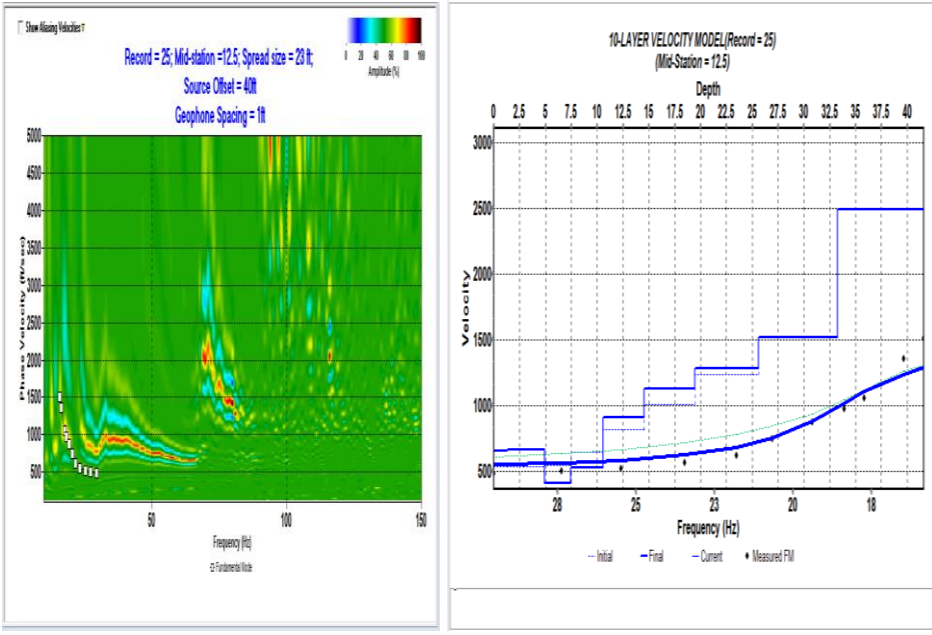


(b) 1-ft spacing and 20-ft offset

Figure 4.11: All the generated dispersion curves and the inverted shear wave velocity model for the different tests (Cont.)

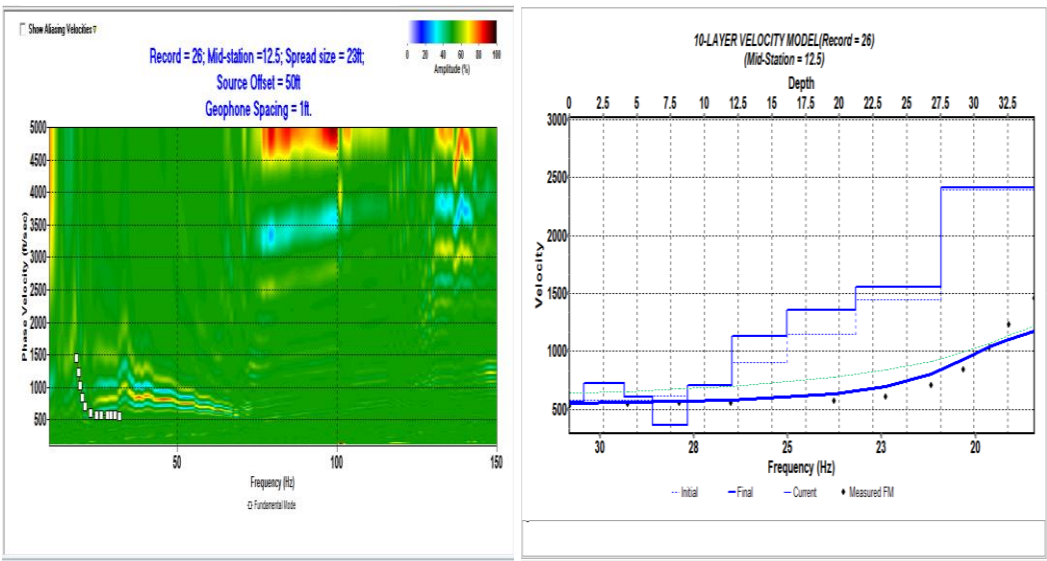


(d) 1-ft spacing and 30-ft offset

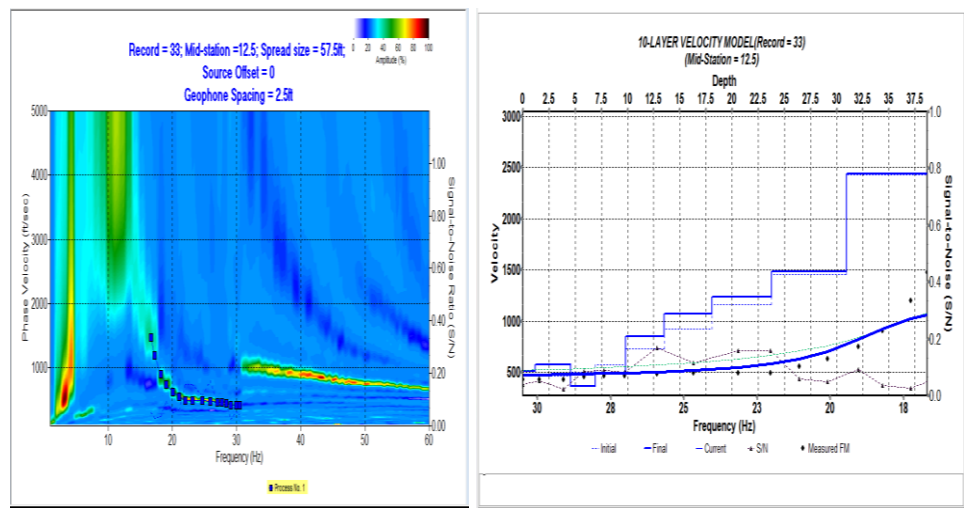


(e) 1-ft spacing and 40-ft offset.

Figure 4.11: All the generated dispersion curves and the inverted shear wave velocity model for the different tests (Cont.)

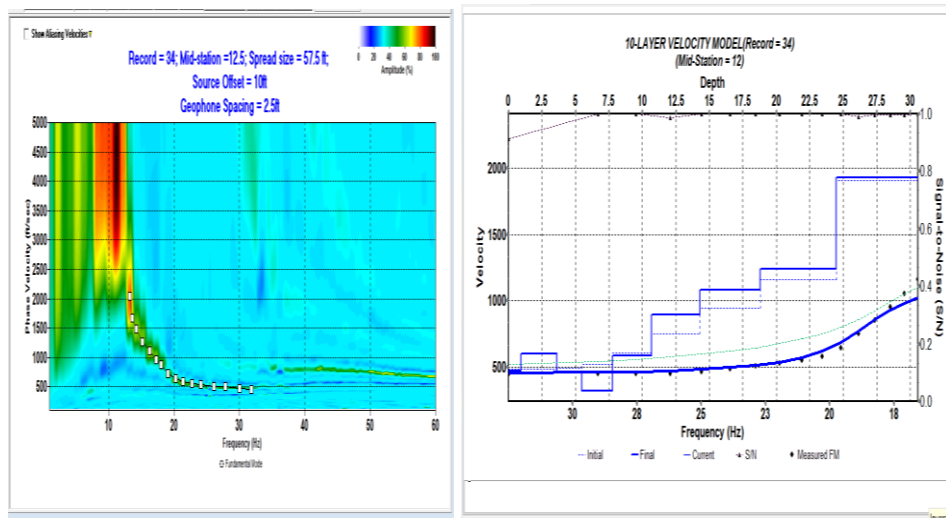


(f) 1-ft spacing and 50-ft offset.

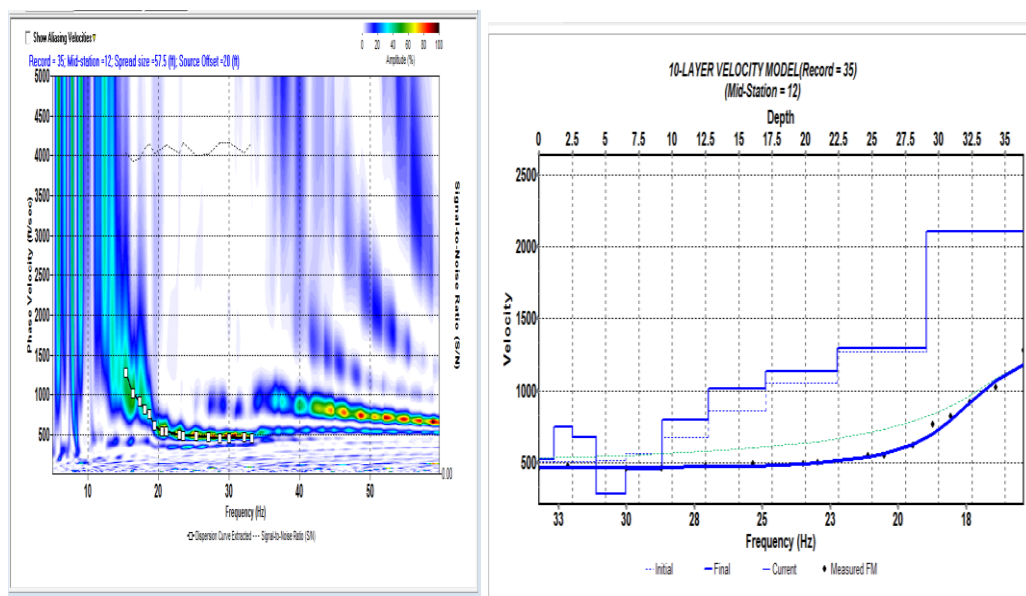


(g) 2.5-ft spacing and 0-ft offset.

Figure 4.11: All the generated dispersion curves and the inverted shear wave velocity model for the different tests (Cont.)

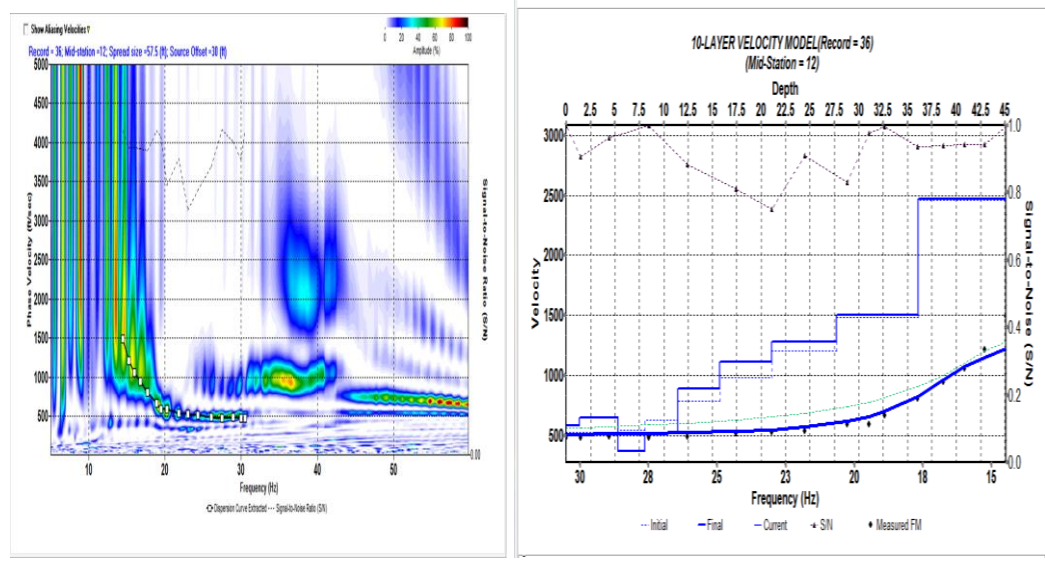


(h) 2.5-ft spacing and 10-ft offset.

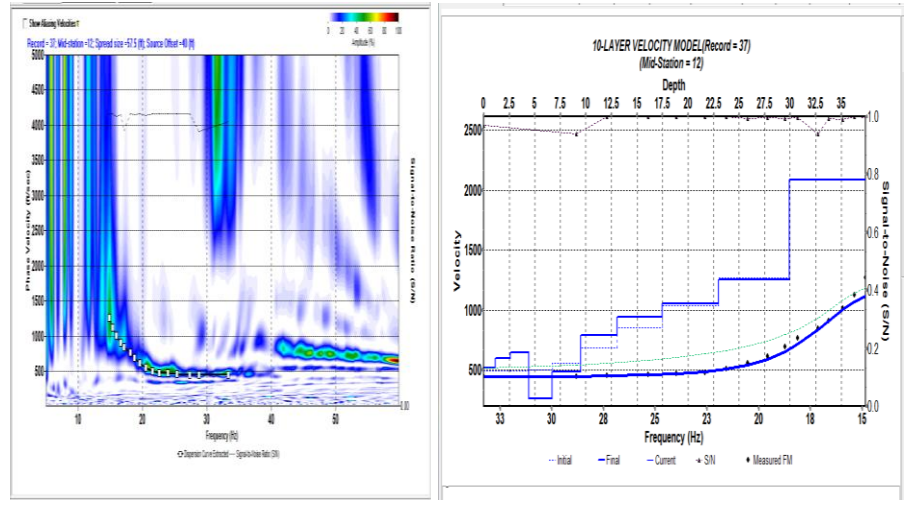


(i) 2.5-ft spacing and 20-ft offset.

Figure 4.11: All the generated dispersion curves and the inverted shear wave velocity model for the different tests (Cont.)

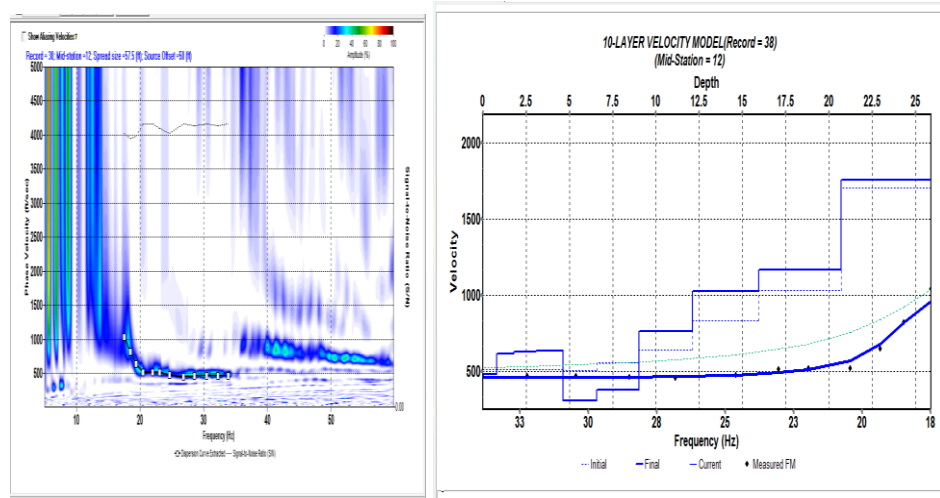


(j) 2.5-ft spacing and 30-ft offset.

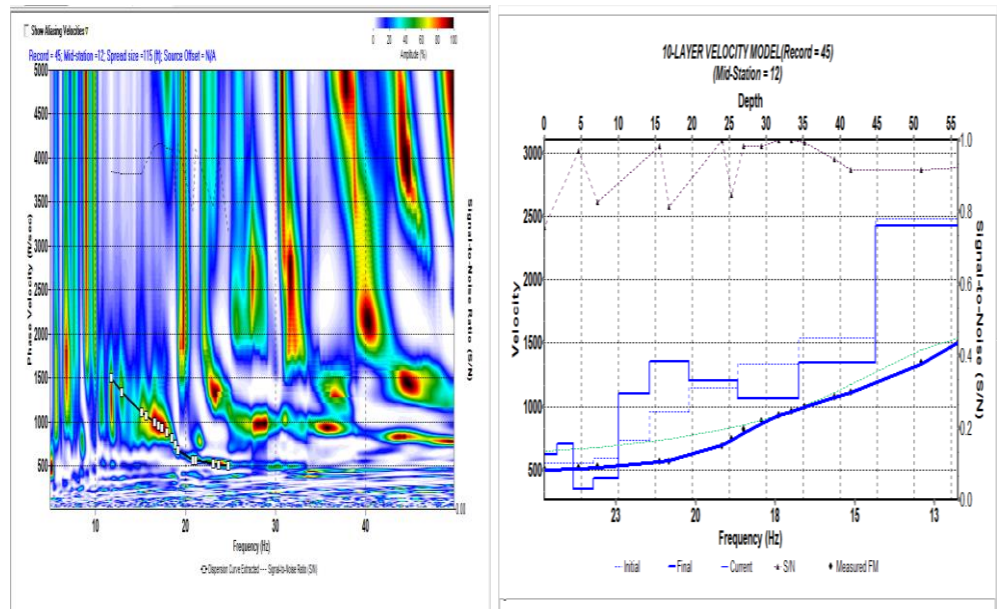


(k) 2.5-ft spacing and 40-ft offset.

Figure 4.11: All the generated dispersion curves and the inverted shear wave velocity model for the different tests (Cont.)

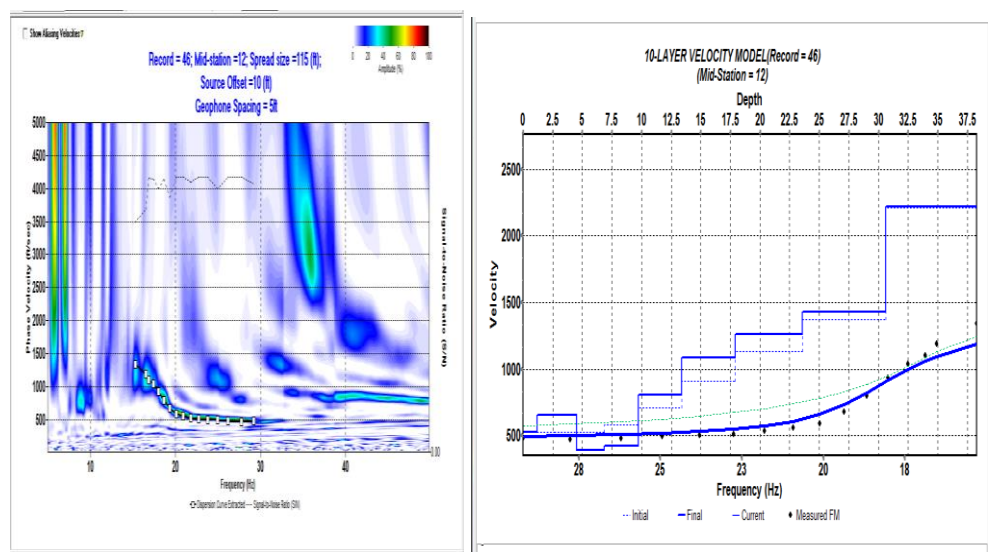


(l) 2.5-ft spacing and 50-ft offset.

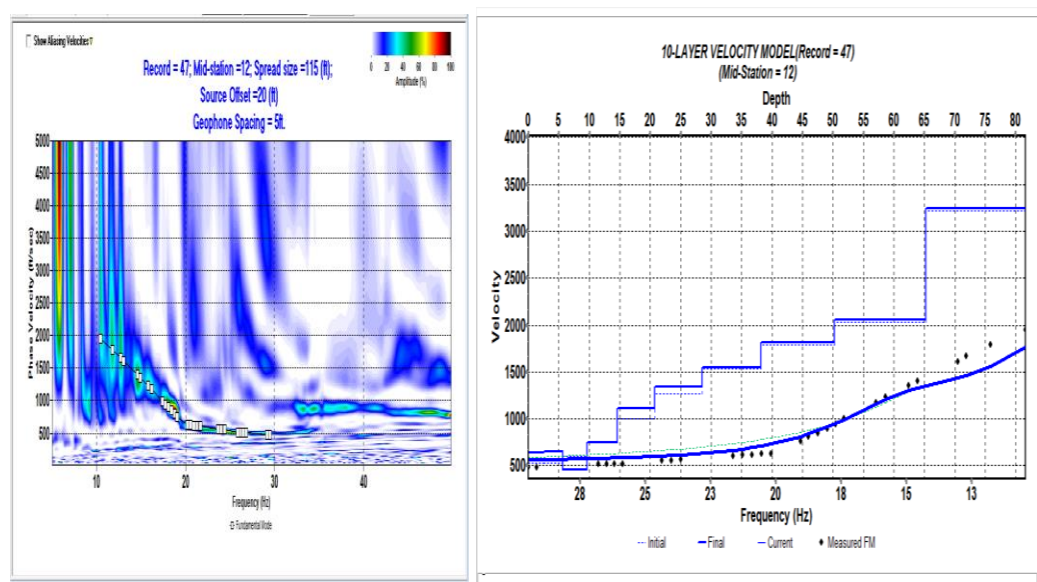


(m) 5-ft spacing and 0-ft offset.

Figure 4.11: All the generated dispersion curves and the inverted shear wave velocity model for the different tests (Cont.)

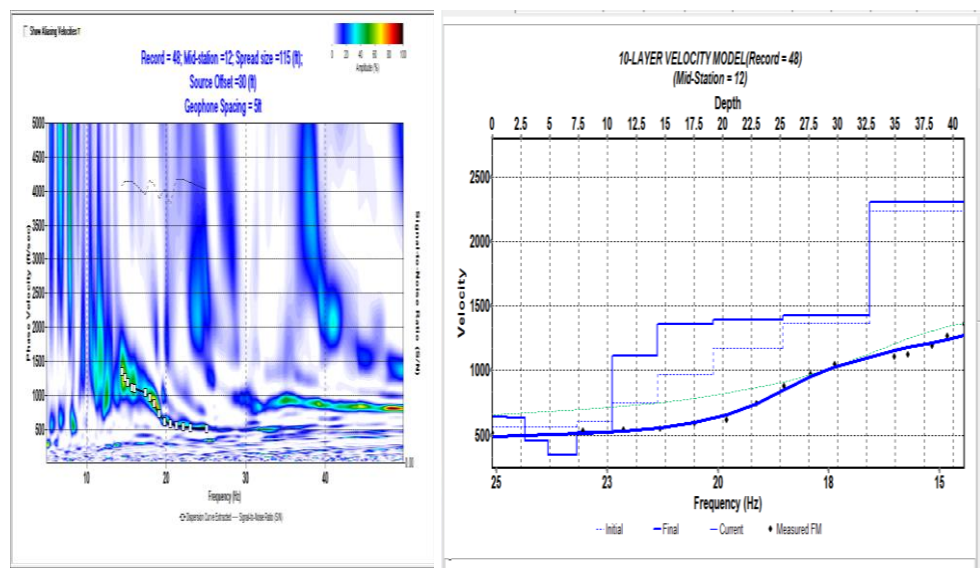


(n) 5-ft spacing and 10-ft offset.

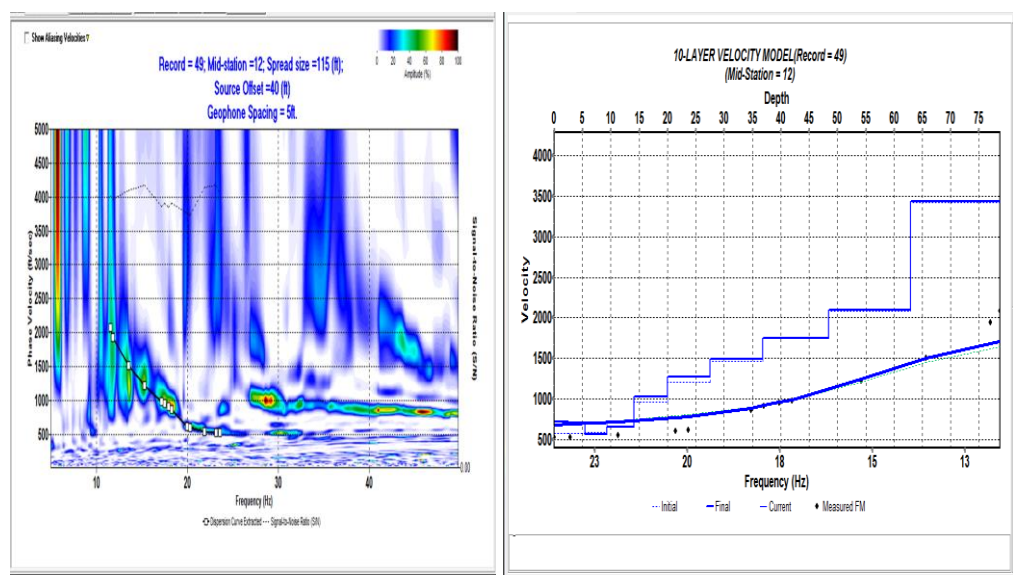


(o) 5-ft spacing and 20-ft offset.

Figure 4.11: All the generated dispersion curves and the inverted shear wave velocity model for the different tests (Cont.)

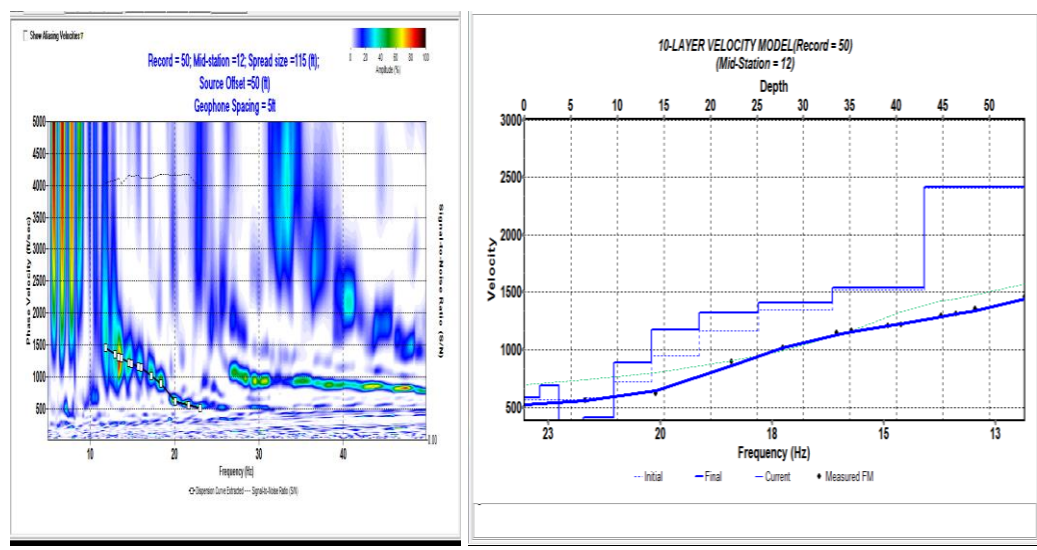


(p) 5-ft spacing and 30-ft offset.

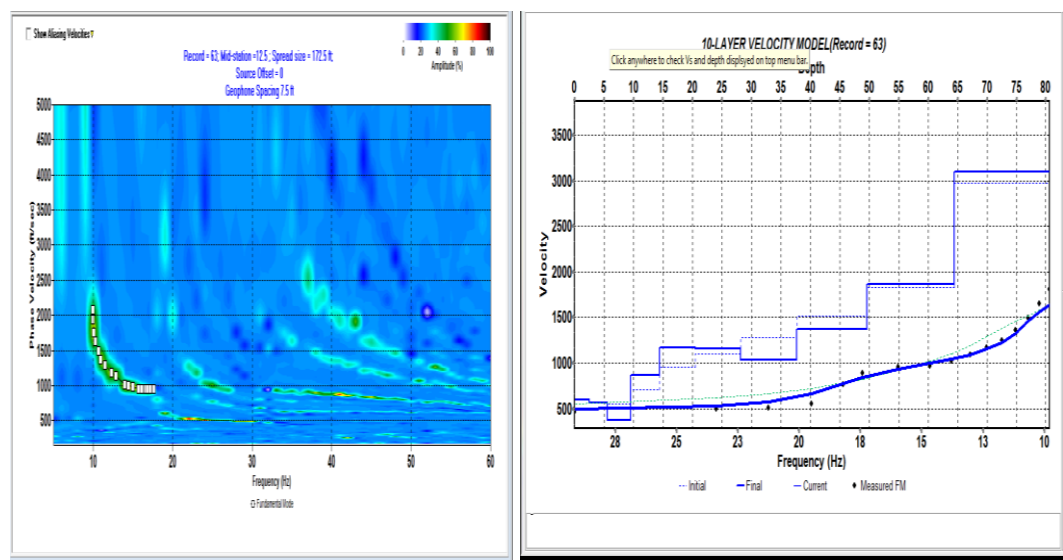


(q) 5-ft. spacing and 40-ft offset.

Figure 4.11: All the generated dispersion curves and the inverted shear wave velocity model for the different tests (Cont.)

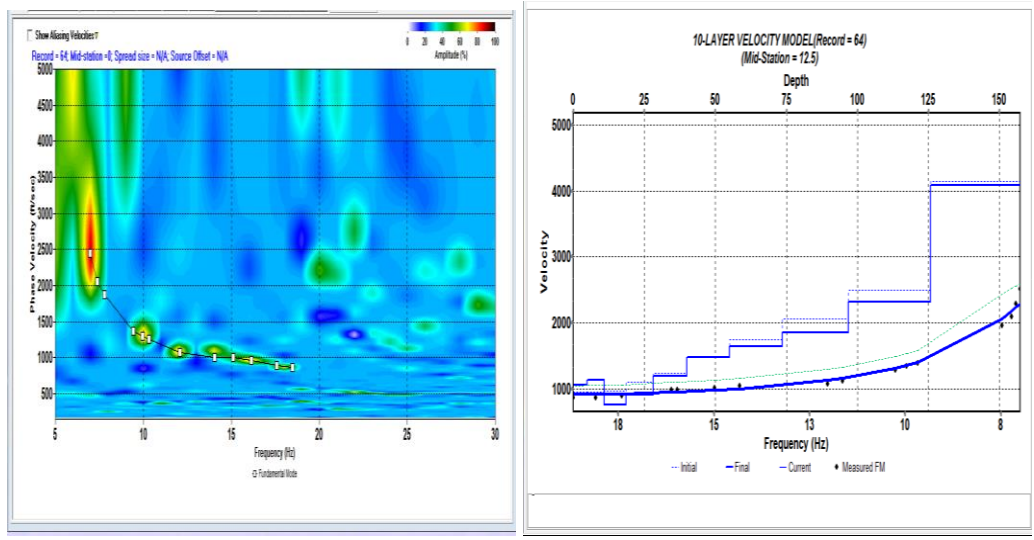


(r) 5-ft spacing and 50-ft offset.

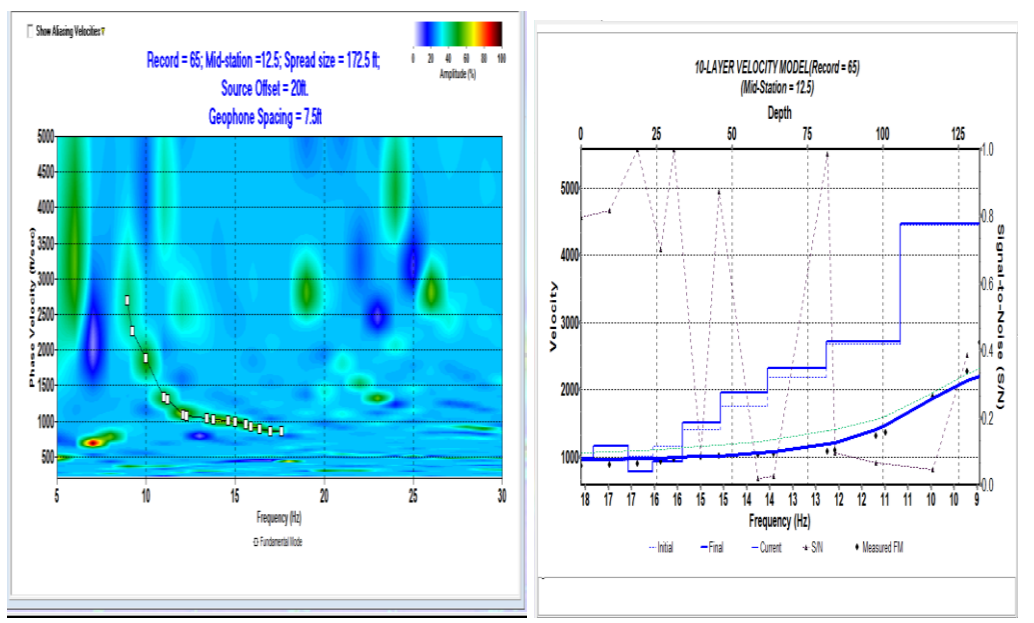


(s) 7.5-ft. Spacing and 0-ft offset.

Figure 4.11: All the generated dispersion curves and the inverted shear wave velocity model for the different tests (Cont.)

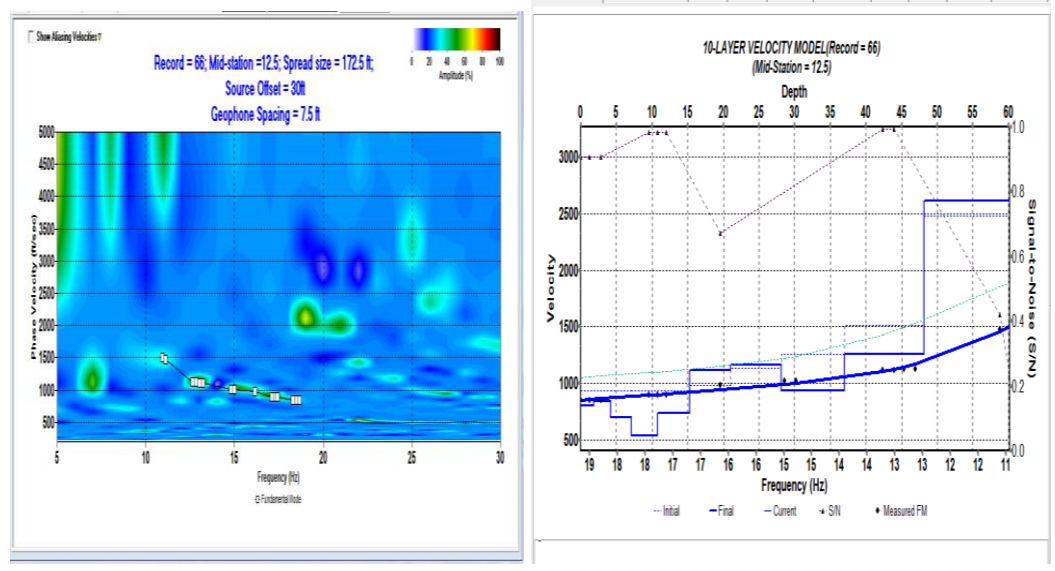


(t) 7.5-ft spacing and 10-ft offset.

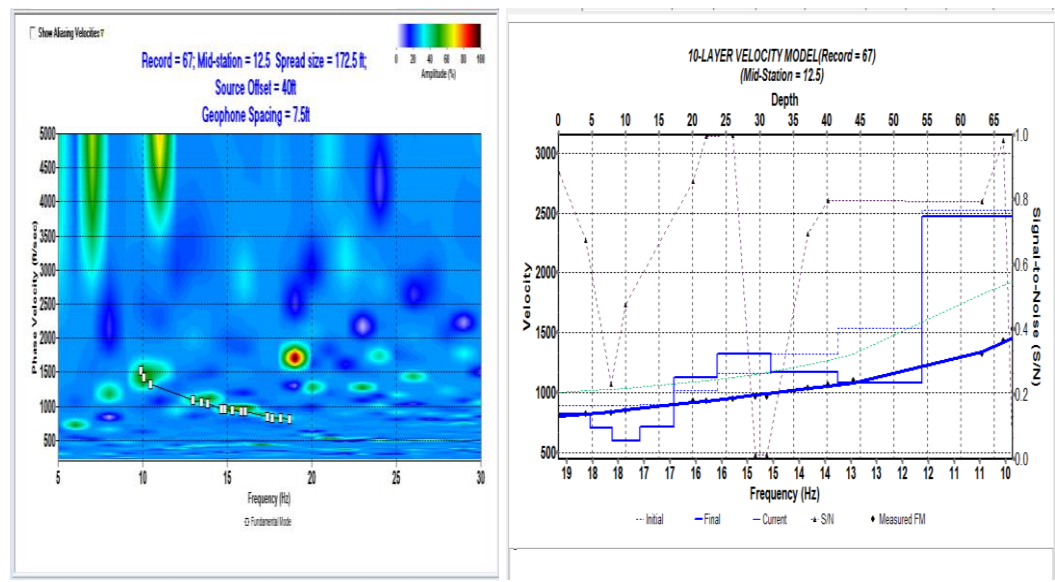


(u) 7.5-ft spacing and 20-ft offset.

Figure 4.11: All the generated dispersion curves and the inverted shear wave velocity model for the different tests (Cont.)

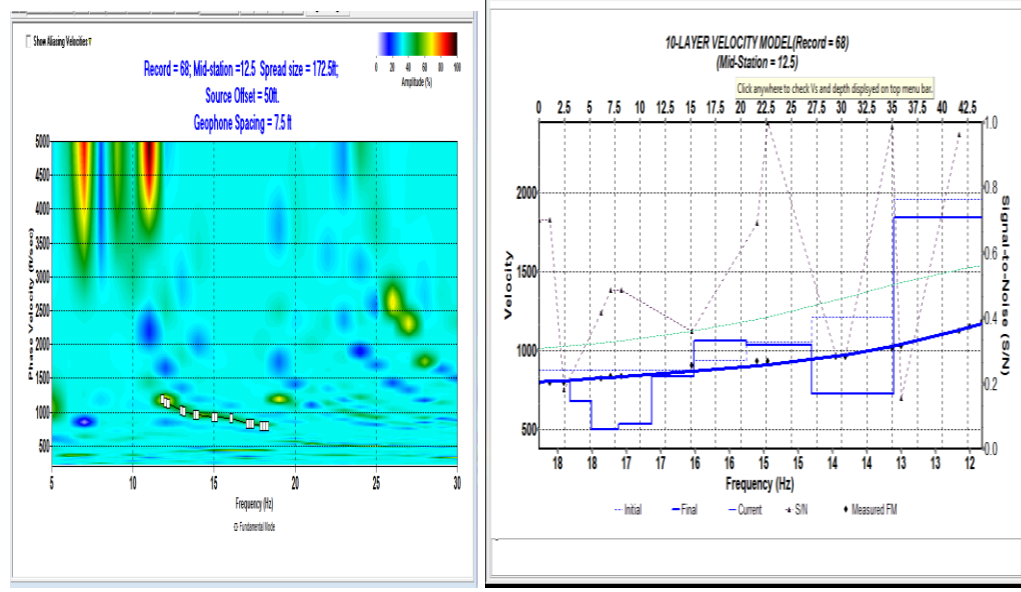


(v) 7.5-ft spacing and 30-ft offset.

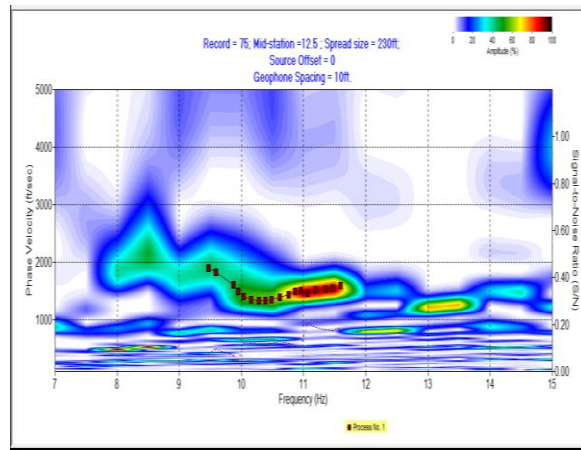


(w) 7.5-ft spacing and 40-ft offset.

Figure 4.11: All the generated dispersion curves and the inverted shear wave velocity model for the different tests (Cont.)

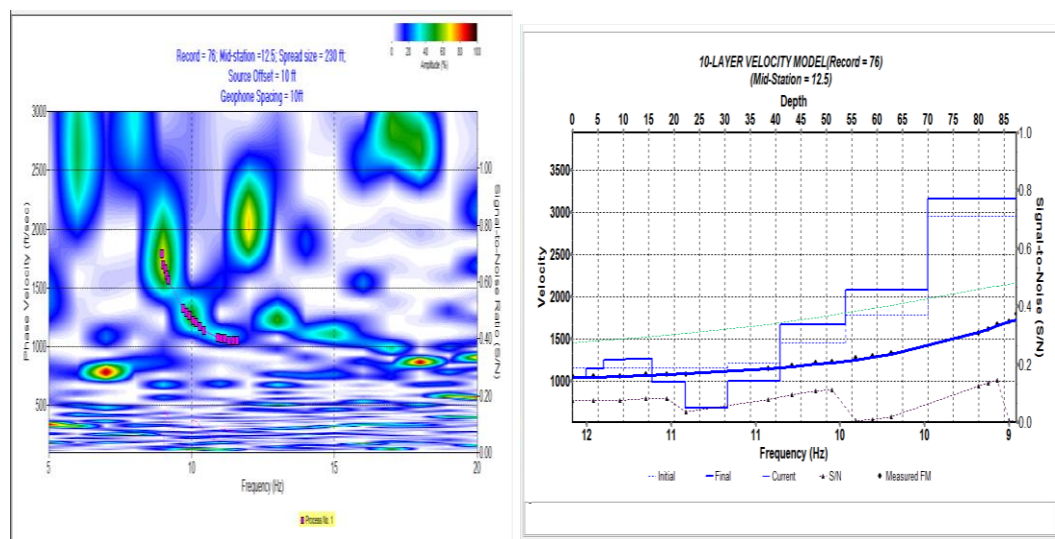


(x) 7.5-ft spacing and 50-ft offset.

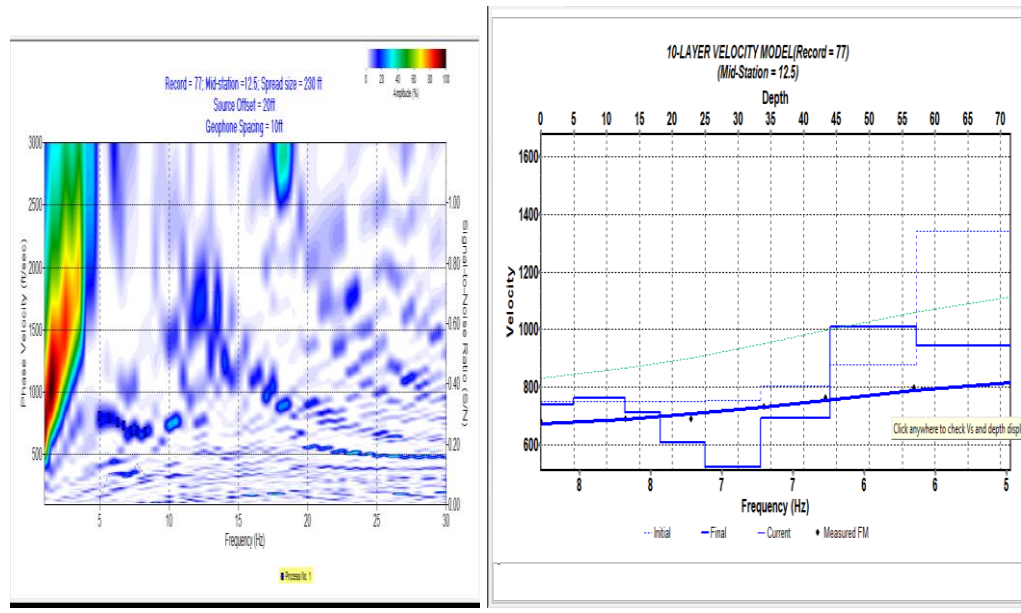


(y) 10-ft spacing and 0-ft offset.

Figure 4.11: All the generated dispersion curves and the inverted shear wave velocity model for the different tests (Cont.)

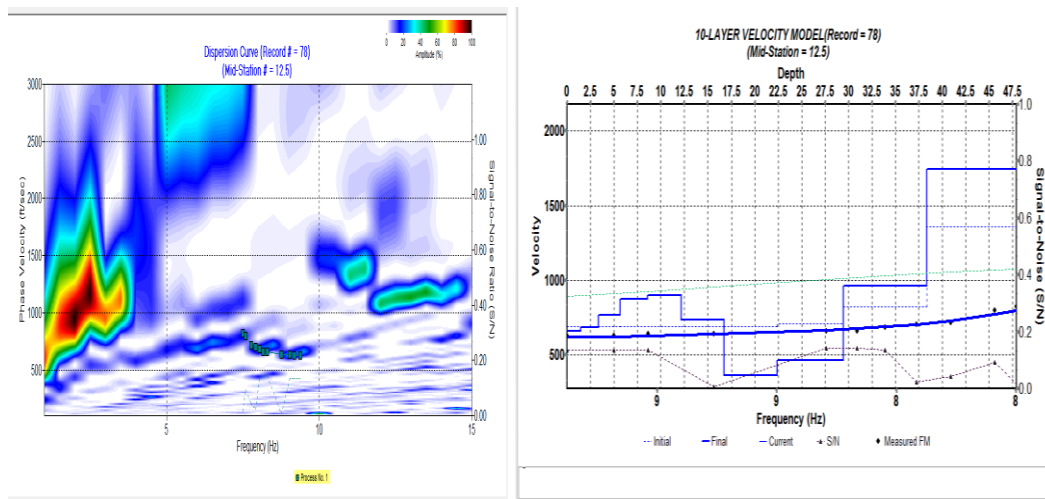


(z) 10-ft spacing and 10-ft offset.

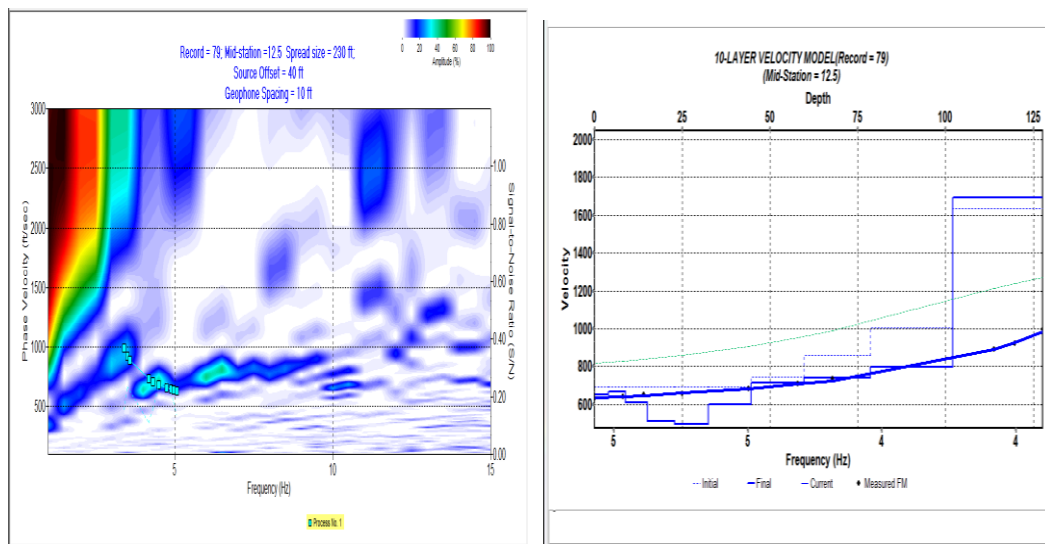


(aa) 10-ft spacing and 20-ft offset.

Figure 4.11: All the generated dispersion curves and the inverted shear wave velocity model for the different tests (Cont.)

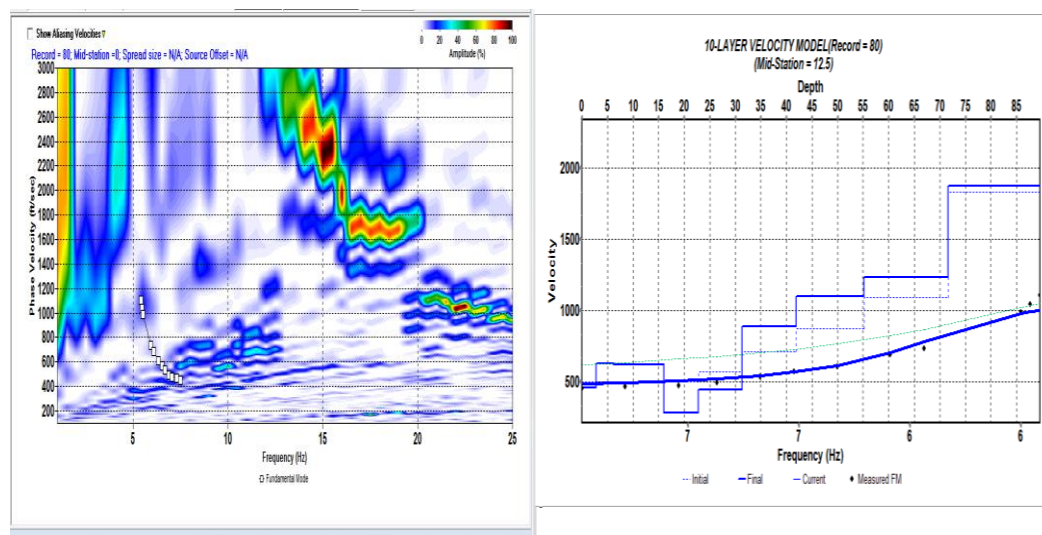


(ab) 10-ft spacing and 30-ft offset.



(ac) 10-ft spacing and 40-ft offset.

Figure 4.11: All the generated dispersion curves and the inverted shear wave velocity model for the different tests (Cont.)



(ad) 10-ft spacing and 50-ft offset.

Figure 4.11: All the generated dispersion curves and the inverted shear wave velocity model for the different tests (Cont.)

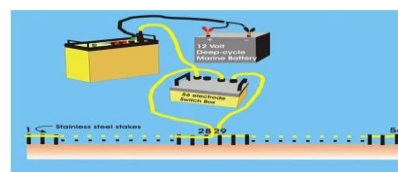
4.4 ELECTRICAL RESISTIVITY TOMOGRAPHY (ERT)

4.4.1 Site Setup. Two measuring tapes were used to measure out the required distance approximately 415- ft. along a flat surface on the site. NW-SE trend was chosen because it makes room for the required length of array. After measuring out the required length, metal stakes were installed at 5-ft. interval along the array making it 84 metal stakes which covered the array length of 415-ft. The installation of the stakes was supervised to make sure they were installed about half of the length of the stakes deep inside the ground. Then four cables each consists of 20 electrodes were spread along the array and each electrode was attached to each metal stakes (84 electrodes attached to 84 metal stakes) the four cable are connected to each other with a connector at both ends of the cable. The first two cables were connected to each other and the last two were also connected to each other, then the tail of the first two cables was connected to the switch

box also the head of the last two cables was connected to the switch box. The switch box has two Amphenol (male and female) connectors (black plastic type) and two female MS3476L18-32S connectors (metal type). The Amphenol connectors are used to connect the switch box to the SuperSting instrument or daisy-chaining to other switch boxes to control more electrodes. The MS3476L18-32S are used to connect the electrodes to the instrument, use mating connector MS3476L18-32P. The connector marked “Low address cable” is used to address electrodes 1-42. Pin 1 of the connector should be connected to electrode 1, pin 2 to electrode 2 and so on. The connector marked “High address cable” is used to address electrodes 43-84. Pin 1 of the connector was connected to electrode 42, pin 2 to electrode 43 and so on. An adapter delivered with the switch box was used for connecting the female connector of a passive cable to the female connector of the switch box. The SuperSting was powered by two external 12 V DC batteries which were in the boost mode. The batteries are attached to the instrument using the power cable. When in main mode, the power cable is connected to the connector marked “Power” on the SuperSting front panel. The red and black Mueller clips were attached to the positive and the negative poles, respectively, of a 12 V battery. Figure 4.12 below show the switch box and how it can be connected to the SuperSting, while Figure 4.13 shows the array set up for the data acquisition.



(a) Switch box



(b) SuperSting, switch box and 12V battery

Figure 4.12: Switch box and SuperSting

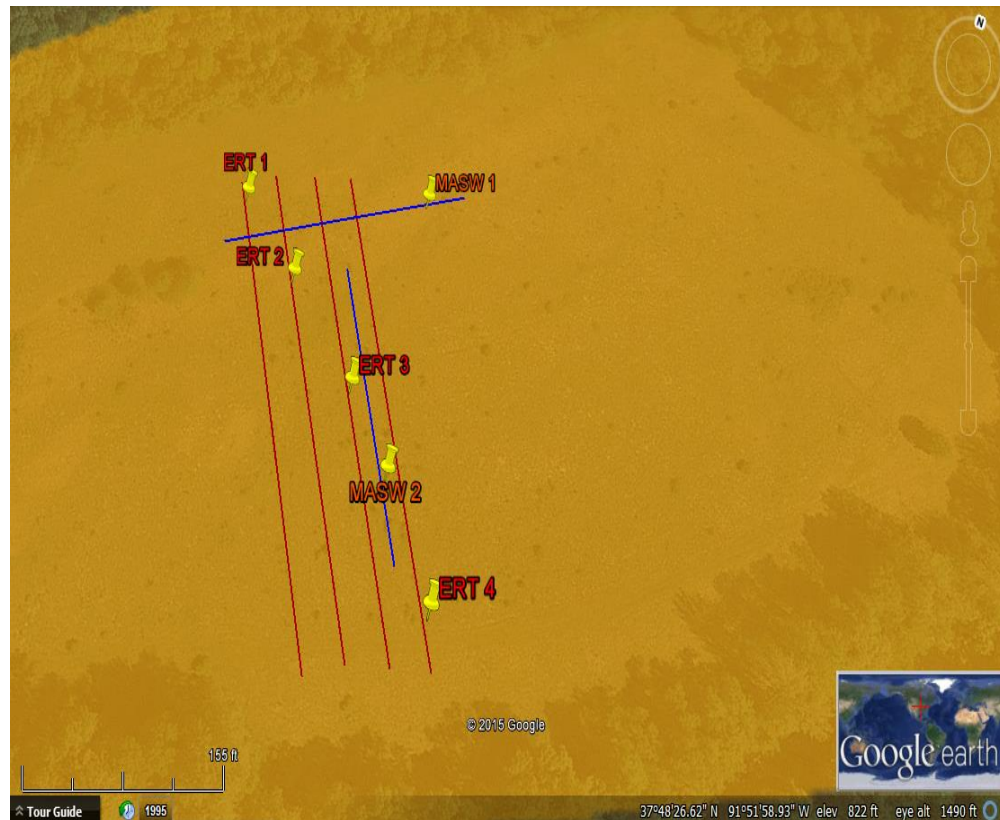


Figure 4.13: Four ERT traverses (red) and two MASW traverses (blue)

4.4.2 Field Procedure and Equipment. The SuperSting Resistivity System, produced by Advanced Geosciences, Incorporated, was used to complete the survey. The SuperSting R8 transmitter/receiver is a self-regulated eight channel digital volt meter, capable of transferring up to two amps of current to the ground. With auxiliary switch boxes, the SuperSting R8 is capable of conducting multiple readings using a string of up to 84 electrodes. The equipment was supplied with the SuperSting R8, 4electrode cables, each cable with 21 electrodes and 84 steel stakes. The SuperSting R8 system requires an external 12 volt battery source; however, the performance of the equipment can be optimized by using a pair, volt batteries connected in series (Advanced Geosciences,

Incorporated, 2006). Wet cell batteries were utilized for this application. The use of wet cell batteries is preferred due to the ability to repeatedly drain the battery source and recharge, within minimal impact to the battery core (Advanced Geosciences Incorporated, 2008). The SuperSting R8 requires commands in order to properly trigger electrodes for current induction and measurement of potential difference (Advanced Geosciences Incorporated, 2008).

AGI Administrator software package, provided with the SuperSting Resistivity System, allows the user to input array parameters to model resulting survey pseudosections. The generated model will give the user an estimate of penetration depth, data point coverage, and an estimation of time required to perform the survey. An example of a generated pseudosection is provided in Figure 4.14. After an array configuration is created, the user can create a unit less command file usable by the SuperSting R8 transmitter/receiver. Another notable feature of the AGI Administrator software is the ability to reverse the array direction, so that points are collected starting from the end of the electrode string and progresses towards the first electrode in the array. This progression is advantageous during a roll-along survey. The SuperSting R8 stores all measurements of current and potential difference during the course of a survey. Each measurement is coordinated with the address of the four electrodes associated with the respective reading. With the capability of referencing coordinate or nodal locations of past readings, the equipment can conclude a survey once all readings within a new domain are acquired. By not overlapping existing data, the use of a reverse array provides an efficient means of surveying and data storage for roll along applications (Advanced Geosciences Incorporated, 2008).

For the purposes, of this survey, a dipole-dipole array was selected due to the need for high lateral resolution and the relatively shallow depth of interest approximately 50-feet. The array was modeled in the AGI Administrator program, and then transferred to the SuperSting R8 equipment for surveying purposes.

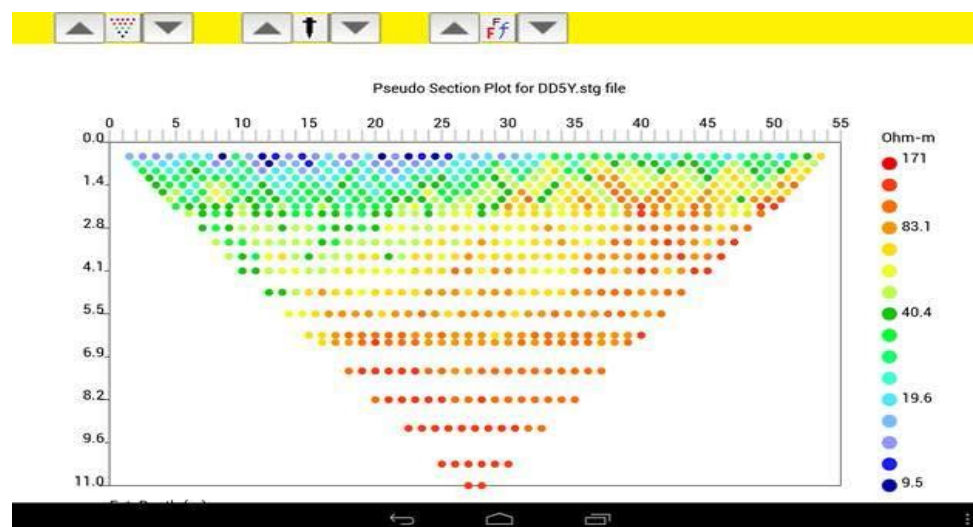


Figure 4.14: SuperSting Manager App, Plot pseudo section (Advanced Geosciences Incorporated, 2008).

4.4.3 Data Acquisition. Consideration was given to the desired resolution, depth of investigation, and available equipment. For the purposes of this study it was determined that an interval spacing of 5 feet would adequately profile the bedrock as well as the surficial materials. It was estimated that for electrodes, at an interval spacing of 5 feet, the approximate depth of penetration would be approximately 83 feet. This is based on the assumption that the penetration depth is approximately 20 percent of the survey length (Advanced Geosciences Incorporated, 2008). Each run would cover 415 linear feet

of the site. It should be noted that the AGI Administrator program generates a generic command file which can be used with any given interval spacing (Figure 4.15)

For the purpose of this research, ERT data was acquired along four different traverses trending NW-SE in order to have more coverage of the study area. Each of the traverses is 20-ft apart from the other and the same array configurations were used for all of the traverses.



(a) Set up



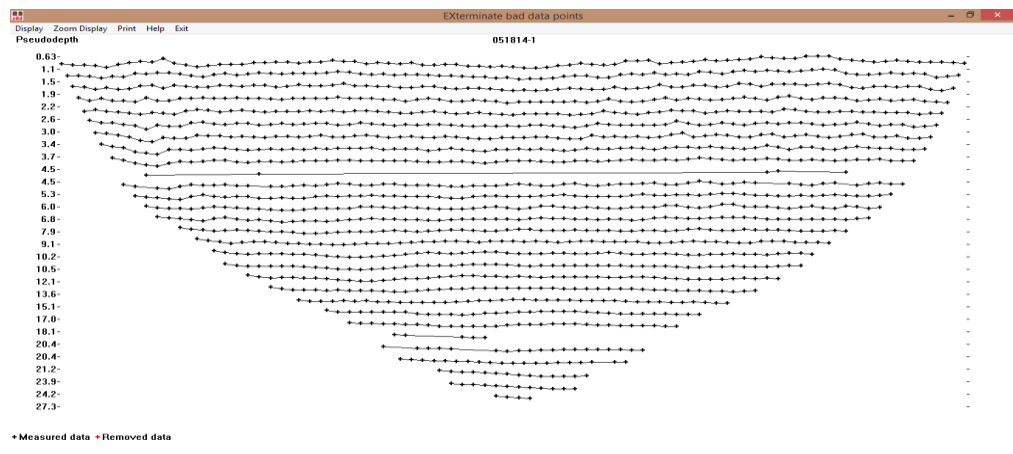
(b) Acquisition in progress.

Figure 4.15: Equipment set up for the ERT acquisition

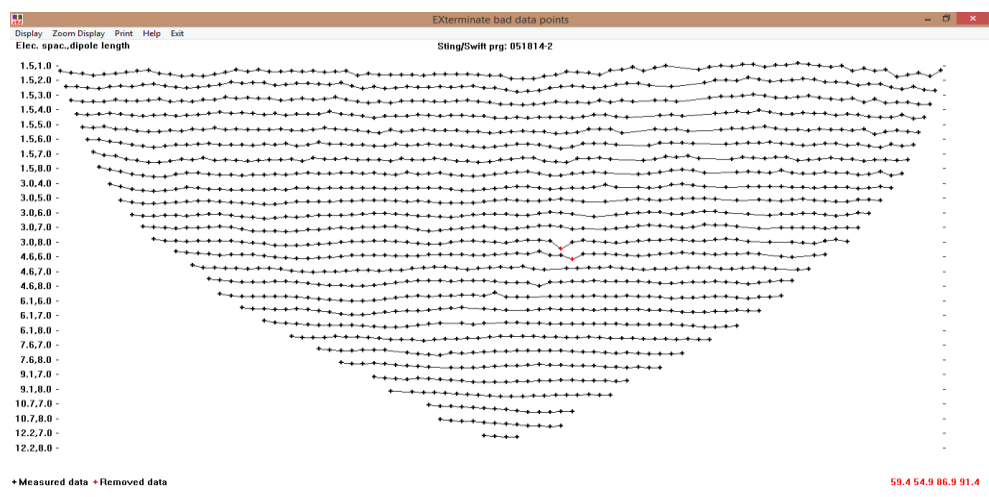
4.4.4 Data Processing and Inversion. The raw data stored in the SuperSting R8 must be extracted and converted into a form suitable for processing. The AGI Administrator software is used to download and convert field data into a form readable for the AGI EarthImager 2D analysis software. In the raw form, measurements of apparent resistivity can be plotted into the respective pseudosection. The EarthImager 2D software uses the measured apparent resistivity pseudosection during the inversion process to recreate an earth model fitting the conductive characteristics of the recorded raw model. The default model used to begin the inversion process is a homogenous half-space with an assigned resistivity equivalent to measured apparent resistivity values, in log form. Other models may be used to begin the inversion by manually selecting available user-defined functions (Advanced Geosciences, Incorporated, 2009).

The inversion process is iterative in two ways. First, EarthImager uses an iterative routine to develop a matching earth model, using an error tolerance or maximum number of iterations as criteria for terminating the inversion. Secondly, if the level of error in a given model is beyond acceptable limits (i.e. root mean square or L2 Normalization terms), the raw data can be evaluated to determine whether outlier measurements are causing unwanted error in the inverted model. Disruptive points, or noise, can result from cultural conditions present at the time of the survey, recordings of negative values, or malfunctioning equipment. Corrupting data points can be isolated by using the misfit histogram generated in the EarthImager program, manually eliminating data points in the pseudosection or by suppressing the readings collected from particular electrodes. The iteration process can stop when the user is satisfied that the represented model demonstrates the subsurface condition, within the accepted error tolerances for the survey

(Advanced Geosciences Incorporated, 2009). Figure 4.16 below show all the pseudosections and data points generated for the ERT traverses while Figure 4.17 show final the inversion results for the four ERT traverses.

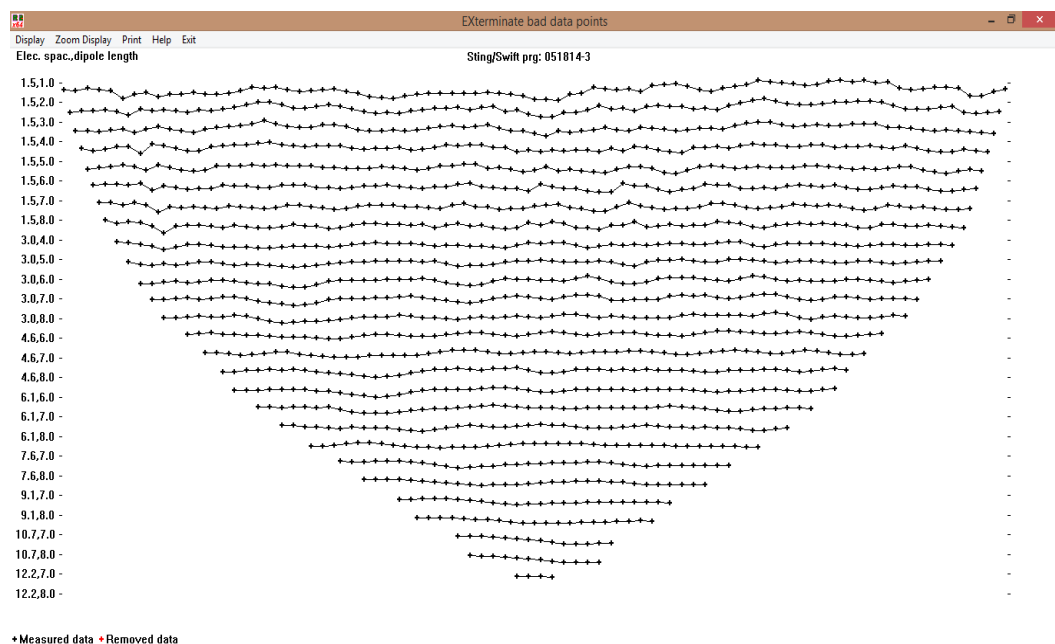


(a) ERT line 1 showing all the data points and 84 electrodes

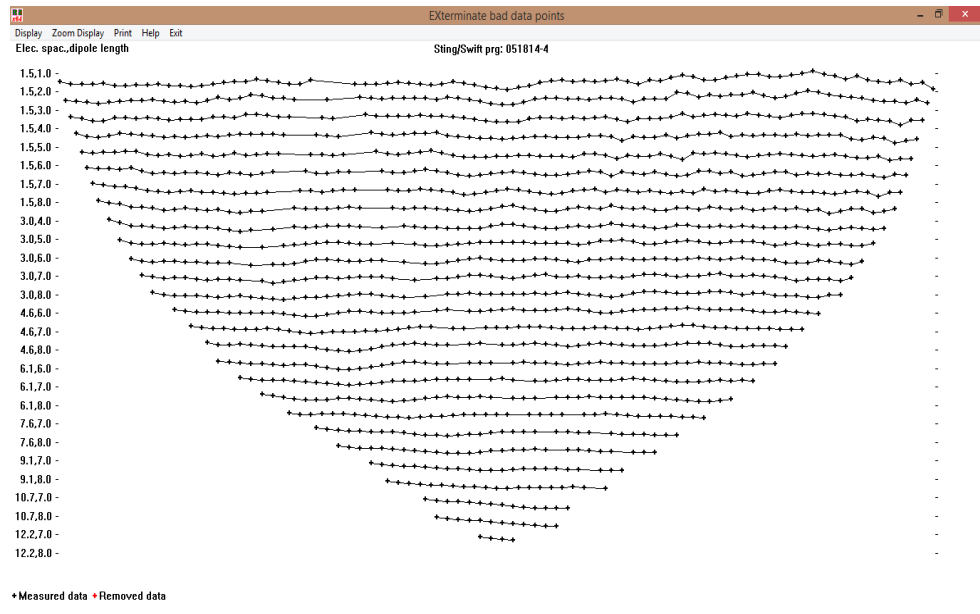


(b) ERT line 2 showing all the data points and 84 electrodes.

Figure 4.16: Pseudo sections and data points generated for the ERT traverses

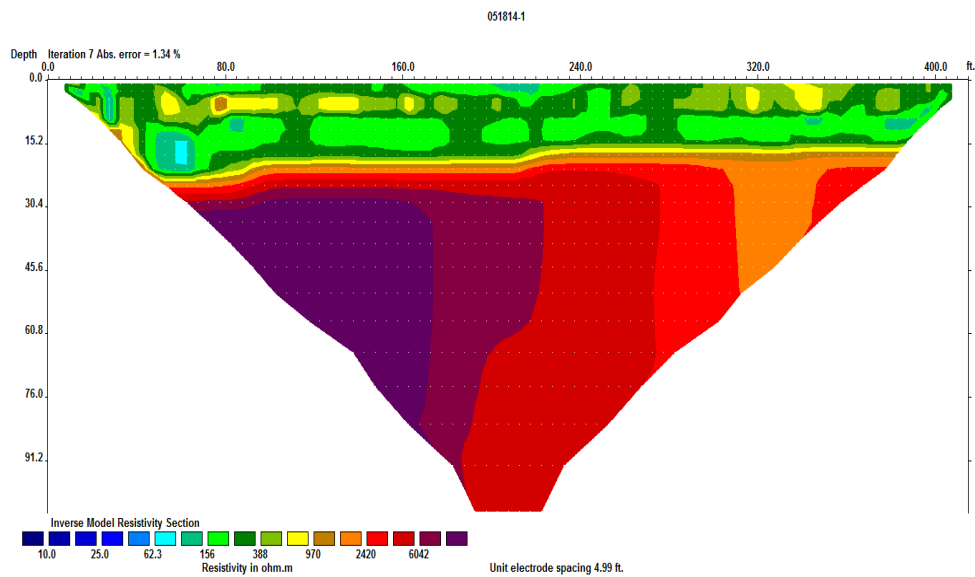


(c) ERT line 3 showing all the data points and 84 electrodes

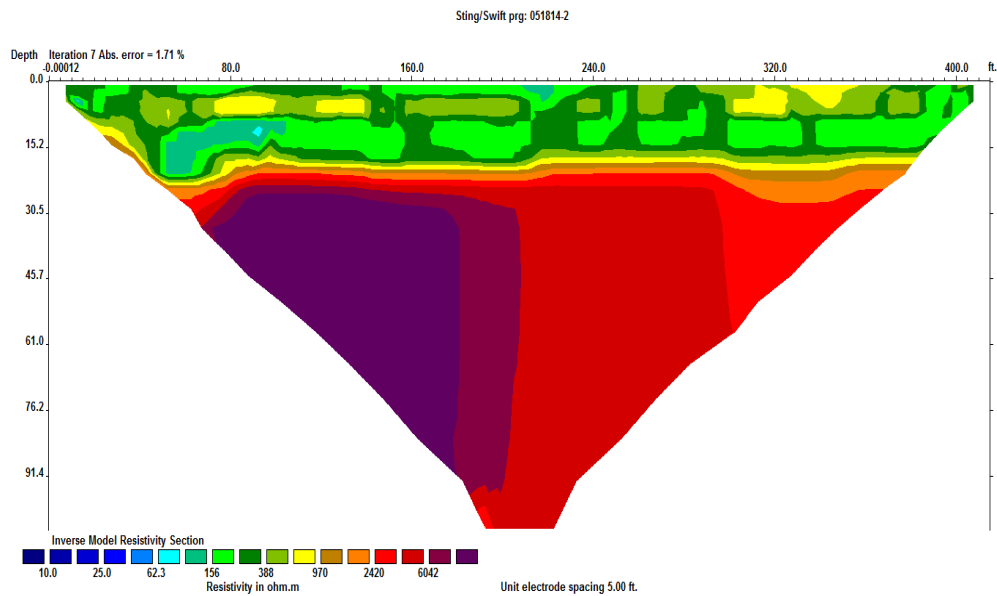


(d) ERT line 4 showing all the data points and 84 electrodes.

Figure 4.16: Pseudo sections and data points generated for the ERT traverses (Cont.)

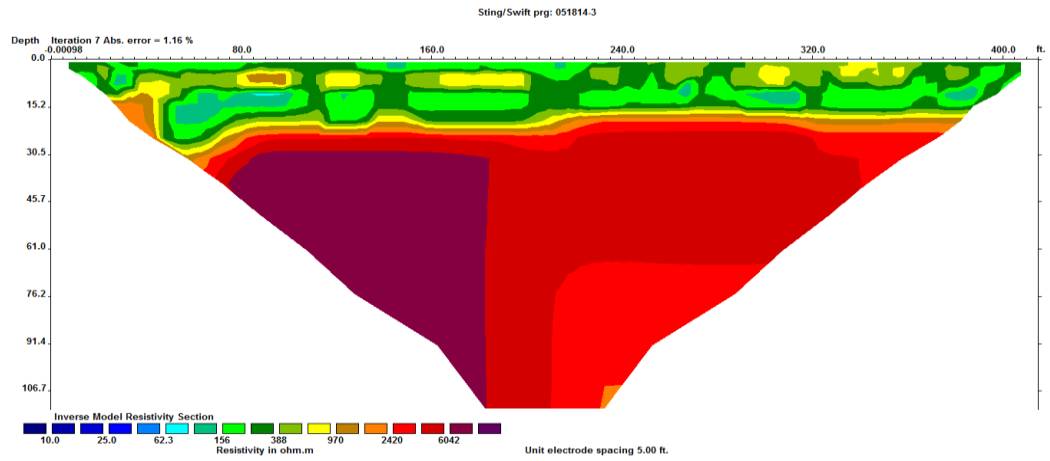


(a) ERT line 1

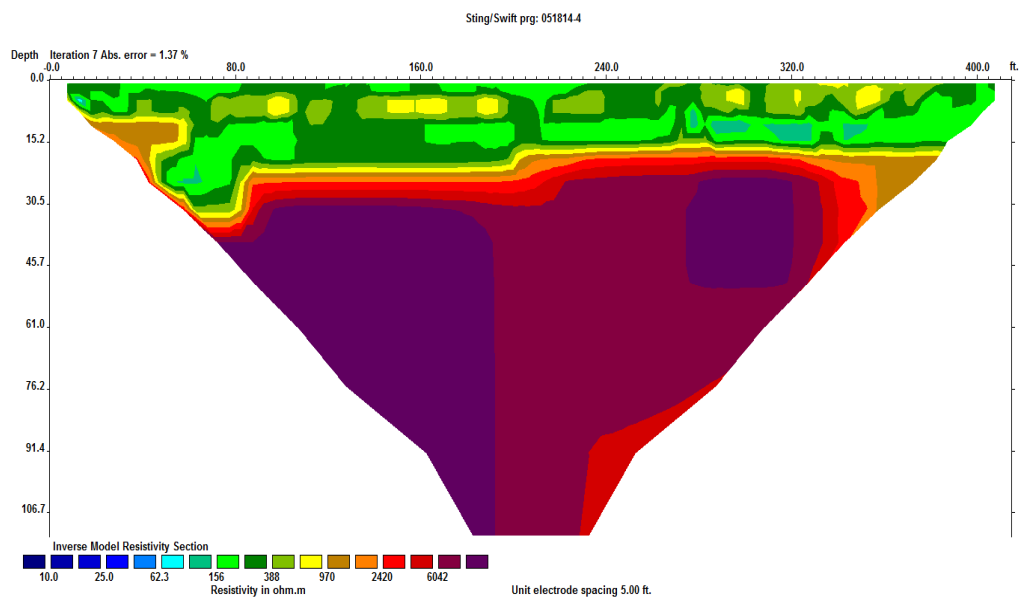


(b) ERT line 2

Figure 4.17: Final inverted section for the resistivity analysis



(c) ERT line 3



(d) ERT line 4

Figure 4.17: Final inverted section for the resistivity analysis (Cont.)

Furthermore, data points from four different ERT lines were collated to generate three dimensional model (3D) using Voxler 3 software produced by Golden software Inc.

Voxler 3 creates powerful, fast, customized 3D images of any scientific data, it is user friendly and easy to import data in a multitude of file formats to create stunning models that visualize the relationships across your data set. This robust, yet user-friendly program gives you the power to display your data in a variety of formats and colors, capture video animation of your moving model, and select from several image and data export options (Golden Software, Inc., 2013). Voxler gives you full control of your 3D data. You can filter anomalies, duplicates, or areas you want eliminated. Interactively manipulate your data while viewing the results, and personalize Voxler with a variety of settings. It offers a multitude of computational modules and graphics display modules that will simply get your modeling. Figure 4.18 show 3D model for all the four lines of ERT generated with Voxler 3 software.

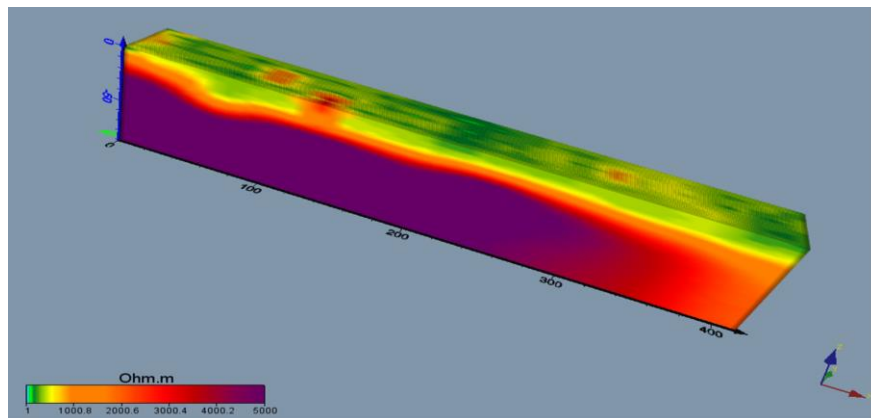
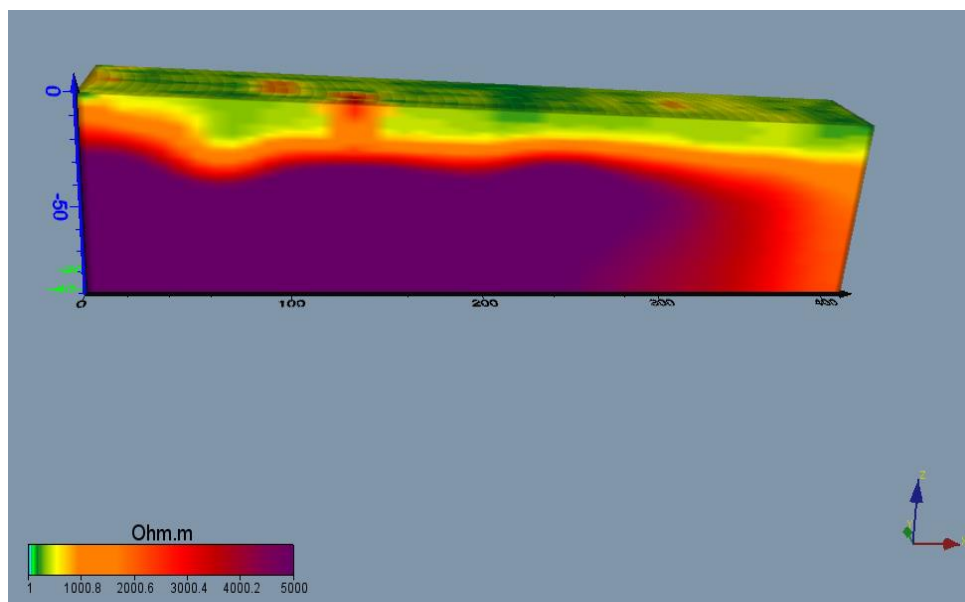
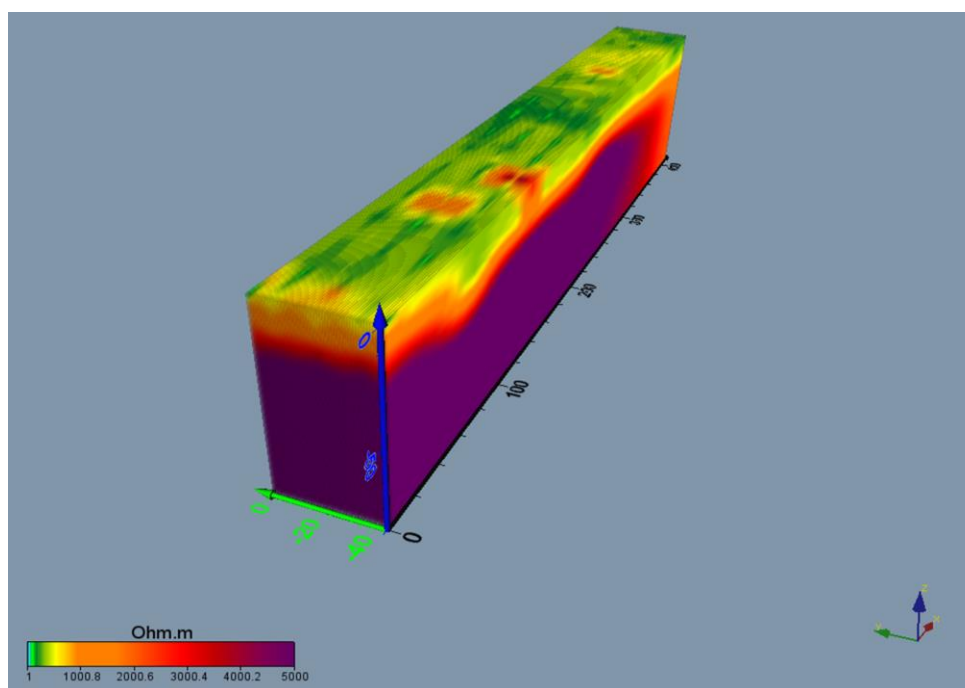


Figure 4.18: 3-D ERT Model generate with Voxler software. (a) Inclined view



(b) Lateral view.



(c) Orthogonal view.

Figure 4.18: 3-D ERT Model generate with Voxler software (Cont.)

4.5 CONCLUSIONS

These tests were conducted to determine the optimum acquisition parameters (source offset and receiver spacing) for MASW data collection along with the accuracy of the MASW dispersion curves and Vs profiles when compared to the 2D and 3D electrical resistivity tomography.

5. RESULTS

5.1 OVERVIEW

The MASW results from the data collected will be presented herein. My concentration will be focused on results from different geophone spacing and offset distance and their respective frequency ranges, phase velocities and depth of investigation. The results are presented in a tabular form that compare the surface wave dispersion curves obtained from various source offset distances and receiver spacings, while keeping the other parameters unchanged. The dispersion curve result presented herein are the same with the generated dispersion curves and shear wave velocity profiles presented in chapter four. Also results from the final inverted section for the resistivity analysis for ERT traverses will be presented as well.

Finally, results from muting as a processing tool will presented with emphasis on the importance and limitations of muting.

5.2 RESULTS FROM MASW DATA

Results from dispersion curves and shear wave velocity profiles for all the tested parameters are presented in Table 5.1 below. The discussion will be focused on the comparison of these parameters (Geophone spacing and Offset distances) with respect to frequency range, phase velocity range, depth to top of bedrock and the maximum depth of investigation. From the overall dispersion curves and shear wave velocity profiles, the shear wave velocity of the rock was set to be 1250-ft/sec and the fundamental mode

ranges from 15Hz to 32 Hz, while that phase velocity for the fundamental mode ranges from 500-ft/sec to 1500-ft/sec.

(i) 1-ft Geophone Spacing

At 1-ft geophone spacing and 0-ft offset, the frequency range picked from the dispersion curve is 55Hz to 110Hz, phase velocity ranges from 1000-ft/sec to 1350-ft/sec. Velocity model could not be generated because fundamental modes could not be picked. The result shows that the frequency range picked were not fundamental modes and phase velocity range was high, there by depicting higher mode. The velocity model was inaccurate; it was only included here to show problems that arise if higher modes are picked.

For 1-ft geophone spacing and 10-ft offset, the frequency ranges from 15Hz to 30Hz, phase velocity ranges from 400-ft/sec to 1500-ft/sec, depth to bedrock is 17.5-ft and the maximum depth of investigation is 37-ft. The frequency range picked fall within the fundamental mode likewise the phase velocity ranges.

When using 1-ft geophone spacing and 20-ft offset, frequency ranges from 15Hz to 20Hz, phase velocity ranges from 400-ft/sec to 1600-ft/sec, depth to bedrock is 17.5-ft and the maximum depth of investigation is 50-ft. The frequency range picked fall within the fundamental mode likewise the phase velocity ranges.

For 1-ft geophone spacing and 30-ft offset, the frequency ranges from 20Hz to 30Hz, phase velocity ranges from 500-ft/sec to 1450-ft/sec, depth to bedrock is 14-ft and the maximum depth of investigation is 22.5-ft. The frequency range picked were not fundamental mode likewise the phase velocity ranges.

For 1-ft geophone spacing and 40-ft receiver offset, the frequency ranges from 15Hz to 30Hz, phase velocity ranges from 1450-ft/sec to 1500-ft/sec, depth to bedrock is 19.5-ft and the maximum depth of investigation is 42.5-ft. The frequency range picked fall within the fundamental mode likewise the phase velocity ranges.

Finally, 1-ft geophone spacing and 50-ft receiver offset, the frequency ranges from 15Hz to 30Hz, phase velocity ranges from 500-ft/sec to 1500-ft/sec, depth to bedrock is 16-ft and the maximum depth of investigation is 35-ft. The frequency range picked fall within the fundamental mode likewise the phase velocity ranges.

(ii) 2.5-ft Geophone Spacing

At 0-ft receiver offset, the frequency ranges from 15Hz to 30Hz, phase velocity ranges from 500-ft/sec to 1500-ft/sec, depth to bedrock is 18-ft and the maximum depth of investigation is 38-ft. The frequency range picked fall within the fundamental mode likewise the phase velocity ranges.

At 10-ft receiver offset, the frequency ranges from 15Hz to 32Hz, phase velocity ranges from 500-ft/sec to 1500-ft/sec, depth to bedrock is 19-ft and the maximum depth of investigation is 31-ft. The frequency range picked fall within the fundamental mode likewise the phase velocity ranges.

At 20-ft receiver offset, the frequency ranges from 15Hz to 33Hz, phase velocity ranges from 500-ft/sec to 1600-ft/sec, depth to bedrock is 22.5-ft and the maximum depth of investigation is 38-ft. The frequency range picked fall within the fundamental mode likewise the phase velocity ranges.

At 30-ft receiver offset, the frequency ranges from 15Hz to 30Hz, phase velocity ranges from 500-ft/sec to 1500-ft/sec, depth to bedrock is 21-ft and the maximum depth

of investigation is 35-ft. The frequency range picked fall within the fundamental mode likewise the phase velocity ranges.

At 40-ft receiver offset, the frequency ranges from 15Hz to 33Hz, phase velocity ranges from 500-ft/sec to 1500-ft/sec, depth to bedrock is 23-ft and the maximum depth of investigation is 37-ft. The frequency range picked fall within the fundamental mode likewise the phase velocity ranges.

At 50-ft receiver offset, the frequency ranges from 18Hz to 35Hz, phase velocity ranges from 500-ft/sec to 1000-ft/sec, depth to bedrock is 15-ft and the maximum depth of investigation is 27-ft. The frequency range picked fall within the fundamental mode likewise the phase velocity ranges.

(iii) 5-ft Geophone Spacing

At 0-ft receiver offset, the frequency ranges from 13Hz to 35Hz, phase velocity ranges from 500-ft/sec to 1500-ft/sec, depth to bedrock is 15-ft and the maximum depth of investigation is 55-ft. The frequency range picked fall within the fundamental mode likewise the phase velocity ranges.

At 10-ft receiver offset, the frequency ranges from 15Hz to 28Hz, phase velocity ranges from 500-ft/sec to 1400-ft/sec, depth to bedrock is 18-ft and the maximum depth of investigation is 38-ft. The frequency range picked fall within the fundamental mode likewise the phase velocity ranges.

At 20-ft receiver offset, the frequency ranges from 10Hz to 30Hz, phase velocity ranges from 500-ft/sec to 2000-ft/sec, depth to bedrock is 20-ft and the maximum depth of investigation is 80-ft. The frequency range picked fall within the fundamental mode likewise the phase velocity ranges.

At 30-ft receiver offset, the frequency ranges from 15Hz to 25Hz, phase velocity ranges from 500-ft/sec to 1500-ft/sec, depth to bedrock is 15-ft and the maximum depth of investigation is 40-ft. The frequency range picked fall within the fundamental mode likewise the phase velocity ranges.

At 40-ft receiver offset, the frequency ranges from 12Hz to 25Hz, phase velocity ranges from 500-ft/sec to 2000-ft/sec, depth to bedrock is 20-ft and the maximum depth of investigation is 80-ft. The frequency range picked fall within the fundamental mode likewise the phase velocity ranges.

At 50-ft receiver offset, the frequency ranges from 15Hz to 23Hz, phase velocity ranges from 500-ft/sec to 1500-ft/sec, depth to bedrock ranges 19-ft and the maximum depth of investigation is 55-ft. The frequency range picked fall within the fundamental mode likewise the phase velocity ranges.

(iv) 7.5-ft Geophone Spacing

At 0-ft receiver offset, the frequency ranges from 10Hz to 18Hz, phase velocity ranges from 1000-ft/sec to 2000-ft/sec, depth to bedrock is 37-ft and the maximum depth of investigation is 80-ft. The frequency range picked were not fundamental mode likewise the phase velocity ranges.

At 10-ft receiver offset, the frequency ranges from 5Hz to 18Hz, phase velocity ranges from 900-ft/sec to 2500-ft/sec, depth to bedrock is 26-ft and the maximum depth of investigation is 150-ft. The frequency range picked were not fundamental mode likewise the phase velocity ranges.

At 20-ft receiver offset, the frequency ranges from 8Hz to 18Hz, phase velocity ranges from 900-ft/sec to 2600-ft/sec, depth to bedrock is 30-ft and the maximum depth

of investigation is 130-ft. The frequency range picked were not fundamental mode likewise the phase velocity ranges.

At 30-ft receiver offset, the frequency ranges from 12Hz to 18Hz, phase velocity ranges from 900-ft/sec to 1500-ft/sec, depth to bedrock is 36-ft and the maximum depth of investigation is 60-ft. The frequency range picked were not fundamental mode likewise the phase velocity ranges.

At 40-ft receiver offset, the frequency ranges from 10Hz to 18Hz, phase velocity ranges from 900-ft/sec to 1500-ft/sec, depth to bedrock is 24-ft and the maximum depth of investigation is 70-ft. The frequency range picked were not fundamental mode likewise the phase velocity ranges.

At 50-ft receiver offset, the frequency ranges from 12Hz to 18Hz, phase velocity ranges from 900-ft/sec to 1200-ft/sec, depth to bedrock is 35-ft and the maximum depth of investigation is 43-ft. The frequency range picked were not fundamental mode likewise the phase velocity ranges.

(v) 10-ft Geophone Spacing

At 0-ft receiver offset, the frequency ranges from 9.5Hz to 18Hz and phase velocity ranges from 1500-ft/sec to 2000-ft/sec. shear wave velocity profile of this data could not be generated hence, no information regarding depth to bedrock nor the maximum depth of investigation. The frequency range picked were not fundamental mode likewise the phase velocity ranges.

At 10-ft receiver offset , the frequency ranges from 8Hz to 12Hz , phase velocity ranges from 1000-ft/sec to 1800-ft/sec, depth to bedrock is 10-ft and the maximum depth

of investigation is 86-ft. The frequency range picked were not fundamental mode likewise the phase velocity ranges.

At 20-ft receiver offset, the frequency ranges from 5Hz to 8Hz, phase velocity ranges from 600-ft/sec to 800-ft/sec, depth to bedrock is 45-ft and the maximum depth of investigation is 70-ft. The frequency range picked were not fundamental mode likewise the phase velocity ranges.

At 30-ft receiver offset, the frequency ranges from 7Hz to 9Hz, phase velocity ranges from 600-ft/sec to 800-ft/sec, depth to bedrock is 38-ft and the maximum depth of investigation is 47.5-ft. The frequency range picked were not fundamental mode likewise the phase velocity ranges.

At 40-ft receiver offset, the frequency ranges from 3Hz to 5Hz, phase velocity ranges from 600-ft/sec to 1000-ft/sec, depth to bedrock is 100-ft and the maximum depth of investigation is 125-ft. The frequency range picked were not fundamental mode likewise the phase velocity ranges.

Finally at 50-ft receiver offset, the frequency ranges from 5Hz to 7Hz, phase velocity ranges from 400-ft/sec to 1100-ft/sec, depth to bedrock is 55-ft and the maximum depth of investigation is 90-ft. The frequency range picked were not fundamental mode likewise the phase velocity ranges. Results from all the dispersion curves and generated shear wave velocity profiles are listed in the Table 5.1 below.

Table 5.1: Results from all the dispersion curves and generated shear wave velocity profiles.

S/N	Spacing (Ft.)	Offset (Ft.)	Source (lb)	Frequency Range (Hz)	Phase Velocity (Ft./sec)	Depth to bedrock(Ft.)	Max. depth (Ft.)	Quality
1	1	0	20	55 -110	1000- 1350	-	-	N/A
2	1	10	20	15 - 30	400 -1500	17.5	37	Good quality
3	1	20	20	15 - 20	400 -1600	17.5	50	Good quality
4	1	30	20	20 - 30	500 -1450	14	22.5	Good quality
5	1	40	20	15 - 30	1450-1500	19.5	42.5	Good quality
6	1	50	20	15 - 30	500 -1500	16	35	Good quality
7	2.5	0	20	15 - 30	500 - 1600	18	38	Good quality
8	2.5	10	20	15 - 32	500 - 1500	19	31	Good quality
9	2.5	20	20	15 - 33	500 -1600	22.5	38	Good quality
10	2.5	30	20	15 - 30	500 - 1500	21	45	Good quality
11	2.5	40	20	15 - 33	500 - 1500	22.5	37	Good quality
12	2.5	50	20	18 - 35	500 - 1000	21	27	Good quality
13	5	0	20	13 - 35	500 - 1500	15	55	Good quality
14	5	10	20	15 - 28	500 - 1400	18	38	Good quality
15	5	20	20	10 - -30	500 - 2000	20.5	80	Excellent quality
16	5	30	20	15 - 25	500 - 1500	15	40	God quality
17	5	40	20	12 - 25	500 - 2000	20	80	Excellent quality
18	5	50	20	15 - 23	500 - 1500	19	55	Excellent quality
19	7.5	0	20	10 -18	1000-2000	37	80	Poor quality
20	7.5	10	20	5 - 18	900-2500	26	150	Poor quality
21	7.5	20	20	8 - 18	900 - 2600	30	130	Poor quality
22	7.5	30	20	12 - 18	900-1500	36	60	Poor quality
23	7.5	40	20	10 - 18	900 - 1500	24	70	Poor quality
24	7.5	50	20	12 -18	900 - 1200	35	43	Poor quality
25	10	10	20	8 - 12	1000-1800	10	86	Poor quality
27	10	20	20	5 - 8	600 -800	45	70	Poor quality
28	10	30	20	7 - 9	600 - 800	38	47.5	Poor quality
29	10	40	20	3 - 5	600 - 1000	100	125	Poor quality
30	10	50	20	5 - 7	400 - 1100	55	90	Poor quality

5.3 RESULTS FROM ERT DATA

Results for all the four ERT traverses show that top layer of the site are mainly alluvium with pockets of consolidated sand dominating at the western part of the array.

Top of bedrock in this site is gradational ranging from 17-ft to the excess of 22-ft with resistivity ranging from 388 Ohm-meters to excess of 615 Ohm-meters. There is an indication of a low resistivity zone at the western part of the array, this could depict moist soil which is deposited by the Corn creek which flows 20-ft away from the array. Also parts of the bedrock at the western part of the array have been eroded thereby deepening the bedrock in that area. Figure 5.1 to Figure 5.4 show the details of the ERT results, while Figure 5.5 confirmed the assumption that the top of bedrock ranges from 17-ft to 23-ft.

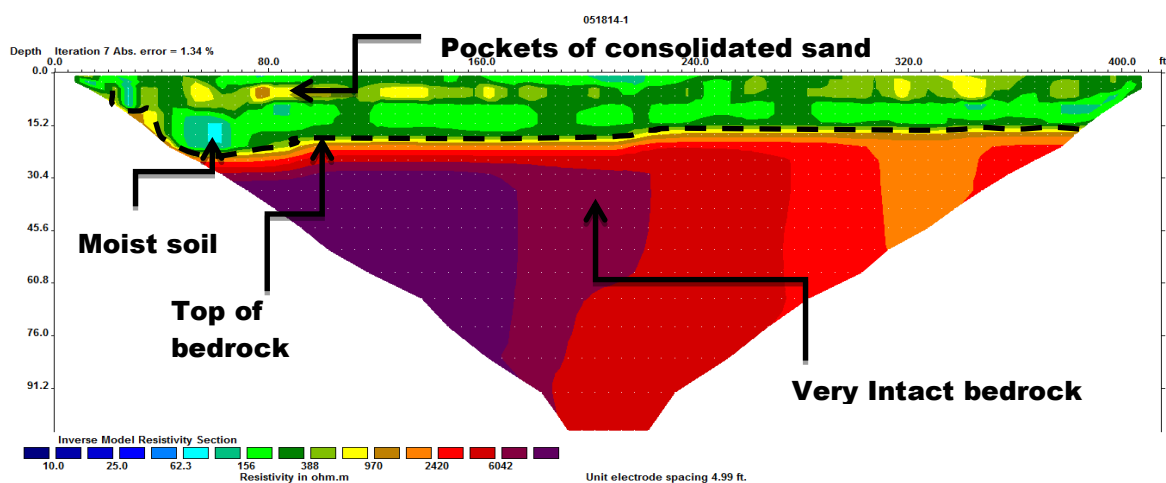


Figure 5.1: Final inverted section for the resistivity analysis for ERT line 1 showing top of bedrock in black dotted lines, pockets of consolidated sand layer, moist soil and very intact bedrock.

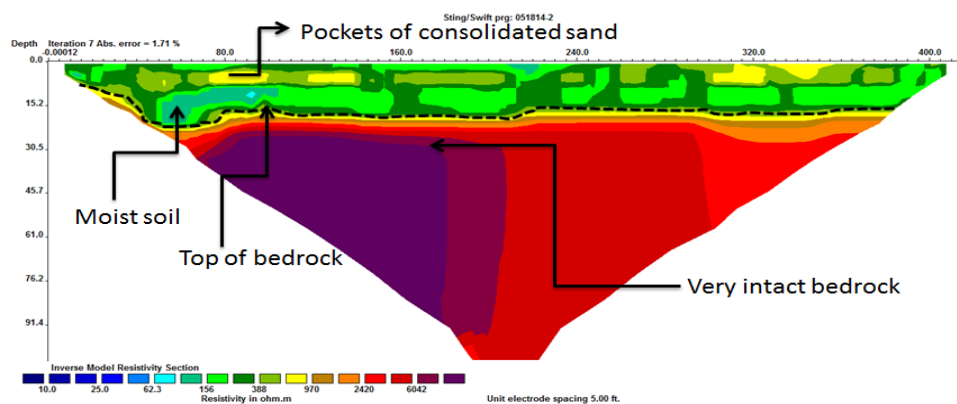


Figure 5.2: Final inverted section for the resistivity analysis for ERT line 2 showing top of bedrock in black dotted lines, pockets of consolidated sand layer, moist soil and very intact bedrock.

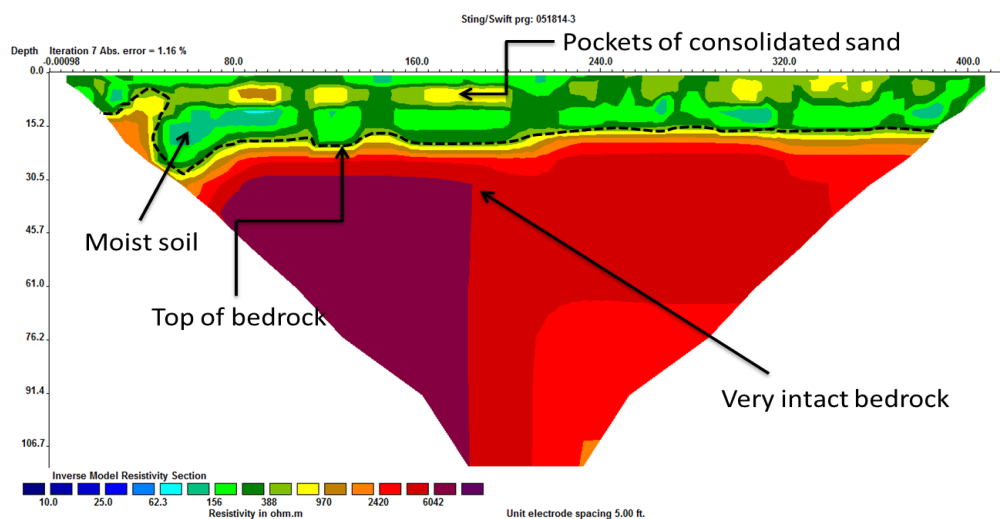


Figure 5.3: Final inverted section for the resistivity analysis for ERT line 3 showing top of bedrock in black dotted lines, pockets of consolidated sand layer, moist soil and very intact bedrock.

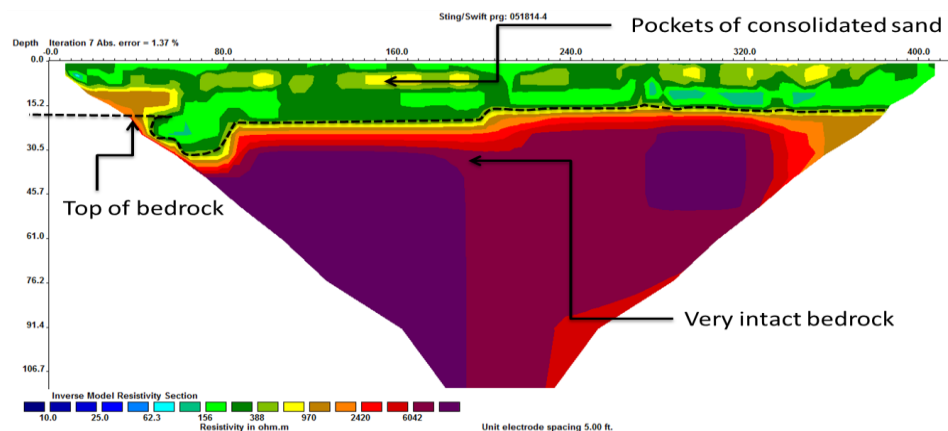


Figure 5.4: Final inverted section for the resistivity analysis for ERT line 4 showing top of bedrock in black dotted lines, pockets of consolidated sand layer, moist soil and very intact bedrock.

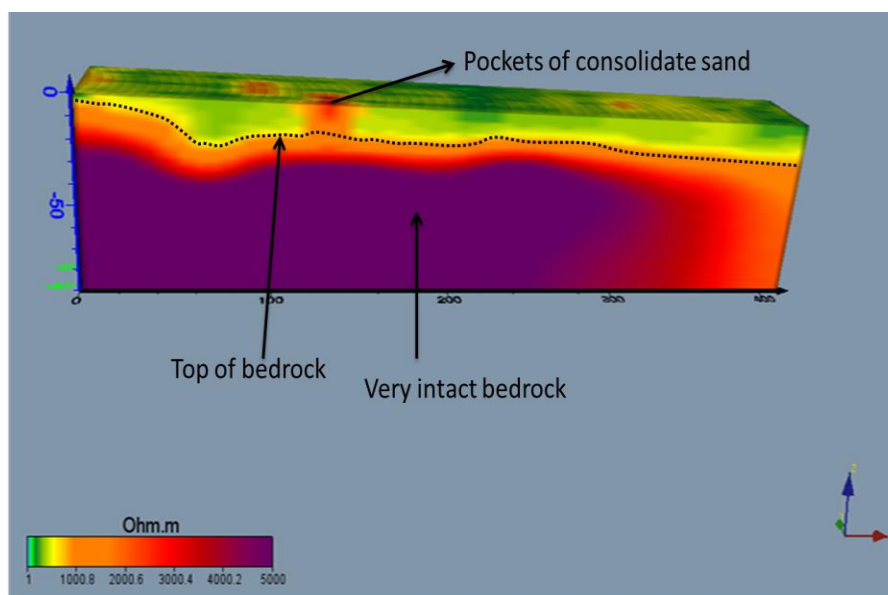


Figure 5.5: 3-D model generated by combining the four ERT traverses using Voxler software.

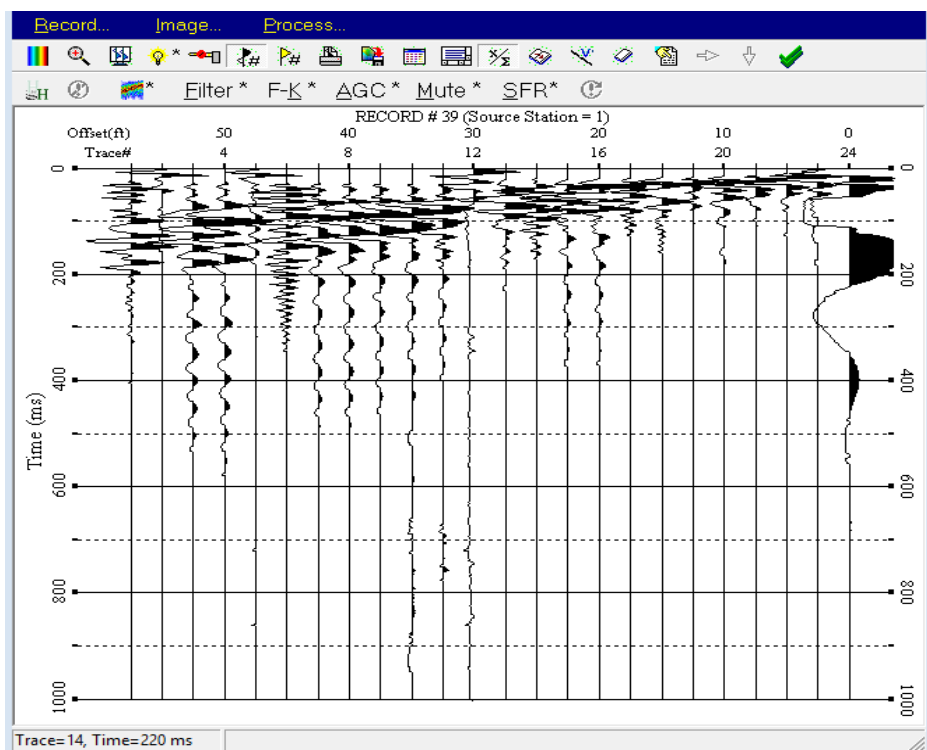
5.4 MUTING

The purpose of muting is to remove specific seismic energy (e.g., dispersion curve), which arrives in specific time frame as a result of its velocity of propagation characteristics (Miller, Ivanov, et al., 2001). For example, in the context of the surface

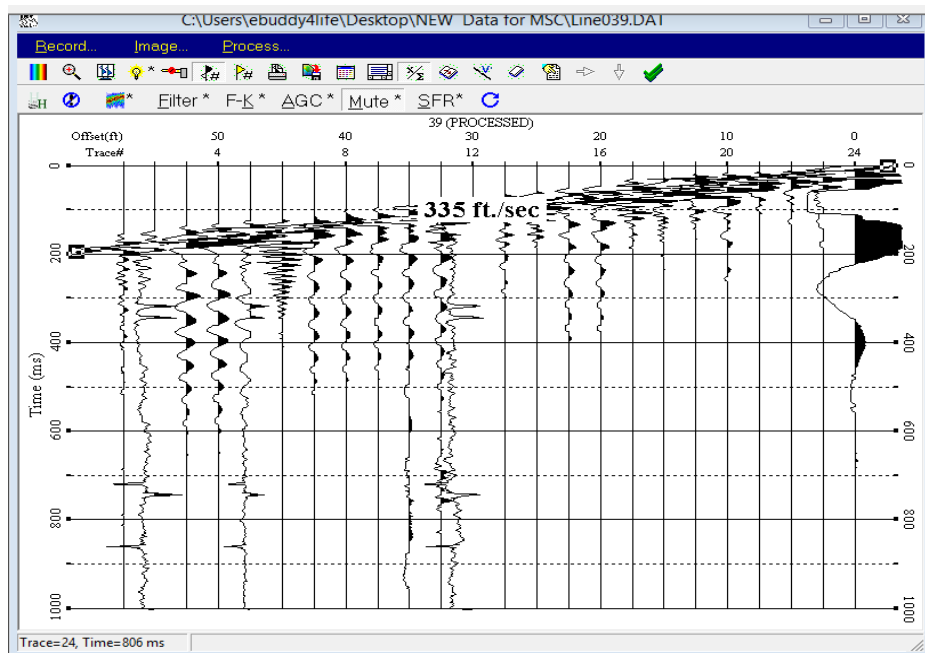
wave method, part of the higher mode energy that propagates faster than the fundamental mode will arrive first on the seismic record. Thus, the fundamental mode energy will begin to appear after certain time, after the arrival of the higher modes. The main condition for the application of the muting method for event separation is the observation of different apparent velocity trends on the raw seismic data. In this research, I demonstrate a method for removing components of seismic wave-field, mainly higher modes of surface wave energy that appear as noise in the phase-velocity – frequency domain, in which dispersion curves are estimated. After proper muting, the quality and observation range of the desired mode (i.e., fundamental mode) improve significantly.

The basis for the application of the method is eliminating certain arrival-time ranges in the offset-time domain, within which certain wave-field components arrive as a result of their overall propagation velocity. For example, higher mode components are expected to arrive earlier on the shot record because of their velocity than the fundamental mode. After muting, the corresponding phase-velocity – frequency domain will lack the noisy event (which appears at a different arrival-time range). The proposed filtering method is effective when it is applied on a seismic shot gathers that have more than one and clearly different surface-wave velocity trends, which can be straightforwardly distinguished.

To show the effect of muting, muting method was applied to shot gather from 2.5-ft geophone spacing at 0-ft receiver offset Figure 5.6 and Figure 5.7 show their dispersion curves before and after muting was applied.

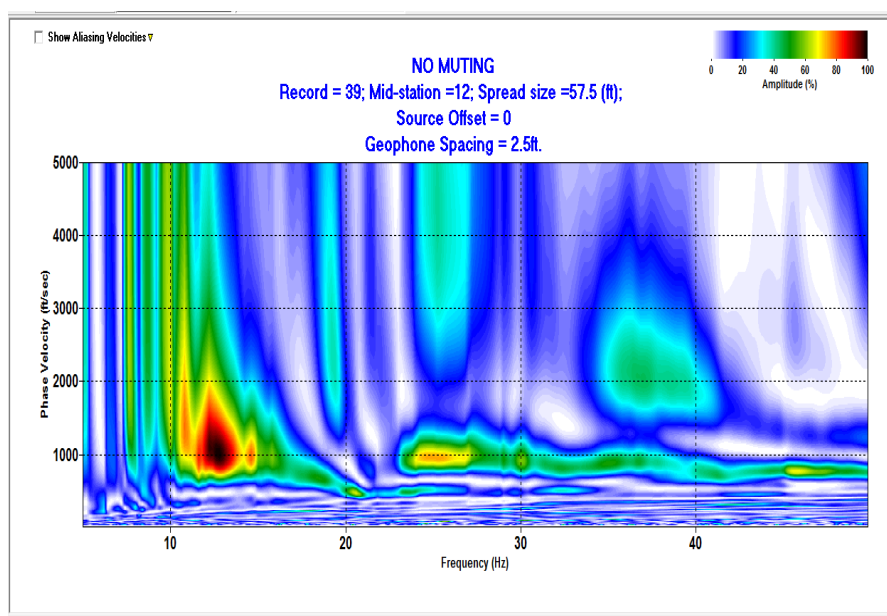


(a) Before Muting

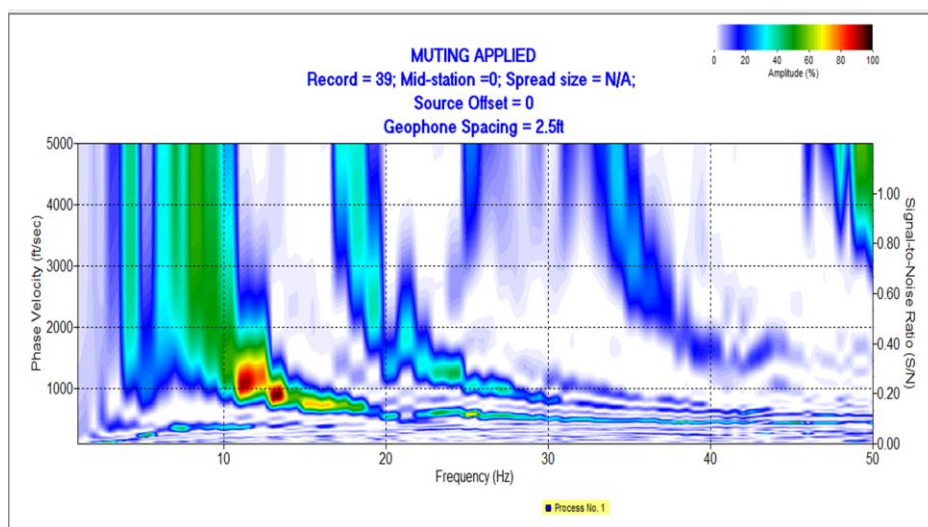


(b) After Muting.

Figure 5.6: Raw shot gather from a 2.5-ft geophone spacing and 0-ft receiver offset before and after muting



(a) Before Muting.



(b) After Muting.

Figure 5.7: Dispersion curve for 2.5-ft spacing and 0-ft offset

5.4.1 Results from Muting. From the example above, it can be seen that surface-wave energy dominates the seismic record (Fig 5.6). The dispersion curve reveals two dispersive events of the surface-wave, the fundamental mode and a high mode (Fig. 5.6c). The fundamental mode can be observed within a narrow frequency range between 10 and 30 Hz (and velocity between 500-1600-ft/sec) while the higher mode dominates a wide frequency range between 25 and 50Hz (and velocities between 700-1500-ft/sec). Efforts to observe the fundamental mode between 15 and 50 Hz by boosting the amplitude of the phase-velocity – frequency spectrum did not bring any success. Thus, the higher-mode energy is significantly higher, and it inhibits the estimation of the fundamental mode dispersion-curve trend above 15 Hz. There are 3 stages to apply muting successfully in MASW processing. The first stage is the estimation of the phase velocities of the fundamental mode of the surface waves in the low-frequency zone. The phase velocity of the fundamental mode ranges from 400 to 1500-ft/sec. The second stage is the muting of the shot gathers from energy dominated by the higher modes and estimating the phase velocities of the fundamental mode of the surface waves in this frequency range (fig 5.6b), which is no longer dominated by higher modes in the raw shot gathers. I muted the surface wave energy below 335-ft/sec and above 1600-ft/sec. The final step is to combine the two curves into a single dispersion curve using the overlapping zone for confirmation of the evaluation and ignoring the steep velocity-gradient portion (at lower frequencies) of the second curve. The acquired fundamental mode dispersion curve now spans over a wide frequency range (10-40 Hz). Thereby eliminating the higher mode energy of the surface wave in the range 15 – 40 Hz in the phase velocity – frequency domain and boosting the weaker fundamental mode energy

within the same frequency range (Fig. 5.6 d). The muting also has completely eliminated the fundamental mode of the surface wave in the range of 5 – 10 Hz (Fig. 5.6c) that has high phase velocity values which inhibit the estimation of the fundamental mode with low phase velocity values. This however, was expected because the low frequency components of the fundamental mode have velocities that are in the velocity range of the muted high mode (Miller, Ivanov, et al., 2001).

5.4.2 Importance of Muting. Fundamental mode dispersion curve energy can be boosted in the phase- velocity – frequency domain after examining a multichannel shot record, recognizing and muting harmful higher mode dispersive energy in the shot record domain. Also muting can significantly improve the bandwidth of the fundamental mode and the dispersion curve picking when using MASW. The downside of muting is that it introduces a high-velocity gradient feature at the low frequency end of the dispersion curve, which is not present before muting. This artifact can be easily handled by using the dispersion curve from the non-muted data that covers the same frequency range, so the artificially high-velocity values can be ignored and are thus considered harmless (Miller, Ivanov, et al., 2001).

6. DISCUSSIONS

6.1 OVERVIEW

Results from MASW data are compared herein with ERT data to determine their accuracy in imaging the top of bedrock in the study area. The acoustic top of bedrock in the study area is 1250-ft. /Sec while the resistivity of top of bedrock ranges from 388 Ohms-meter to excess of 615 Ohms-meter. The estimated top of bedrock based on the resistivity data shows that it ranges from 17-ft to 23-ft and the expected depth of investigation would be 50-ft. In this section, results from the dispersion curves and shear wave velocity profiles of the tested parameters (off set distances and geophone spacings) will be compared with ERT results to determine their accuracy and variations in imaging the top of bedrock and maximum depth of investigation in the study area.

6.2 COMPARISON OF MASW RESULTS WITH 2-D ERT RESULTS

(i) 1-ft Geophone Spacing

Now starting with 10-ft offset and 1-ft geophone spacing, the estimated top of bedrock was 17.5-ft and the maximum depth of investigation would be 37-ft. This result corresponds with the ERT result which shows that the top of bedrock ranges from 17-ft to 23-ft, but maximum depth of investigation would shallower (less than 50-ft.) which is the targeted depth of investigation for this research. Therefore, these parameters would only be useful for a shallower depth of investigation (about 35-ft).

When imaging the top of bedrock using 20-ft offset and 1-ft geophone spacing, the estimated top of bedrock was 17.5-ft and the maximum depth of investigation would

be 50-ft. This result corresponds with the ERT result which shows that the top of bedrock ranges from 17-ft to 23-ft. Also, the maximum depth of investigation would be 50-ft which is the targeted depth of investigation for this research. Therefore, these parameters would be useful and appropriate for mapping acoustic top of bedrock and image the required depth of investigation in the study area.

Also, when imaging the top of bedrock using 30-ft offset and 1-ft geophone spacing, the estimated top of bedrock was 14-ft and the maximum depth of investigation would be 22-ft. This result does not correspond with the ERT result which shows that the top of bedrock ranges from 17-ft to 23-ft. Also, maximum depth of investigation would be shallower (less than 50-ft.) which the targeted depth of investigation for this research is. Therefore, these parameters would only be useful for a shallower depth of investigation of about 20-ft.

When imaging the top of bedrock using 40-ft offset and 1-ft geophone spacing, the estimated top of bedrock was 19.5-ft and the maximum depth of investigation would be 42.5-ft. This result corresponds with the ERT result which shows that the top of bedrock ranges from 17-ft to 23-ft, but maximum depth of investigation would be shallower (less than 50-ft.) which is the targeted depth of investigation for this research. Therefore, these parameters would only be useful for a shallower depth of investigation (about 40-ft).

Finally, when imaging the top of bedrock using 50-ft offset and 1-ft geophone spacing, the estimated top of bedrock was 16-ft and the maximum depth of investigation would be 35-ft. This result corresponds slightly with the ERT result which shows that the top of bedrock ranges from 17-ft to 23-ft, but maximum depth of investigation would be

shallower (less than 50-ft.) which is the targeted depth of investigation for this research. Therefore, these parameters would only be useful for a shallower depth of investigation (about 30-ft).

(ii) 2.5-ft Geophone Spacing

When imaging the top of bedrock using 0-ft offset and 2.5-ft geophone spacing, the estimated top of bedrock was 18-ft and the maximum depth of investigation would be 38-ft. This result corresponds with the ERT result which shows that the top of bedrock ranges from 17-ft to 23-ft, but maximum depth of investigation would be shallower (less than 50-ft.) which is the targeted depth of investigation for this research. Therefore, these parameters would only be useful for a shallower depth of investigation (about 35-ft).

When imaging the top of bedrock using 10-ft offset and 2.5-ft geophone spacing, the estimated top of bedrock was 19-ft and the maximum depth of investigation would be 31-ft. This result corresponds with the ERT result which shows that the top of bedrock ranges from 17-ft to 23-ft, but maximum depth of investigation would be shallower (less than 50-ft.) which is the targeted depth of investigation for this research. Therefore, these parameters would only be useful for a shallower depth of investigation (about 30-ft).

When imaging the top of bedrock using 20-ft offset and 2.5-ft geophone spacing, the estimated top of bedrock was 22.5-ft and the maximum depth of investigation would be 38-ft. This result corresponds with the ERT result which shows that the top of bedrock ranges from 17-ft to 23-ft, but maximum depth of investigation would be shallower (less than 50-ft.) which is the targeted depth of investigation for this research. Therefore these parameters would only be useful for a shallower depth of investigation (about 35-ft).

When imaging the top of bedrock using 30-ft offset and 2.5-ft geophone spacing, the estimated top of bedrock was 21-ft and the maximum depth of investigation would be 35-ft. This result corresponds with the ERT result which shows that the top of bedrock ranges from 17-ft to 23-ft, but maximum depth of investigation would be shallower (less than 50-ft.) which is the targeted depth of investigation for this research. Therefore these parameters would only be useful for a shallower depth of investigation (about 30-ft).

When imaging the top of bedrock using 40-ft offset and 2.5-ft geophone spacing, the estimated top of bedrock was 23-ft and the maximum depth of investigation would be 37-ft. This result corresponds with the ERT result which shows that the top of bedrock ranges from 17-ft to 23-ft, but maximum depth of investigation would be shallower (less than 50-ft.) which is the targeted depth of investigation for this research. Therefore, these parameters would only be useful for a shallower depth of investigation (about 35-ft).

When imaging the top of bedrock using 50-ft offset and 2.5-ft geophone spacing, the estimated top of bedrock was 15-ft and the maximum depth of investigation would be 27-ft. This result does not correspond with the ERT result which shows that the top of bedrock ranges from 17-ft to 23-ft, but maximum depth of investigation would be shallower (less than 50-ft.) which is the targeted depth of investigation for this research. Therefore, these parameters would only be useful for a shallower depth of investigation (about 25-ft).

(iii) 5-ft Geophone Spacing

When imaging the top of bedrock using 0-ft offset and 5-ft geophone spacing, the estimated top of bedrock was 15-ft and the maximum depth of investigation would be 55-ft. This result does not correspond with the ERT result which shows that the top of

bedrock ranges from 17-ft to 23-ft, but maximum depth of investigation would be appropriate and accurate (more than 50-ft.) which is the targeted depth of investigation for this research. Therefore, these parameters would be appropriate for imaging a deeper depth of investigation (more than 50-ft).

When imaging the top of bedrock using 10-ft offset and 5-ft geophone spacing, the estimated top of bedrock was 18-ft and the maximum depth of investigation would be 38-ft. This result corresponds with the ERT result which shows that the top of bedrock ranges from 17-ft to 23-ft, but maximum depth of investigation would be shallower (less than 50-ft.) which is the targeted depth of investigation for this research. Therefore, these parameters would only be useful for a shallower depth of investigation (about 35-ft).

When imaging the top of bedrock using 20-ft offset and 5-ft geophone spacing, the estimated top of bedrock was 20-ft and the maximum depth of investigation would be 80-ft. This result corresponds with the ERT result which shows that the top of bedrock ranges from 17-ft to 23-ft. Also, maximum depth of investigation would be appropriate and accurate (more than 50-ft.) which is the targeted depth of investigation for this research. Therefore, these parameters would be appropriate for imaging a deeper depth of investigation (more than 50-ft).

When imaging the top of bedrock using 30-ft offset and 5-ft geophone spacing, the estimated top of bedrock was 15-ft and the maximum depth of investigation would be 40-ft. This result does not correspond with the ERT result which shows that the top of bedrock ranges from 17-ft to 23-ft, also, the expected maximum depth of investigation would be shallower (less than 50-ft.) which is the targeted depth of investigation for this

research. Therefore, these parameters would be appropriate for imaging a shallower depth of investigation (less than 40-ft).

When imaging the top of bedrock using 40-ft offset and 5-ft geophone spacing, the estimated top of bedrock was 20-ft and the maximum depth of investigation would be 80-ft. This result corresponds with the ERT result which shows that the top of bedrock ranges from 17-ft to 23-ft. Also, maximum depth of investigation would be appropriate and accurate (more than 50-ft.) which is the targeted depth of investigation for this research. Therefore, these parameters would be appropriate for imaging a deeper depth of investigation (more than 50-ft).

When imaging the top of bedrock using 50-ft offset and 5-ft geophone spacing, the estimated top of bedrock was 19-ft and the maximum depth of investigation would be 55-ft. This result corresponds with the ERT result which shows that the top of bedrock ranges from 17-ft to 23-ft. Also, maximum depth of investigation would be appropriate and accurate (more than 50-ft.) which is the targeted depth of investigation for this research. Therefore, these parameters would be appropriate for imaging a deeper depth of investigation (more than 50-ft).

(iv) 7.5-ft Geophone Spacing

When imaging the top of bedrock using 0-ft offset and 7.5-ft geophone spacing, the estimated top of bedrock was 37-ft and the maximum depth of investigation would be 80-ft. This result does not correspond with the ERT result which shows that the top of bedrock ranges from 17-ft to 23-ft. But expected maximum depth of investigation would be appropriate and accurate (more than 50-ft.) which is the targeted depth of investigation

for this research. Therefore, these parameters would be appropriate for imaging a deeper depth of investigation (more than 50-ft).

When imaging the top of bedrock using 10-ft offset and 7.5-ft geophone spacing, the estimated top of bedrock was 26-ft and the maximum depth of investigation would be 150-ft. This result does not corresponds with the ERT result which shows that the top of bedrock ranges from 17-ft to 23-ft. But expected maximum depth of investigation would be appropriate and accurate (more than 50-ft.) which is the targeted depth of investigation for this research. Therefore, these parameters would be appropriate for imaging a deeper depth of investigation (more than 50-ft).

When imaging the top of bedrock using 20-ft offset and 7.5-ft geophone spacing, the estimated top of bedrock was 30-ft and the maximum depth of investigation would be 130-ft. This result does not corresponds with the ERT result which shows that the top of bedrock ranges from 17-ft to 23-ft. But expected maximum depth of investigation would be appropriate and accurate (more than 50-ft.) which is the targeted depth of investigation for this research. Therefore, these parameters would be appropriate for imaging a deeper depth of investigation (more than 50-ft).

When imaging the top of bedrock using 30-ft offset and 7.5-ft geophone spacing, the estimated top of bedrock was 30-ft and the maximum depth of investigation would be 60-ft. This result does not corresponds with the ERT result which shows that the top of bedrock ranges from 17-ft to 23-ft. But expected maximum depth of investigation would be appropriate and accurate (more than 50-ft.) which is the targeted depth of investigation for this research. Therefore, these parameters would be appropriate for imaging a deeper depth of investigation (more than 50-ft).

When imaging the top of bedrock using 40-ft offset and 7.5-ft geophone spacing, the estimated top of bedrock was 24-ft and the maximum depth of investigation would be 70-ft. This result does not correspond with the ERT result which shows that the top of bedrock ranges from 17-ft to 23-ft. But expected maximum depth of investigation would be appropriate and accurate (more than 50-ft.) which is the targeted depth of investigation for this research. Therefore, these parameters would be appropriate for imaging a deeper depth of investigation (more than 50-ft).

When imaging the top of bedrock using 50-ft offset and 7.5-ft geophone spacing, the estimated top of bedrock was 35-ft and the maximum depth of investigation would be 43-ft. This result does not correspond with the ERT result which shows that the top of bedrock ranges from 17-ft to 23-ft. Also, expected maximum depth of investigation would be shallower (less than 50-ft.) which the targeted depth of investigation for this research is. Therefore, these parameters would be appropriate for imaging a shallower depth of investigation (less than 50-ft).

(v) 10-ft Geophone Spacing

When imaging the top of bedrock using 10-ft offset and 10-ft geophone spacing, the estimated top of bedrock was 10-ft and the maximum depth of investigation would be 86-ft. This result does not correspond with the ERT result which shows that the top of bedrock ranges from 17-ft to 23-ft, but maximum depth of investigation would be appropriate and accurate (more than 50-ft.) which is the targeted depth of investigation for this research. Therefore, these parameters would be appropriate for imaging a deeper depth of investigation (more than 50-ft).

When imaging the top of bedrock using 20-ft offset and 10-ft geophone spacing, the estimated top of bedrock was 45-ft and the maximum depth of investigation would be 70-ft. This result does not correspond with the ERT result which shows that the top of bedrock ranges from 17-ft to 23-ft. But expected maximum depth of investigation would be appropriate and accurate (more than 50-ft.) which is the targeted depth of investigation for this research. Therefore, these parameters would be appropriate for imaging a deeper depth of investigation (more than 50-ft).

When imaging the top of bedrock using 30-ft offset and 10-ft geophone spacing, the estimated top of bedrock was 38-ft and the maximum depth of investigation would be 47.5-ft. This result does not correspond with the ERT result which shows that the top of bedrock ranges from 17-ft to 23-ft. Also, expected maximum depth of investigation would be shallower (less than 50-ft.) which the targeted depth of investigation for this research is. Therefore, these parameters would be appropriate for imaging a shallower depth of investigation (less than 50-ft).

When imaging the top of bedrock using 40-ft offset and 10-ft geophone spacing, the estimated top of bedrock was 100-ft and the maximum depth of investigation would be 125-ft. This result does not correspond with the ERT result which shows that the top of bedrock ranges from 17-ft to 23-ft. But expected maximum depth of investigation would be appropriate and accurate (more than 50-ft.) which is the targeted depth of investigation for this research. Therefore, these parameters would be appropriate for imaging a deeper depth of investigation (more than 50-ft).

When imaging the top of bedrock using 50-ft offset and 10-ft geophone spacing, the estimated top of bedrock was 55-ft and the maximum depth of investigation would be

90-ft. This result does not corresponds with the ERT result which shows that the top of bedrock ranges from 17-ft to 23-ft. But expected maximum depth of investigation would be appropriate and accurate (more than 50-ft.) which is the targeted depth of investigation for this research. Therefore, these parameters would be appropriate for imaging a deeper depth of investigation (more than 50-ft).

6.3 FINAL ANALYSIS

Analysis of the discussed are analyzed in this section based there appropriate matches with the ERT results. The analyses are divided into three categories (Excellent, Good and Poor) in Table 6.1

Table 6.1: Final result analysis for MASW and ERT testing

Excellent Quality (Top of bedrock and Max. depth of investigation accurate with ERT result)		Good Quality (Top of bedrock is accurate with ERT result but shallower depth investigation)		Poor Quality (Deeper depth of investigation at deeper top of bedrock)	
Offset (ft)	Spacing (ft)	Offset (ft)	Spacing (ft)	Offset (ft)	Spacing (ft)
20	5	10	1	0	7.5
40	5	20	1	10	7.5
50	5	30	1	20	7.5
		40	1	30	7.5
		50	1	40	7.5
		0	2.5	50	7.5
		10	2.5	10	10
		20	2.5	20	10
		30	2.5	30	10
		40	2.5	40	10
		50	2.5	50	10
		0	5		
		10	5		
		30	5		

7. CONCLUSIONS

The primary objective of this study was to image the subsurface of the study area to 50-ft using Multichannel Analysis of Surface Waves and Electrical Resistivity Tomography and compare the estimated top of bedrock from the MASW results and ERT results. From the comparison of these results, the optimum acquisition parameters for the MASW for this site would be selected based on how accurate they match with the ERT results in estimating the top of bedrock and imaging a maximum depth of investigation of 50-ft.

Observations from the final analysis of the MASW results show

- (1) Profile data from electrical resistivity and MASW analyses was comparable with each other.
- (2) Dissimilarities between MASW data and ERT data can exist due to the heterogeneity of the earthen structure, as well as the resolution capabilities and data smoothing associated with each method
- (3) 1-ft geophone spacing at 20-ft offset distance, 5-ft geophone spacing at 20-ft offset and 5-ft geophone spacing at 40-ft offset distance were the most accurate parameters because they corresponded with the ERT result for the estimation of top of bedrock and also will be appropriate for imaging the subsurface to 50-ft.
- (4) 2.5-ft geophone spacing at 0-ft, 10-ft, 20-ft, 30-ft, 40-ft, 50-ft offset distance and 1-ft geophone spacing at 10-ft, 40-ft, 50-ft offset distance gave a good quality result because they corresponded with the ERT result for the estimation of the top of rock, but would not be advisable for imaging the subsurface more than 40-ft.

Conclusively, the most appropriate parameters for estimating the top of bedrock and imaging the subsurface of this study area to 50-ft would be 5-ft geophone spacing at 20-ft offset and 5-ft geophone spacing at 40-ft offset distance. These parameters were chosen as the optimum acquisition parameters for this site because they gave the accurate top of bedrock and were able to image the subsurface at 50-ft.

8. RECOMMENDATIONS

The performance of similar analyses is needed in order to validate the primary objective of this study. It is believed that future studies would benefit by utilizing and/or incorporating the following measures in the methodology:

- Perform all testing and data acquisition during the same analysis period to limit any potential variations in site conditions.
- Incorporate GPS and/or GIS information into data acquisition and presentation of findings to enhance the location of survey features and testing results.
- Higher source like drop source or vibrator should be used to enhance the quality of the MASW data.
- Borehole data should be available as a ground truth for estimating the top of bedrock and calibrating MASW and ERT with borehole data would be highly recommended.
- On the basis of data that were acquired it is recommended that 2.5ft spacing be used if depth of investigation is about 40ft, but if the depth of investigation is about 80-ft, using a sledge hammer source then 5-ft geophone spacing at 20-ft shot-receiver offset distance is recommended.

BIBIOGRAPHY

Advanced Geosciences Incorporated. "Workshop/Seminar on Resistivity Imaging." Austin, April 29, 2008.

Advanced Geosciences, Inc. January 23, 2009.<http://www.agiusa.com> (accessed April 16, 2009).

Advanced Geosciences, Incorporated. "Instruction Manual for the Super Sting with Swift Automatic Resistivity and IP System." Austin, January 2006.

Callister Jr, William D. Fundamentals of Material Science and Engineering. New York: John Wiley and Sons, Inc., 2001.

Clinton .M. Wood "The impact of source type, source offset, and receiver spacing on experimental masw data at soft-over-stiff sites, Master's degree thesis University of Arkansas, 2009.

Geometrics Incorporated. "ES-3000, Geode, and Strata Visor NZ/NZC Operator's Manual, P/N 28519-01 Rev K." San Jose, June 2003.

Gibson, Paul J, and Dorothy M George. Environmental Applications of Geophysical Surveying Techniques. Hauppauge: Nova Science Publishers, 2003.

Golden Software, Inc. 2013. (<http://www.goldensoftware.com/voxler-videos/voxler-3-loading-and-visualizing-well-data?ml=1>).

Hazmira Liyana (2013, December 13) Gujarat Earthquake [Web log post].Retrieved May 3, 2015, from <http://geohazardsearthquake.blogspot.com>.

Ivanov, Julian, Choon Park, and Jianghai Xia. "MASW/Surfseis 2 Workshop." Fort Worth: Kansas Geologic Survey, March 28, 2009.

Kearey, Brooks and Hill, 2002. Introduction to Geophysical Exploration. Williston: Blackwell Publishing, 2002.

Loke, M.H. "Electrical Imaging Survey for Environmental and Engineering Studies." 2000.

MASW to investigate subsidence in the Tampa, Florida area: Kansas Geological Survey Open-file Report 99-33.2014.

Milson, John. Field Geophysics. New York: John Wiley & Sons, 1996.

Missouri Department of Natural Resources (FGDC-STD-001-1998) Geographic Information System. Retrieved May 3, 2015, <http://dnr.mo.gov/gis/geology.surficial.xml>

Multichannel Analysis of Surface Waves (2013, March 13) Dispersion Analysis. Retrieved May 3, 2015, from <http://www.masw.com/DispersionAnalysis.html>.

Nazarian, 1984; Nazarian S, Stokoe II KH. In situ shear wave velocities from spectral analysis of surface waves. Proceedings of 8th Conference on Earthquake Engineering, San Francisco, 1984. vol. 3. P.38-45.

Parasnis, D.S. Principles of Applied Geophysics. New York: Chapman & Hall, 1997.

Park CB, Miller RD, Xia J. Imaging dispersion curves of surface waves on multichannel record. 68th Annual International Meeting, Society of Exploration Geophysicists, Expanded Abstracts; 1998. p. 1377-1380.

Park CB, Miller RD, Xia J. Multichannel analysis of surface waves. Geophysics 1999; 64(3):800-808.

Park, Choon B, Miller, Richard D., Xia Jianghai. (1997) "Multi-Channel Analysis of Surface Waves (MASW) a summary report of technical aspects, experimental results, and perspective" Kansas Geological Survey Open-file Report #97-10.

Park, Choon B, Richard D Miller, Jianghai Xia, and Julian Ivanov. "MASW - An easy seismic Method to map shear-wave velocity of the ground." Chun Cheon: Korean Society of Engineering Geology, 2004.

Park, Choon B, Richard D Miller, Jianghai Xia, and Julian Ivanov. "Multichannel Seismic Surface-Wave Methods for Geotechnical Applications." First International Conference on the Application of Geophysical Methodologies to Transportation Facilities and Infrastructure. St. Louis, 2000.

Park, Choon B, Richard Miller, Jianghai Xia, Nils Ryden, and Peter Ulriksen. "The MASW Method - What and Where it is." EAGE 65th Conference and Exhibition. Stavanger, 2003.

Park, Choon B. MASW - Horizontal Resolution in 2D Shear-Velocity (V_s) Mapping. Open-File Report, Lawrence: Kansas Geologic Survey, 2005.

Park, Choon B. Miller, Richard D. and Xia, Jianghai (1999). "Multichannel Analysis of Surface Waves." Geophysics. Vol 64. (3), pp 800-808.

Park, Choon B., Miller, Richard D., Xia, Jianghai and Ivanov, Julian (2001). "Seismic Characterization of Geotechnical Sites by Multichannel Analysis of Surface Waves (MASW) Method.

Park, Choon B., Miller, Richard D., Xia, Jianghai and Ivanov, Julian (2001). "Seismic Characterization of Geotechnical Sites by Multichannel Analysis of Surface Waves (MASW) Method.

Sanchez-Salintero, I. (1987). "Analytical Investigation of Seismic Methods used for Engineering Applications.", Ph.D. Dissertation, The University of Texas at Austin, pp. 401.

Seistronix (2015, April 30) RAS-24 Exploration Seismograph. Retrieved May 5, 2015, from <http://www.seistronix.com>.

Society of Exploration Geophysicist of Japan. Application of Geophysical Methods to Engineering and Environmental Problems. Tokyo: Society of Exploration Geophysicist of Japan, 2004.

Stokoe II KH, Wright GW, James AB, Jose MR. Characterization of geotechnical sites by SASW method. In: Woods RD, Ed. Geophysical characterization of sites, A. A. Balkema/Rotterdam, 1994. p. 15-25.

United States Corps of Engineers. "EM 1110-1-1802: Geophysical Exploration for Engineering and Environmental Investigations." Engineering Manual, Washington D.C., 1995.

United States Corps of Engineers. "EM 1110-1-1802: Geophysical Exploration for Engineering and Environmental Investigations." Engineering Manual, Washington D.C., 1995.

United States Corps of Engineers. "Geotechnical Investigations." Engineering Manual No. 1110-1-1804, Washington D.C., 2001.

Wikipedia (2015, April 23) Deformation (engineering). Retrieved May 3, 2015, from http://upload.wikimedia.org/wikipedia/commons/8/84/Stress_Strain_Ductile_Material.png.

Wikipremed (2014, October 8) Physics cards. Retrieved May 3, 2015, from <http://www.wikipremed.com/01physicscards.php?card=312>.

Zonge, Ken, Jeff Wynn, and Scott Urquatt. "Resistivity, Induced Polarization, and Complex Resistivity." In Near-Surface Geophysics, by Dwain K. Butler, 265-300. Tulsa: Society of Engineering Geophysicist, 2005.

VITA

Uchenna Chibuzo Nwafor was born in Oko in Orumba North Local Government Area in Anambra State Nigeria. In 2001 he graduated from Community Secondary School Oko where he served as the Senior Prefect for 2000-2001 academic year and received his West Africa Examination Certificate (WAEC) and National Examination Council (NECO) with academic excellence.

In December 2005, he received his Ordinary National Diploma (OND) in Science Laboratory Technology from the University of Nigeria Nsukka Nigeria. In December 2010 he received his B.S with Honors in Geology from the University of Nigeria Nsukka, Nsukka, Nigeria. He did his summer internship with GeoGlobe Nigeria Limited during the summer of 2009 and in summer 2010, he started working for Regibel Limited in Awka Nigeria as a field Geologist until March 2011.

Uchenna joined APOGEE Engineering Limited in April 2011 as a Procurement Manager and Store Manager in Uyo, Akwaibom state Nigeria and he worked there for three years until gained admission into the Missouri University of Science and Technology graduate school in August 2013 to study Geological Engineering.

In May 2015, he received his M.S degree in Geological Engineering from the Missouri University of Science and Technology, Rolla, United States of America.

He has presented conference papers in the American Association of Petroleum Geologist (AAPG) and Society of Exploration Geophysicists (SEG) students Expo and received awards and grants from Exxon Mobil to attend Students Education Program in 2014. Also he received grant from Chevron in 2010 to attend the Chevron/SEG Students leadership Symposium in Denver, Colorado.